Towards a Targeted Formulation for Treatment of Small Cell Lung Cancer

Mohammad Jamal A Akbar

University of East Anglia

School of Pharmacy

Thesis Submitted for the degree of Master of Science by Research

July, 2016

Towards a Targeted Formulation for Treatment of Small Cell Lung Cancer

Mohammad Jamal A Akbar, 2016

Abstract

Lung cancer is one of the most common cancers with small lung cancer (SCLC) representing 14% of the total lung cancer incidence. It is the major cause of cancer death in the UK. Most patients present with extensive disease, which is difficult to treat with the standard chemotherapy. Liposome-based approach provides a tool for improving treatment outcomes. Liposome is versatile tool, with tuneable features such as composition, size and charge. It can be used as a targeting therapy.

The aim of this study was to synthesis a targeted liposomal drug delivery system for SCLC that enhances delivery to GRPR+ cells through conjugation with an antagonist peptide, cystabn. To do that, the receptor expression evaluated in the SCLC cell line (H345) and NSCLC cell line (A549) by indirect antibody detection using flow cytometed. The cystabn peptide was synthesised using Fmoc-SPPS and coupled to DSPE-PEG_{2000}-Maleimide. The dyalised product was characterised by HPLC, UV and MALDI-TOF MS. PEG-stabilised control liposomes were prepared using the thin film hydration method and characterized by DLS. A targeted liposome formulation was prepared by including 1 mole % DSPE-PEG_{2000}-cystabn in the control formulation. Fluorescent liposomes include 1 mole % DHPE-fluorescein. Cell uptake was measured on by flow cytometer.

Uniform targeted liposome formulation were prepared with good stability. The cystabn peptide showed no growth stimulation in H345 and A549 cells, both of which have been shown to express GRP-R to varying extents. Uptake of targeted liposomes into SCLC cells was equivalent for control and targeted formulations. This indicates that the current formulation approach is inappropriate for the preparation of targeted liposomes.

Acknowledgement

I would like to express my sincere gratitude to my supervisor Dr Chris Morris for his continuous support and encouragement, for his patience, motivation, and immense knowledge during my research study for Mscr degree. His guidance helped me in all the time of research and writing of this thesis. I could not have imagined having a better supervisor and mentor for my Mscr study.

Besides my supervisor, I would like to thank Dr Francesca Baldelli Bombelli and Dr Wafa Al-Jamal for their help and support. I would also like to thank the University of Dammam thorough Saudi Arabia Cultural Bureau in London for granting me this opportunity and for their financial support. Thanks also to several members of the school of Pharmacy who gave me invaluable help throughout my Mscr Degree and gave me access to their laboratory and research facilities.

I would like to thank my very special friends and labmates Mr Carl Webster and Miss Melania Giorgetti for the stimulating discussions, for the sleepless nights we were working together, and for all the fun we have had in the last two years. Also I thank my friends in the department of drug delivary for their help and support.

Last but not the least, I would like to give my special thanks to my wife for her invaluable support and for her patience. Thanks to my family: my parents and to my brothers and sister for supporting me spiritually throughout writing this thesis and my life in general.

Table of Contents

Figures list

Tables list

Abbreviations list

FULL EXPRESSION	ABBREVIATED EXPRESSION
1,2-DIOLEOYL-*SN*-GLYCERO-3-PHOSPHOCHOLINE	DOPC
1,2-DIOLEOYL-SN-GLYCERO-3-PHOSPHOETHANOLAMINE	DOPE
1,2-DISTEAROYL-*SN*-GLYCERO-3-PHOSPHOETHANOLAMINE	DSPE
1^{O}	Primary
2,5-DIHYDROXYBENZOIC ACID	DHB
2^{O}	Secondary
4-METHYLBENZHYDRYLAMINE HYDROCHLORIDE	MBHA
AMINO ACID	AA
ANTIBODY	Ab
APPARENT BINDING CONSTANT	K_D
BOMBESIN RECEPTOR SUBTYPE 3	BRS-3
CENTRAL NERVOUS SYSTEM	CNS

CHOLESTEROL	Chol
CONTROL FORMULATION	CF
DERJAGUIN, LANDAU, VERWEY, OVERBEAK	DLVO
DICHLOROMETHANE	DCM
DILUTION FACTOR	DF
DIMETHYLFORMAMIDE	DMF
DYNAMIC LIGHT SCATTERING	DLS
ELECTRON MICROSCOPY	EM
ENHANCED PERMEABILITY AND RETENTION	EPR
ETHYLENEDIAMINETETRAACETIC ACID	EDTA
ETHYLMETHYL SULFIDE	EDT
FETAL BOVINE SERUM	FBS
FLUORENYLMETHYLOXYCARBONYL	Fmoc
FLUORESCENT LIPOSOME	FL
FORWARD LIGHT SCATTERING	FS
FORWARD SCATTER	FS

GASTRIN RELEASING PEPTIDE	GRP
GASTRIN RELEASING PEPTIDE RECEPTOR	GRP-R
HEAT INACTIVATED	HI
HIGH PERFORMANCE LIQUID CHROMATOGRAPHY	HPLC
HYDROGENATED SOY PHOSPHATIDYLCHOLINE	HSPC
INTENSITY BASED HARMONIC MEAN SIZE	Z-Ave
LARG UNILAMELLAR VESICLES	LUV
LIQUID CHROMATOGRAPHY	LC
L-STATINE	Sta
MALEIMIDE	Mal
MASS SPECTROMETRY	MS
MATRIX ASSISTED LASER DESORPTION/IONIZATION	MALDI
MEDIAN FLUORESCENT INTENSITY	MFI
MOLECULAR WEIGHT CUT-OFF	MWCO
MULTILAMELLAR VESICLE	MLV

N,*N*-DIISOPROPYLETHYLAMINE	DIPEA
NEUROMEDIN B	NMB
NEUROMEDIN B RECEPTOR	NMB-R
NICOTINAMIDE ADENINE DINUCLEOTIDE	NADH
NICOTINAMIDE ADENINE DINUCLEOTIDE PHOSPHATE	NADPH
NON-SMALL CELL LUNG CANCER	NSCLC
PERMEABILIZED	Perm
PHOSPHATE-BUFFERED SALINE	PBS
POLYDISPERSITY INDEX	PDI
POLYETHYLENE GLYCOL	PEG
RETENTION TIME	R_T
RETICULOENDOTHELIAL SYSTEM	RES
REVERSE TRANSCRIPTION POLYMERASE CHAIN REACTION	RT-PCR
ROOM TEMPERATURE	RT
SIDE LIGHT SCATTERING	SS

SIZE EXCLUSION CHROMATOGRAPHY	SEC
SMALL CELL LUNG CANCER	SCLC
SMALL UNILAMELLAR VESICLES	SUV
SOLID PHASE PEPTIDE SYNTHESIS	SPPS
STANDARD DEVIATION	SD
TARGETED FORMULATION	TF
TIME OF FLIGHT	ToF
TRIFLUOROACETIC ACID	TFA
TRIISOPROPYLSILANE	TIPS
ULTRAVIOLET VISIBLE	UV-Vis
UNILAMELLAR VESICLE	ULV
ZETA POTENTIAL	ZP
ZETASIZER	ZS

GENERAL INTRODUCTION

Chapter 1

1.1 Small cell lung cancer (SCLC)

Lung cancer is the second most common malignancy after prostate and breast cancer in men and woman respectively in the UK [1]. However, it is the major cause of cancer deaths among cancer patients [2]. SCLC is a type of lung cancer with unique clinical and histological features in comparison to other lung cancers, which are collectively called non-small cell lung cancer (NSCLC).

SCLC accounts for about 14 % of all diagnosed lung cancer cases [3] and is considered the most aggressive subtype of lung cancer. SCLC has a strong association with tobacco smoking with more than 95% of SCLC patients presenting with a history of tobacco smoking [4]. There is a slight decrease in SCLC incidence recognized in relation to tobacco smoking cessation [5]. There have been limited advances made in the treatment and understanding of the underlying biology of SCLC compared to NSCLC. In order to address this problem, it is crucial to draw efforts on to further our understanding of the biology as well as diagnosis and development of effective treatment for SCLC.

1.1.1 Clinical Presentation

SCLC is characterized by its distinct features such as its high proliferation rate, high probability of early metastasis and high initial response rates to chemotherapy [4]. These characteristics relate to the patient symptoms presentation. For example, most SCLC patients (~80%) present with extensive metastatic disease at the time of diagnosis although at the time of diagnosis relatively mild symptoms such as cough and dyspnoea are the most common findings in addition to symptoms related to metastasis [5].

SCLC is a neuroendocrine type of cancer, which produces a number of hormone-like substances and growth factors. The neuroendocrine nature of SCLC often leads to paraneoplastic syndromes such as inadequate antidiuretic hormone homeostasis [6]. Generally, these syndromes are groups of symptoms, which manifest themselves at body sites distal to that of the causative malignancy and they result from substances produced by the tumour itself. The syndrome symptoms take diverse manifestations, which could be, for example, endocrine, neuromuscular or musculoskeletal in nature [5-7].

1.1.2 Histology of SCLC

SCLC is a lung tumour that originates from small, monomorphic epithelial cells which develop undistinguishable nuclei and clear nuclear chromatin and minimal cytoplasm [3] (Figure 1.1). In general, SCLC can be diagnosed with high reliability based on pathological samples viewed using light microscopy Figure 1.1. The SCLC cells form a dense cell population with granular nuclear chromatin, frequent mitoses and with no nucleoli in addition to scarce cytoplasm.

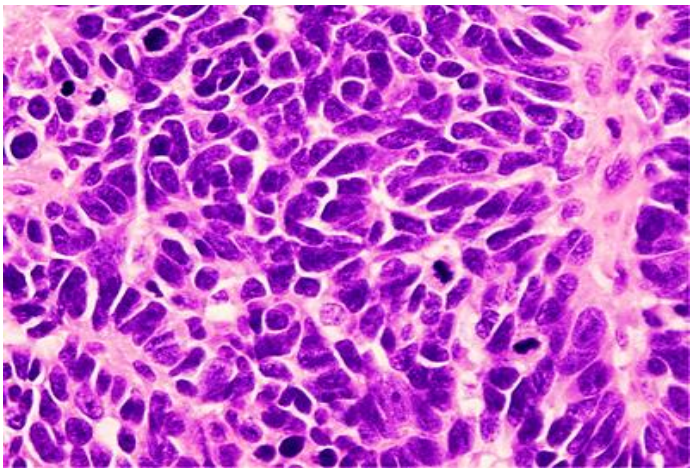

Figure 1.1: High magnification light micrograph of primary SCLC tumour cells. *The image taken from [3].*

For some cases however, immunohistochemistry as well as cytology is used to aid differential diagnosis. SCLC can be classified pathologically into two types including typical SCLC and combined SCLC (C-SCLC, SCLC + NSCLC), which represents about 18% of the cases [8]. Figure 1.2 shows the SCLC tumour sample under the light microscope, which show extensive necrosis and densely packed sheet of malignant cells.

An accurate pathological diagnosis of SCLC is key as it will direct the course of treatment and disease prognoses. For example, SCLC is treated mostly with chemotherapy of platinates and etoposide in combination for limited stage disease. Consecration of thoracic radiotherapy if the disease can be encumbered with the thoracic radiation or the patient is responding to chemotherapy but showing toxicities. For metastatic disease the same protocol without radiotherapy and with continues monitoring throughout the treatment course. the patient with the extensive stage can be treated with thoracic radiotherapy, if there a complete response at distal sites and partial thoracic response to chemotherapy [9].

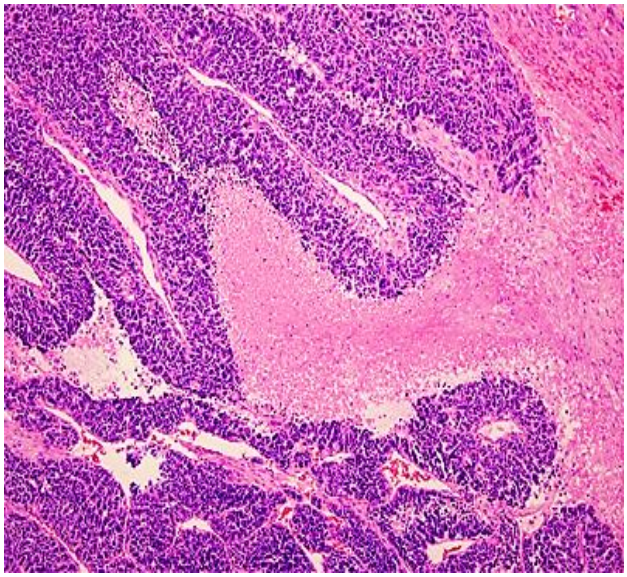

Figure 1.2: Low power light micrograph of SCLC primary tumour. *The biopsy was taken from the tumour periphery and includes regions of high mitoses juxtaposed to the necrotic core. The used stain is hematoxylin and eosin (H&E). Image adapted from [3].*

SCLC, which is a type of neuroendocrine tumours, produces many growth factors. For example, gastrin-releasing peptide (GRP) [10], bombesin [11] and insulin growth factor [12] are expressed by SCLC in autocrine manner to stimulate its own growth.

1.1.3 Bombesin-like peptide family in SCLC

GRP is part of a group of peptides called bombesin-like peptides (BLPs) which bind to the bombesin receptor family. Bombesin is a 14-amino acid peptide first isolated from frog skin [13]. BLPs include GRP and neuromedin B (NMB) which were found in mammalian cells [14, 15]. GRP and bombesin share a highly conserved 7-amino acids C-terminal sequence (shown in Figure 1.3), which is essential for high-affinity to GRP-R [14]. GRP is a neuropeptide that acts through gastrin-releasing peptide receptor (GRP-R) in human to perform numerous functions around the body such as in the gastrointestinal and central nervous systems, including release of gastrointestinal hormones and epithelial cell

proliferation by acting as a hormone [16]. There is growing interest in the bombesin receptor family for a number of reasons. First, this family of receptors, particularly GRP-R , has been shown to be overexpressed in a wide spectrum of human cancers, as well as it found to be involved in tumour growth in various tumours [17].

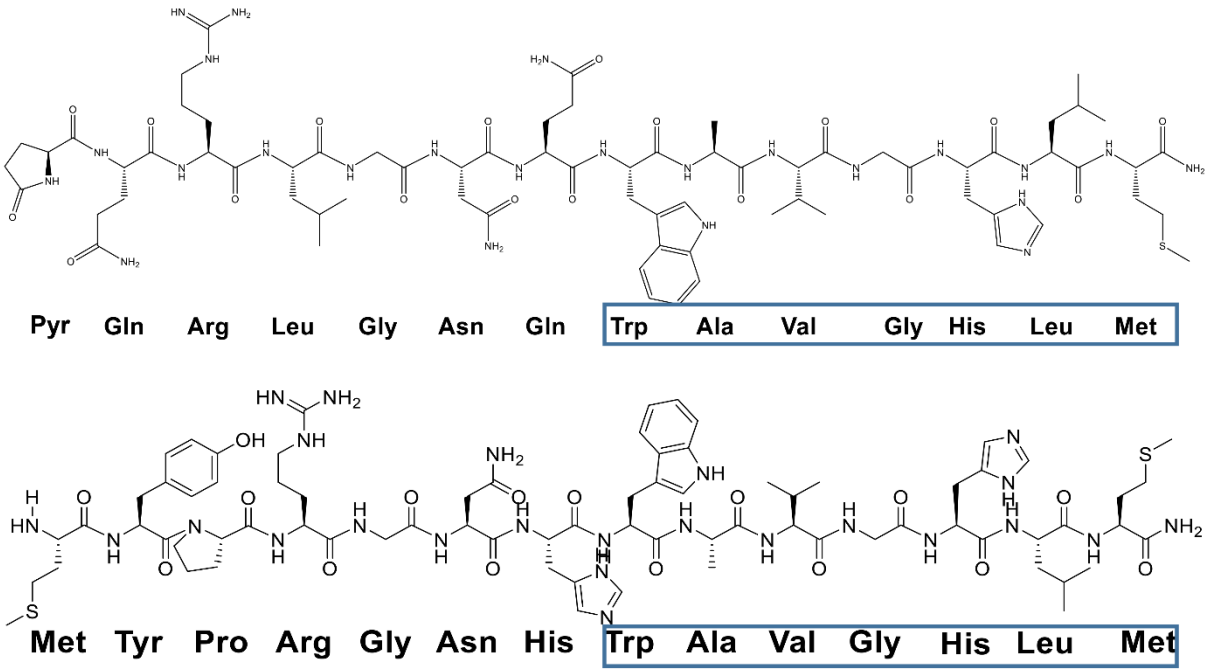

Figure 1.3: amino acids sequence of two peptides- Bombesin(1-14) (top) and GRP(14-27) (bottom). *The 7-amino acids shared sequence between the two peptides is highalited with blue rectangle.*

The human GRP-R is a G-protein coupled receptor comprising 384 amino acids and seven transmembrane regions (**Figure 1.4**). Human GRP-R expressed in the pancreas, the stomach, prostate, skeletal muscle and in the CNS. C-terminal 7-amino acids sequence shared between Bombesin and GRP is the shortest sequence required to cause internalization [18]. Bombesin and GRP bind to GRP-R, which is a G-protein coupled receptor. This triggers the activation of many signalling pathways that transduct the mitogenic signal to the nucleus and promote

cell proliferation. For example, bombesin stimulated Ca^{2+} mobilization [19] and activation of protein kinase C [20]. In regard to internalization, GRP-R has been shown to be internalized upon ligand binding by fluorescence visualization of the receptor trafficking [21].

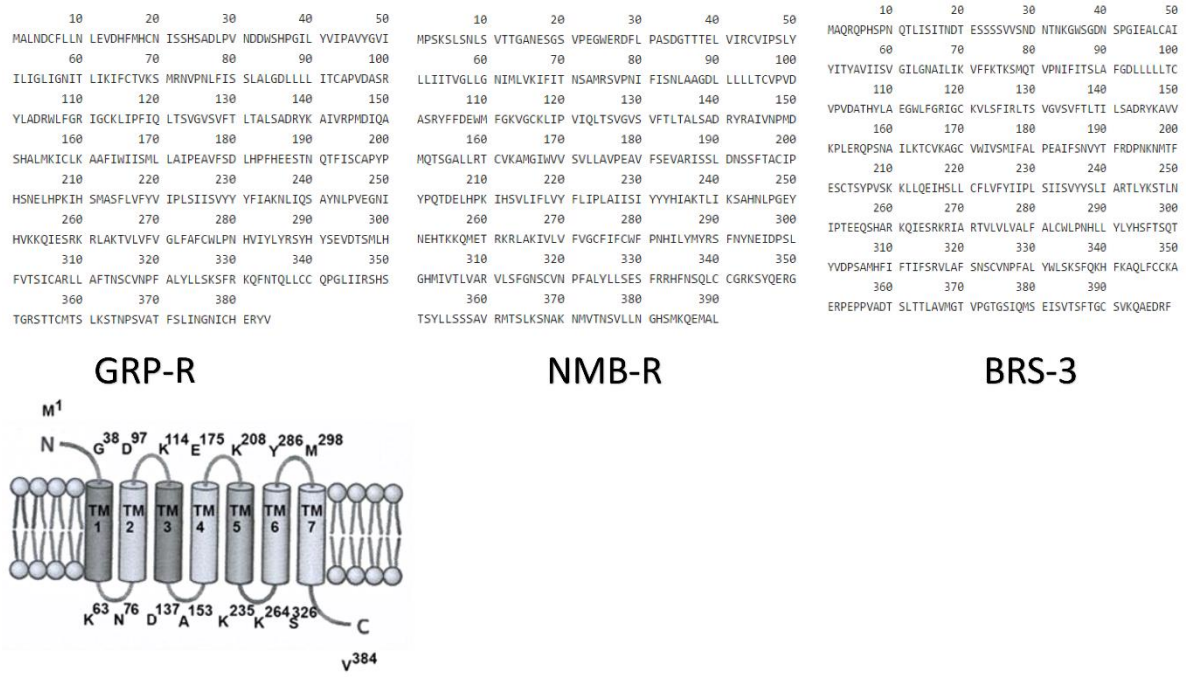

Figure 1.4: The three mammalian bombesin receptors represintation. *Gastrin releasing peptide receptor (GRP-R), neuromedin B receptor (NMB-R) and Bombesin receptor subtype 3 (BRS-3) are shown as amino acids sequences. Repressive structure for GRP-R across cell membrane shown in the bottom right. It features the seven receptor subunits of this G-protein pound receptor.*

GRP was found to be a potent mitogen in cancers such as SCLC [22], breast [23], colon [24] and prostate [25] cancers. NMB has also been found to stimulate growth in SCLC cells *in vitro* [26]. GRP-R is reported to be overexpressed in numerous cancers such as lung, colon, and prostate [17]. SCLC cells express the receptors, GRP-R , NMB-R and the orphan BRS-3, and also secrete the cognate ligands, GRP and NMB [27]. These receptor-ligand pairs

have been shown to fulfil an autocrine growth loop that is unique to malignant cells. Normal lung epithelia dose not express GRP-R [28]. GRP is a 27-amino acid peptide that shows extensive homology with bombesin (57 %) that binds with high affinity (K_D = 1.3 nM) to solubilised GRP-R in the NCI-H345 (H345) SCLC cell line [29]. Ligand-receptor binding in this cell line was later (Corjay et al) shown to cause raised intracellular Ca^{2+} levels consistent with the mechanism of a protein kinase C, G protein linked GPCR [30].

The expression of GRP-R has been evaluated in a variety of human cancers such as SCLC by RT-PCR and immunoreactivity experiments. GRP-R has been shown to be expressed in 17/20 SCLC cell lines (Toi-Scott et al 1996) 85% , which found to be more than other Bombesin receptors in the cells, (NMB-R = 55%, BB_3-R = 25%) [27]. GRP-R was also detected in primary SCLC samples (2/5; 29%) in another study [31]. There is evidence in the literatures in regard to GRP-R expression in NSCLC. GRP-R found to be expressed in 11/13 NSCLC cell lines [27]. The growth of NSCLC tumour in mice was suppressed by more than 30% using GRP-R antagonist [32]. Taken together the expression data for GRP and GRP-R in SCLC offers the opportunity to target this pathway for cancer treatment.

1.1.4 Staging of SCLC

Cancer staging aims to identify the magnitude of cancer cell dissemination. This is one of the most important factors in making successful treatment decisions and subsequently disease prognosis. Patients with SCLC are typically grouped into limited stage or extensive stage disease [4]. Limited stage disease is generally defined as a case where the tumour(s) are to one half of the thorax, with hilar and mediastinal nodes metastases, which can be treated with one tolerable radiotherapy session. Extensive stage disease is any presentation of the disease not labelled as limited stage. Most (65%) patients present with extensive stage disease and the median survival and 5 years survival for this stage are 7–12 months and 2%

of the initial diagnosed patients, respectively. For the limited stage disease, 23 months' median survival and 12–17% survive 5 years after the initial diagnosis. In the UK the TNM staging system is used for a more detailed analysis of the disease. It includes the size of the tumour (T), whether or not the cancer cells have metastasised to local lymph nodes (N) and whether the tumour has metastasised distally (M) [33].

1.1.5 Treatment

Combination chemotherapy is the standard treatment for both limited and extensive stages of SCLC. Etoposide and cisplatin plus chest radiotherapy for patients with good performance status and limited-stage disease is the first line therapy. Good performance status is determined by using a scale for assessing cancer progression, its effects on the daily activities of the patient [34]. In general, this treatment approach for limited stage has complete initial treatment response rate of 80% or higher, increased median survival period, and increased 5-year cancer-free survival before tumour reestablishment. In contrast, patients with extensive stage disease show only 20% response rate and the median survival extends to 7-8 months with a the 5-year cancer-free survival of 2%. Surgical resection of early stage SCLC can extend the 5-year survival to 35–40%, if followed by chemotherapy, chest radiotherapy or both. These statistics highlight the need to improve treatment using novel strategies for early diagnosis and treatment [35-37].

1.2 Cancer Targeting

According to the "magic bullet theory" by Paul Ehrlich, drugs can be selectively targeted toward molecular targets specific to cancer cells [38]. The main advantage of the targeting approach is to enhance drug accumulation in the cancer tumour while limiting the unwanted

toxicity to healthy tissues. In general, there are two ways to target anticancer drugs to the desired site of action, which include passive and active targeting strategies. Passive targeting is achieving by utilizing enhanced permeability and retention (EPR) effect (**Figure 1.5**). This approach exploits the defective vascularisation of solid tumours which display increased permeability to particles in the nanometre range. This leads to enhanced penetration into the tumour mass and prolonged retention within the tumour due to inefficient penetration back into the vasculature or lymphatic drainage [39]. Active targeting of cancer tissue can be achieved by directing drug delivery platforms toward receptors in the tumour cells that are overexpressed on their surface. Optimal active targeting requires the presence of a highly specific tumour receptor that is not expressed of highly under-expressed in non-target (healthy) tissue. Any expression of target receptor in other tissues could result in off-target effects and significant toxicity. Furthermore, a stable expression of the target molecule is required to avoid down regulation of the receptor in cancer cells [40]. It is difficult to find the ideal target, however, there are many targeted cancer therapies developed to percent with great clinical potential. The targeted delivery of nanomaterials can overcome many difficulties encountered with free drugs, including insolubility, rapid clearance, degradation, lack of selectivity and nonspecific toxicity as well as reducing the drug dosage.

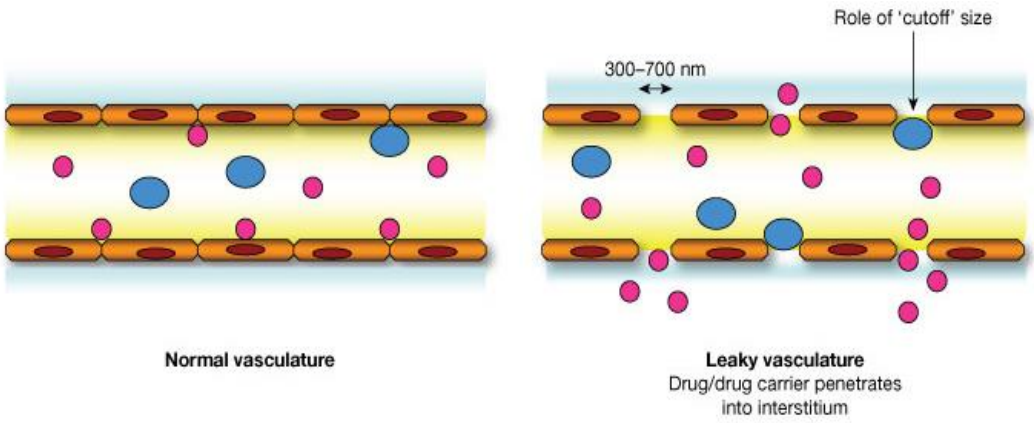

Figure 1.5: Schematic representation of the enhanced permeability and retention (EPR) effect. *Passive targeting is achieved by using EPR. Leaky tumour vascular with impaired lymphatic drainage, increase permeability to nanoparticulates. This image adapted from [41].*

1.2.1 GRP-R as a target in SCLC

Recognising GRP-R as a tumour target a number of groups have developed peptide ligands and antibodies targeting GRP and GRP-R. Cuttitta et al [42] showed in 1985 that an antibody raised against GRP could block GRP binding to its receptor and subsequently blocked clonal growth of SCLC cells in vitro and xenograft growth in vivo. This antibody (named 2A11) was later confirmed by Avis et al to bind to the peptide with high affinity and was taken forward into a number of pre-clinical [40] and later clinical trials, reaching Phase II [43].

In a complementary approach other labs have developed antagonistic peptides that bind the GRP-R, thus blocking ligand binding and autocrine growth stimulation. For example, one non-natural peptide sequence termed RC-3095 is a potent antagonist to the GRP-R receptor which decreased by 50–70% the tumour volume of xenografts in nude mice following subcutaneous administration for 5 weeks [44]. A third approach to the treatment of GRP-R

positive tumours involves the conjugation of a cytotoxic drug (doxorubicin) to a bombesin-derived peptide antagonist (RC-3094) which binds with high affinity to the GRP-R [45]. This approach, which has the benefit of smaller molecular weight and lower immunogenicity was also reported to inhibit growth of H69 SCLC xenografts in vitro and in vivo [155].

There are some synthetic antagonists are produced to bind with high affinity to GRP-R. A study used two GRP-R antagonistic peptides ([d-Cpa1-β-Leu8-des-Met9]litorin and [d-Phe6 , Leu13-CH2NH-Cpa14]bombesin(6–14)) showed inhibition in growth both in vitro and in vivo using GRP-R positive SCLC (SCLC 41M and SCLC 75) [46]. The first GRP-R antagonist used in the study was developed from litorin (pGlu-Gln-Trp-Ala-Val-Gly-His-Phe-Met-NH2), which is an amphibian Bombesin-like peptide. Another study showed that a number of GRP-R antagonist peptides caused inhibition in the growth of SCLC cell line (NCI-H345 cells) as well as in mice [47]. Llinares et al synthesised GRP-R antagonist (JMV594) (H-D-Phe-Gln-Trp-Ala-Val-Gly-His-Sta-NH2) by solution phase peptide synthesis. The peptide tested on rat pancreatic acini and Swiss 3T3 cells. The antagonist recognize the GRP-R receptor on pancreatic acini (binding 34 ± 14 nm) and antagonized GRP stimulated amylase secretion (IC50 = 190.0 ± 57 nm) and also able to recognize the GRP receptor in 3T3 cells (binding Ki 18.9 ± 8.1 nm) [48]. In another study, the selectivity of the JMV94 for GRP-R (IC50 = 2.2 ± 0.1 nm) was demonstrated over the NMB-R (IC50 = >10,000 nm) by using competitive cell binding assay on Balb/c 3T3 cells transfected with ether receptors [49]. Marsouvanidis et al developed the JMV594 peptide further by coupling the chelator DOTA (1,4,7,10 tetraazacyclododecane-1,4,7,10-tetraacetic acid) to the N-terminal end of the peptide by using $(\beta Ala)_2$ as linker and labelled it with ^{111}In. The ^{111}In-DOTA-$(\beta Ala)_2$-JMV594 showed internalized to some extent in PC-3 prostate cell line at37 °C. More than 60% of the radiopeptide remained intact

for 5 min after entering the bloodstream of healthy mice. The radiopeptide also showed high tumor uptake and rapid background clearance via the kidneys [50].

1.3 Liposomes as drug delivery platforms

1.3.1 Definition and background

Alec Bangham discovered closed bilayer structures [51], which were called liposomes later by Sessa [52]. Bangham discovered that when phospholipids are dispersed in water, they form a bilayer vesicle that he termed multilamellar smectic mesophases. Since then, liposomes have gained much interest and contributed to many areas such as pharmaceutics, cosmetics and food science such as in the treatment of cancer [53], anti-ageing creams [54] and flavour retention agent [55] respectively. At first, liposomes were used as a model membrane system in the area of biophysical research before moving to the pharmaceutical industry to be used as drug carriers after Gregoriadis' demonstration of their drug-carrying capacity [56].

Liposomes are self-assembled artificial colloidal spherical vesicles composed of one or more bilayers of amphiphilic molecules called phospholipids (**Figure 1.6**). Liposomes can transport hydrophilic or hydrophobic drugs, depending on the nature of the drug. Liposomes are classified according to their bilayer number into multilamellar vesicles (MLV) and unilamellar vesicles (ULV). ULV subclassified into large unilamellar vesicles (LUV) and small unilamellar vesicles (SUV). Liposomes range in size from tens of nanometres to tens of micrometres. Liposomes are commonly used as drug delivery carriers for a number of reasons. They are biocompatible, biodegradable and they have the capacity to encapsulate both hydrophilic and hydrophobic drugs.

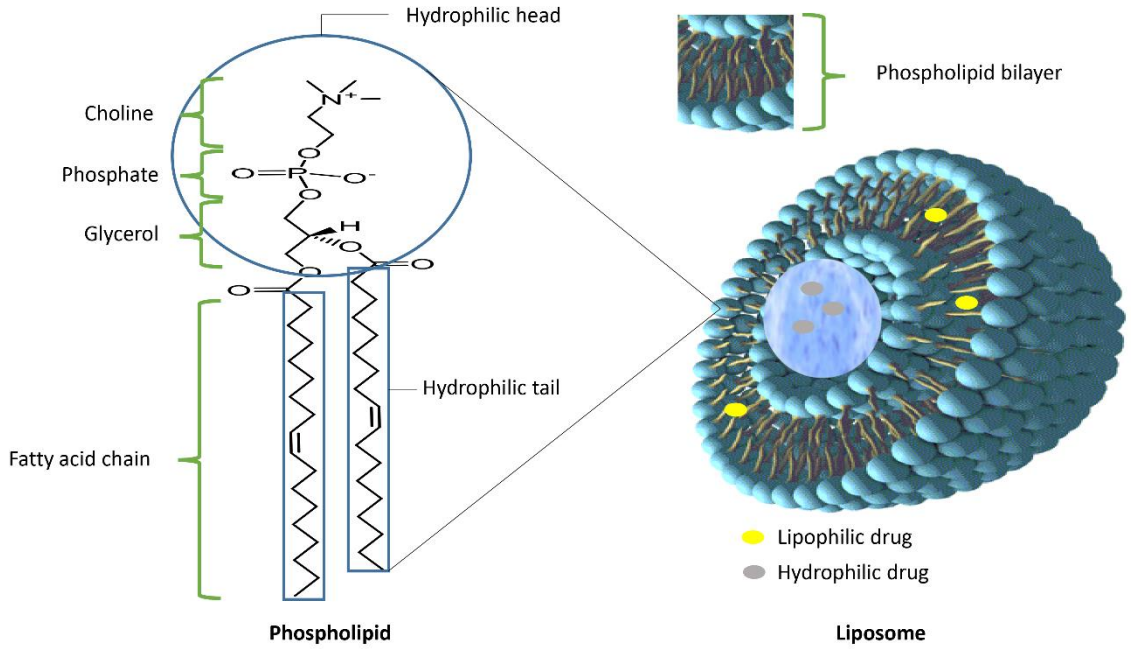

Figure 1.6: schematic representation for liposome and a component phospholipid. *Liposome vesicles consist from aqueous core, in which hydrophilic molecules can be encapsulated and phospholipid bilayer, in which lipophilic molecules can be encapsulated. The bilayer consists mainly from amphiphilic phospholipids. Phospholipids consist from hydrophilic head (phosphate group) and hydrophobic fatty acid chains joined together by a glycerol molecule. The phosphate molecule can be modified for instance by choline to form 1,2-dioleoyl-sn-glycero-3-phosphocholine (DOPC), which shown in the left of the figure. The liposome image modified from [57].*

1.3.2 Liposomes for targeting

Liposomes can be designed to target specific cell types. In cancer drug delivery, there are two types of targeting, which include passive and active targeting. This can be done by designing liposomes in a size range of 100 nm to 200 nm, which promote the accumulation in the target tumour site. Smaller liposomes in the size range of 20 nm are cleared by kidney glomerulus and larger liposomes (>200 nm) tend to be recognised and cleared by the

reticuloendothelial system (RES) [58]. For the active targeting, functionalization of the liposomal surface with antibodies, ligands and other biomolecules is used encourage selective liposomal interaction with the targeted cells. This can improve cellular drug accumulation by increasing the local concentration of drug in the vicinity of the target call and thus increase passive drug uptake into the cell. Alternatively, the liposome encapsulated drug can be delivered directly into the cell by internalisation / endocytosis. Liposomal composition and physical characteristics, such as size and surface charge, are crucial determinants to the liposome stability and application [59-61].

1.3.3 Liposome role in enhancing the pharmacology of the drug

Liposomes greatly improve the drug pharmacokinetics, pharmacodynamics and toxicity profile when compared to the free drug [62]. Non-targeted liposomal anticancer drug formulations of the appropriate size passively accumulate in tumour tissues by the EPR effect and this is associated with greater amounts of drug in tumour tissues compared to free drug. For example, Doxil®, a pegylated liposomal doxorubicin offers unique pharmacokinetic profile compared to free drug (**Figure 1.7**)

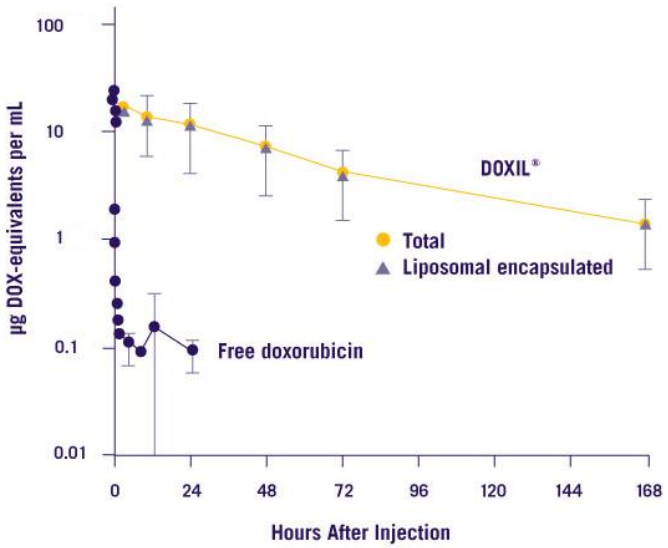

Figure 1.7: Plasma pharmacokinetics of free doxorubicin compared to liposomal doxorubicin (Doxil®). *Figure adapted from [63].*

The liposomal carrier (Doxil®) slowed the plasma clearance combared to the free drug from 45 L/h to 0.1 L/h in patients after IV dose of 25 mg/m^2 or 50 mg/m^2 of both free and liposomal drug. Doxil® also showed smaller volume of distribution combared to free drug (4 L versus 254 L respectively). The liposomal drug also enhanced the drug level in the tumer to > 4 folds [63]. Doxil is an example of a "stealth liposome" in which a hydrophilic PEG polymer shields the liposomal surface in such a way to reduce detection by the immune system and rapid clearance by the mononuclear phagocyte system (MPS) [64, 65].

1.3.4 Phospholipids – the building blocks of liposomes

Phospholipids are naturally occurring amphiphilic molecules that contribute to cellular membrane of prokaryotes and eukaryotes. The basic unit of a phospholipid (**Figure 1.6** above) comprises two fatty acids, a glycerol molecule and a phosphate group that it generally modified with a small organic molecule. The fatty acid tails impart a hydrophobic character

that is contrasted by the hydrophilic character if the glycerophosphate unit. Together these characteristics promote amphiphilic characteristics which allow self-assembly into complex structures such as bilayers, multilayers and vesicle like structures. The variation in these components, either naturally through biosynthesis or synthetically through hydrogenation, affords a wide range of phospholipids [66].

The chemical structures of phospholipids can be classified by the alcohol molecule (glycerophospholipids and sphingomyelins), head group (e.g. phosphatidylethanolamine (PE), phosphatidylserine (PS)), the length and the saturation of hydrophobic side chains; the type of bonding between the aliphatic moieties and alcohol backbone; and the number of aliphatic chains [66]. This variability in phospholipid structure is an important factor in designing the drug delivery system as it affects the assembly and physio-chemical properties of the system. In aqueous media, phospholipids can form many kinds of assemblies, such as spherical micelles, cylindrical micelles, liposomes, planar bilayers and inverted micelles, depending on the molecular shapes of the phospholipids. Bilayer preferring lipids, such as PC, are usually used to form liposomes via self-assembly. However, non-bilayer lipids, such as unsaturated PE, can be incorporated to certain extent in a bilayer structure, which is stabilized by bilayer preferring lipids [66].

1.3.4.1 Cholesterol

Another very important factor in the liposomal composition and design is the addition of cholesterol. Cholesterol is naturally occurring hydrophobic sterol with four hydrocarbon rings and a pendant branched aliphatic chain (**Figure 1.8**). The presence of the hydroxyl group (OH) gives it weak amphiphlic character which facilitates insertion into the lipid bilayers of eukaryotic cell membranes with its hydrophilic part oriented towards the aqueous medium, and the rigid hydrophobic ring structure toward the bilayer interior (**Figure 1.8**).

Cholesterol enhances bilayer stability and reduces aggregation by modulating the bilayer rigidity. Cholesterol also act as permeability buffer by controlling the fluidity of liposomal membrane. It changes the molecular packing and dynamics in the fluid crystalline and gel phases. Below the phase transition temperature (T_C) of lipids, cholesterol addition increases the fluidity of lipids, while above T_C the mobility and fluidity of the lipid chains are restricted, reducing the bilayer permeability and drug incorporation efficiency. The membrane elasticity found to be increased with an increase in cholesterol content. The maximum amount of cholesterol that has been reported and can be incorporated into liposome is widely assumed to be about 50 mole %. However, the optimal ratio between cholesterol and lipid is not understood. The most frequently used proportion is 2:1 ratio or 1:1 ratio lipids to cholesterol parts [67].

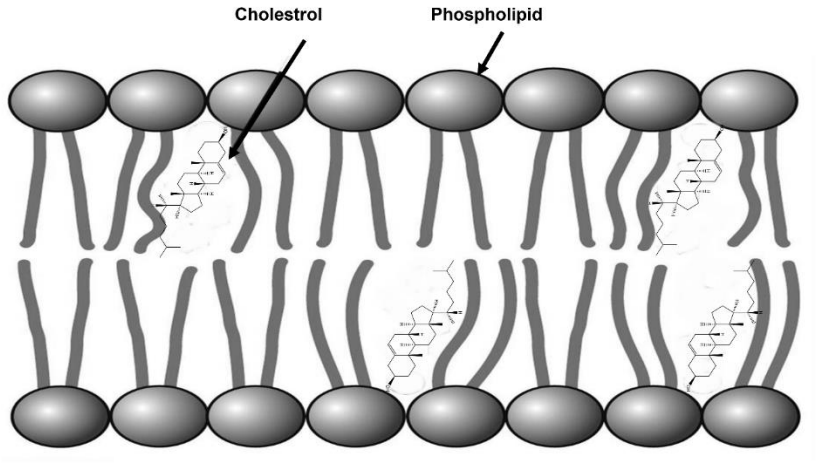

Figure 1.8: Schematic representation of cholesterol insertion into a phospholipid bilayer.

1.3.5 Liposome classification

Liposomes can be classified according to their size and lamellarity into multilamellar vesicles (MLVs, 0.1–20 μm), large unilamellar vesicles (LUVs, 0.1–1 μm) and small unilamellar vesicles (SUVs, 25–100 nm) [68]. The size and lamellarity of liposomes depends on their composition and their method of preparation. MLVs are more suitable for lipophilic drug encapsulation due to their increased lamellarity which provides a larger volume into which hydrophobic drugs can partition. On the other hand, LUVs and SUVs are more suitable for parenteral administration due to their homogenous size distribution. However, the smaller the size of the vesicles the lower the amount of encapsulation of hydrophilic drugs.

The traditional method of making MLVs is the thin film hydration technique. The lipidic components are dissolved in organic solvent (e.g. chloroform and methanol) followed by the removal of the organic solvents using a rotary evaporator to produce a thin lipid film. The addition of an aqueous phase above the phase transition temperature of the lipid mixture with shaking results in the formation of the MLVs [69].

Extrusion of MLVs through polycarbonate membrane filters was an important methodological development in SUV/LUV manufacture. This method allows the production of homogenous vesicles with improved trapping efficiency. Moreover, using a reverse phase evaporation method or ethanol-based proliposome technology, oligolamellar vesicles (0.1–1 μm) have been produced. The manual extrusion system with relatively low pressure is usually used for lab scale production. For large scale production, higher pressure systems were developed. The production of SUVs with diameters less than 50 nm is only possible

using sonication or homogenization. However, for a large scale production of SUVs in the 20 nm to 50 nm size range, microfluidic mixing techniques can be used [59].

Liposome can also be classified according to their compositions to four general classes of liposome for delivery of drugs. These include conventional liposomes, sterically-stabilized liposomes, ligand-targeted liposomes and stimuli-responsive liposomes. Traditionally, liposomes were formulated from phospholipids and cholesterol with neutral, cationic, or anionic phospholipids as well as cholesterol. Further developments led to the formulations of the other types of liposomes [61].

1.3.6 Factors affecting the efficacy of liposomal drug delivery systems

Factors such as lipid composition, size and surface charge are important in determining the properties of liposomes and their clearance route from the body. Liposomes can range in size from 10 nm to 5 μm. Adjustment of the size of the nanoparticles is crucial to take advantage of the EPR effect. *In vivo*, nanoparticles generally within the size range of 20 nm to 400 nm will diffuse through the gaps in the cancer vascular endothelium, which is not the case in normal tissue. The porous nature of the cancer vasculature varies in size depending on the cancer type, site, and the stage of the disease, but the upper size threshold is generally around 300 to 400 nm. In addition, nanoparticles must be larger than 10 nm to avoid kidney first pass elimination and smaller than 150 to 200 nm to avoid clearance by the liver and spleen [60].

Liposome opsonisation and clearance by the reticuloendothelial system (RES) is dependent on vesicle composition and size. RES is part of the immune system and their main function is to eliminate foreign materials from the blood. RES consists of cells such as blood monocytes and macrophages found mainly in liver, the lung and the spleen. Naked

phospholipid liposomes can be rapidly cleared by RES cells due to coating of liposomal surface with serum proteins called opsonins. Large liposomes (>200 nm in diameter) are rapidly opsonised and taken up by the RES. Opsonisation decreases with a reduction in liposome size. Small liposomes have a relatively larger surface area, and will have a lower density of opsonins on the membrane surface which results in lower uptake by the macrophages. Liposomes with a size of 70 to 200 nm will have a greater chance to escape from RES and remain in the circulation longer and then reach the target. Due to extravasation through the fenestrated capillary walls in the liver, the small liposomes (< 70 nm in diameter) show shorter circulation time and therefore reduced drug activity [70].

1.3.7 From conventional to targeted liposomes

Rapid clearance of naked phospholipid liposomes by RES typically limits their application to therapies such as immune-related medicine (e.g. liposomal hepatitis A vaccine). To address the problem, coating the liposome surface with inert, biocompatible polymers, such as PEG was suggested and adapted [71, 72]. Polymer flexibility is an important factor because it allows a relatively small number of grafted polymers to protect the liposomal surface. In addition, polymer coated liposome, such as pegylated liposome, provide stability to the colloidal liposomal system through steric repulsion and decreased aggregation. A recently discovered drawback of pegylated liposomes is their activation of the complement system. As a consequence of this, it can give hypersensitivity reactions and decrease circulation time due to clearance by RES [73].

With the development of Doxil an improvement of clinical parameters was observed [74]. The passive targeting of tumours via the EPR effect was inefficient due to drug release in sites other than the tumour. The formulation of targeted liposomes for cell-specific targeting

was proposed (**Figure 1.9**) as a means to delivery drug only to the tumour site. The major challenge is the identification of biological targets that are expressed exclusively or significantly over-expressed by cancer cells.

The targeting moiety could be antibody, peptide or carbohydrate-based. The used of the monoclonal antibodies as targeting moieties is one of the most effective methods for liposome targeting due to the exquisite specificity of antibody-antigen interactions. However, it has some disadvantages such as difficulty of production due to bulky nature, immunogenicity and poor pharmacokinetic profile. The use of peptides as targeting moieties is one of the good approaches because of its small size, ease of synthesis and modification such as attachment to pegylated lipids [61, 75].

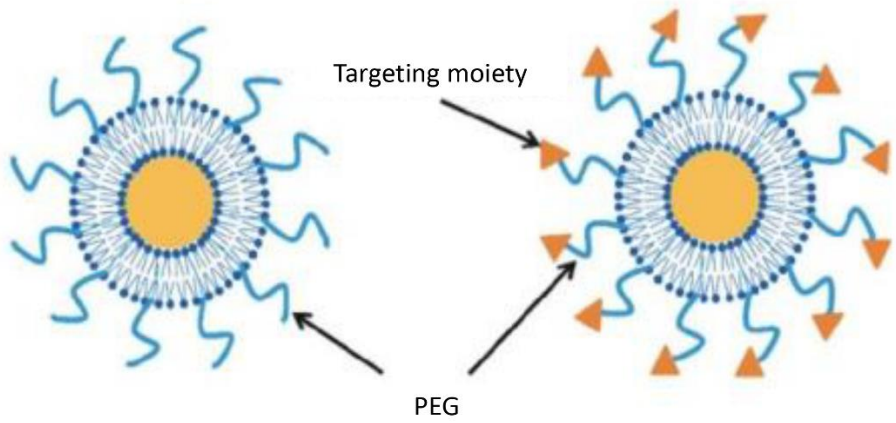

Figure 1.9: representation of the Pegylated and targeted liposomes. *On the left side, the liposome is coated with peg polymer and on the other side the liposomes features targeting moiety. The targeting moiety% can be controlled and the nature of the moiety can be varied such as using peptides or antibody. The image adapted from [76]*

Tethering of targeting peptides to pegylated lipids offers the advantages of simultaneous cell targeting while maintaining the steric stabilisation afforded by polymer grafting. Typically the peptide is presented on the surface of the liposome surface (via a spacer which separates the phospholipid head group) or at the terminal end of the polymer (e.g. PEG) chain. Further development of this approach evolved into the concept of stimuli-responsive liposomes. For example, pH-sensitive liposomes release their content in a pH-sensitive manner inside the target cells by incorporating pH-sensitive components. Following cellular internalisation of the intact liposome the endosomal pH decreases causing a conformational of chemical change in the liposomal system that destabilises the membrane and permits drug release into the endosomal lumen and subsequent diffusion into the cytoplasm [59-61, 70].

1.4 Liposomal delivery in SCLC

SCLC is a challenging disease in terms of both diagnosis and management/treatment. We hypothesised that a GRP-R targeted liposomal delivery system could be developed for enhanced delivery of cytotoxic drugs to the primary and metastatic tumours. Towards this aim it was necessary to confirm the expression of GRP-R in lung cancer cells and to develop a prototypical targeted liposome that bears an efficient targeting peptide for GRP-R. To achieve therapeutic efficacy, it was necessary to study stability in simple formulation buffers as well as physiological media such as serum. Such a delivery system could be delivered locally to the tumour site before and after surgical resection of the primary tumour in order to localise the delivery of drug to the tumour site. Alternatively, parenteral administration of such a system would rely on the efficient homing of the targeted liposomes to distal tumour sites.

Aims and objectives of this thesis:

- **To evaluate the GRP-R expression in SCLC cell line (H345) and NSCLC cell line (A549)**
- **To synthesise cystabn-targeted liposome toward SCLC cells**
- **Evaluate cell uptake by fluorescently labelled liposomes**

MATERIALS AND METHODS

Chapter 2

2.1 Introduction

This project aimed to develop a targeted liposomal formulation for the treatment of small cell lung cancer (SCLC). This chapter provides the general information of the source of materials used through the project, the sample preparation procedures and theoretical background and methodology development of the characterisation methods used. The GRP-R receptor targeting peptide (cystabn) was synthesised using Fmoc-SPPS before coupling to a commercially available pegylated lipid. The peptide and conjugate was characterised by HPLC, UV and MALDI-TOF MS. The cystabn-PEG-lipid conjugate was included in targeted at 1 mole % using the thin film hydration method and the liposomes characterized by DLS. The stability of targeted and control liposomes in buffer solution and biological media was also studied by DLS. Targeting of SCLC cells with cystabn peptide was examined using flow cytometry analysis of fluorescent liposomes which included 1 mole % DHPE-fluorescein.

2.2 Manual Fmoc solid phase peptide synthesis (SPPS)

The classical solution phase synthesis (SPS) of peptides has several disadvantages. These include the need to remove intermediates and reaction by-products at each step of peptide growth; the requirement to characterise the purified product at each step; and, poor solubility of some intermediate peptides in the synthesis solvent. The standard SPPS, introduced by Merrifield in 1963, is a convenient and efficient method for peptide production that utilises solid insoluble polymeric resin beads as a support covalently bonded with the growing peptide chain [77]. The peptide chain is constructed from the C' terminal end by the step-wise addition of amino acids that are alpha amino-protected by Fmoc group, as illustrated in (Figure 2.1). Orthogonal functional groups within the amino acid are typically protected by acid-sensitive protecting groups (e.g. Boc or trityl) in order to avoid their interference with the coupling of the required α amino and carboxylic acid groups to form a peptide bond [78]. Examples of amino acid side chains that are protected include the side-chain (ε) amine of lysine or the δ side chain carboxylic acid group of glutamic acid.

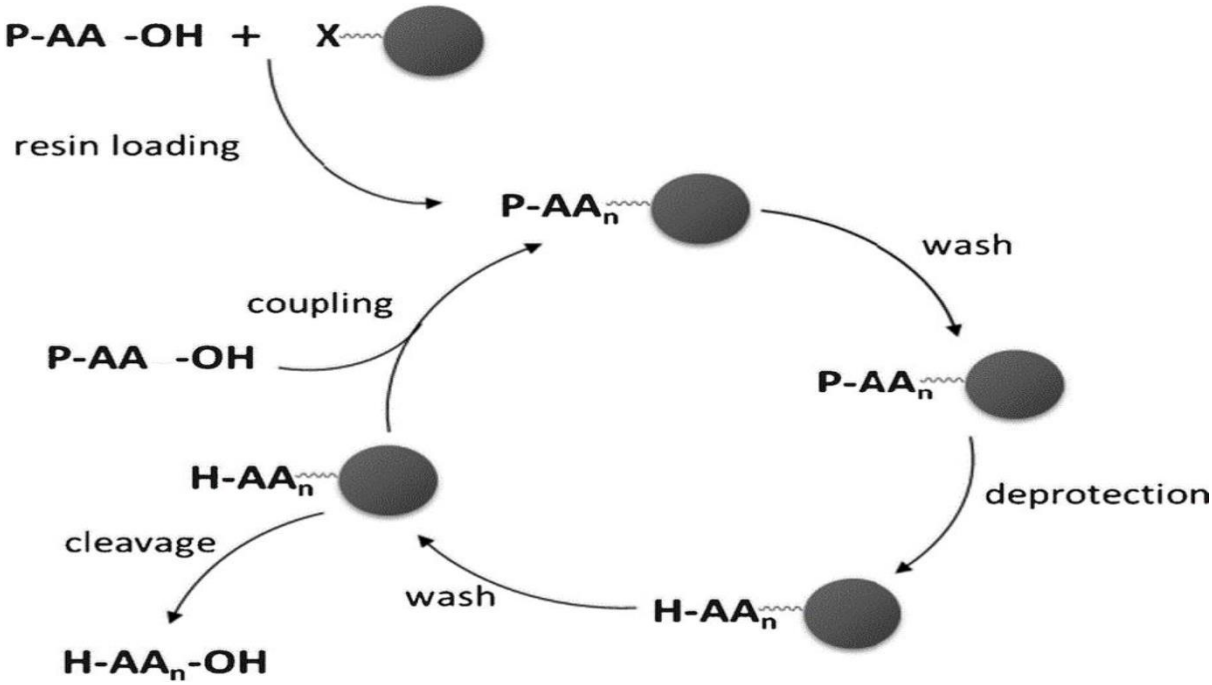

Figure 2.1: General solid phase peptide synthesis scheme, *where P-AA-OH represents a N^{α}-terminal and side-chain protected amino acid and H-AA-OH represents an unprotected amino acid. The first amino acid is loaded onto a solid support, the N-terminal protection group is removed and the subsequent amino acid is coupled. At the end of the synthesis the peptide is cleaved from the solid support and fully deprotected [79].*

The use of an insoluble, high porosity resin allows for high peptide loading and the removal of unreacted coupling reagents and by-products by simple filtration and washing. In addition, this method is highlighted by short coupling reaction time, simplicity of set-up and automation using robotic liquid handling. Other advantages include the flexibility of resin attachment chemistries. For example, cyclic peptide synthesis is achievable through by coupling the first amino acid to resin through a side chain carboxyl group. Limitations include a decrease in the peptide coupling efficiency with growing chain length and potential for aggregation. This results in reduced final purity and yield of the peptide [80].

2.2.1 Amino Acid Protecting Groups

Modern SPPS generally uses the Fmoc approach. This is an orthogonal approach in which, for example, a base-labile Fmoc group is used to protect the alpha carbon primary amine and an acid-sensitive protecting group is used to protect other side chain functional groups which could either interfere with peptide chain growth (e.g. the carboxylic acid in Asp or Glu) or when side chains are sensitive to modification by the synthesis conditions e.g. the oxidation of tryptophan residues. The Fmoc group is base sensitive and can be cleaved using mild conditions such as 20% piperidine or 5% piperazine after successful peptide coupling. There is an extensive range of orthogonal protecting groups for amino acid side chains which are generally acid-sensitive and are cleaved at the end of the synthesis. For example, the Boc protecting group is labile to treatment with TFA but is stable to base treatment during Fmoc removal. In addition to that, the resin linker, which covalently links the resin beads with the C-terminal amino acid, should typically be cleavable under the acidic deprotection conditions of the side chains protecting group. Therefore, the choice of the N^{α}-protecting group will define the choice of the side chains protection and the linker, thus it also define the name of the SPPS technique (Fmoc SPPS or Boc SPPS). Boc SPPS, initially introduced by Merrifield, require TFA to be removed from the alpha amino group and highly toxic hydrogen fluoride for the final peptide to be cleaved from the resin. However, Fmoc SPPS require milder and safer conditions [81].

Moreover, new resin derivatives have been developed, which allowed broader scope for chemical synthesis. For example, enhanced degree of polymer crosslinking promotes optimal stable swelling of the resin and increased loading. In addition to that, development of super-acid sensitive resin-peptide linkers allows the cleavage of peptides from the resin which retain all necessary side chain protecting groups. These cleaved products can be

further coupled or processed, before side chain deprotection at the end of the procedure. The choice of linker also provide the opportunity to determine the *C*-terminal functionality such as free carboxylic group (e.g. chlorotrityl resin) or amide group (e.g. Rink Amide resin) [80].

2.2.2 The SPPS synthetic cycle

The C-terminal N^{α}-protected amino acid is anchored to the insoluble resin by the addition of peptide coupling agents. After filtration to remove excess synthesis reagents and by-products only correctly coupled peptide remains on the resin. Prior to coupling of the next amino acid a deprotection step involving the removal of the base-labile N^{α}-protecting group is required. After washing to remove base, the next N^{α}-protected amino acid is linked to the resin-bound C terminal amino acid by coupling reagents. This cycle is repeated until the peptide chain completed (Figure 2.1). When designing the synthesis procedure of a natural linear peptide sequence it is imperative to use amino acid reagents with all necessary orthogonal side chain protecting groups to the allow selective coupling of the alpha amino and carboxylic acid groups. At the end of the synthesis these orthogonal protecting groups are cleaved from the washed and dried resin with a cocktail of trifluoroacetic acid (TFA) and scavenger molecules. These scavenger molecules prevent reattachment of orthogonal protecting groups and modification of deprotected side chains under the harsh cleavage conditions. The choice of scavenger cocktail depends on the primary sequence of the peptide. For example, the orthogonal protecting groups of methionine, cysteine histidine and tryptophan are easily removed but the deprotected side chains are labile in acid conditions. Some side chain protecting groups e.g. Mtr protecting group of arginine undergoes very slow acid-mediated cleavage and therefore requires scavengers to drive the deprotection reaction to completion. Finally, some protecting groups are extremely reactive once cleaved and therefore need to be sequestered by scavengers to prevent modification of the deprotected peptide [80].

2.2.3 Choice of coupling agents

The key step in peptide synthesis is amide bond formation by coupling between the N^{α}-protected carboxylic acid moiety and the amino group of the anchored peptide chain. The first coupling reaction forms a peptide bond between the resin amino group and the C-terminal amino acid of the peptide sequence. In this work, Rink Amide resin was used to liberate a C terminal amidated peptide after cleavage. Scheme 2.1 shows the reaction between the resin and the Fmoc-protected amino acid.

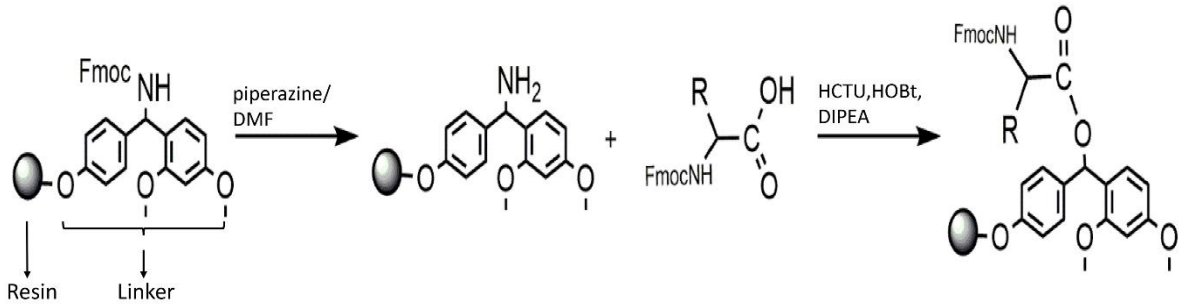

Scheme 2.1: the reaction between the Rink Amide resin and the Fmoc-protected amino acid.

The first step in this reaction is the activation of the carboxylic acid moiety of the N^{α}-protected amino acid followed by amide bond formation. These two steps can be ether performed consecutively or at once depending on the choice of the coupling reagent. Couplings are achieved via formation of an active ester of the Fmoc- amino acid followed by attack of the peptide chain's alpha amino group (Scheme 2.2). This can be done by reacting the amino acid with a coupling reagent to form a stable reactive intermediate. Secondly, the intermediate can be attacked by a nucleophile such as the amino group of a carboxy-protected amino acid.

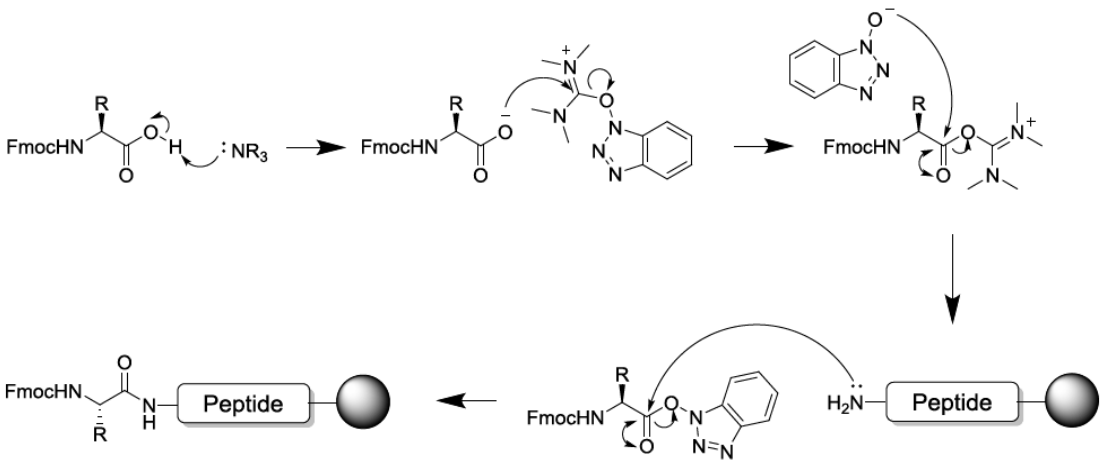

Scheme 2.2: reaction scheme of amino acid activation by nucleophile and coupling reaction. *The base deprotonates the carboxylic acid. The carboxylate anion then attacks the electron deficient carbon atom of HBTU. The resulting HOAt anion (1-Hydroxy-7-azabenzotriazole) reacts with the newly formed activated carboxylic acid derived intermediate to form an OAt- activated ester. The amine reacts with the OAt activated ester to form the amide.*

Many coupling agents are available for the formation of these active ester, including carbodiimides (DIC, EDCI), uronium salts (HBTU, HATU) and phosphonium salts (PyBOP, PyAOP). Each of these coupling agents has advantages and disadvantages including, for example, high coupling efficiency and low racemisation or, on the contrary, high cost and a propensity to propensity to favour racemisation of chiral amino acids. Aminium coupling reagents (e.g. HCTU) are among the most potent coupling reagents used in Fmoc SPPS method. They are commonly used as *in situ* activators in the presence of tertiary amine as a base (e.g. NMM, DIPEA). The base serve as proton extractor from the carboxylic acid moiety to facilitate the intermediate formation. However, this increase the rate of

racemization, which can be suppressed by the use of an auxiliary nucleophile (e.g. HOBt) as an additive (Scheme 2.2) [82].

In this work HCTU was used to maximise coupling efficiency while limiting high costs that are associated with the use of modern reagents such as PyBOP. The coupling reaction typically involves the use of a 4-8 fold excess of both coupling agents, base and amino acids in order to drive the reaction to completion. It is not uncommon, however, for the coupling reaction to be incomplete after a single coupling reaction step so a second reaction with fresh base, coupling agents and base is performed. This maximises the yield of intact peptide and avoids complex purification of multiple reaction products that include truncated peptide or those with missing residues. Following a second coupling step the resin is tested for reaction completion using a colourimetric Kaiser test.

2.2.4 The Kaiser test:

The Kaiser test is a convenient colourimetric test to detect the presence of free amines on the SPPS resin. It is used to qualitatively confirm successful completion of two key steps in the SPPS process. Firstly, successful Fmoc deprotection should reveal a free alpha amino group which gives a positive Kaiser result. i.e. reaction of the ninhydrin with primary amines generates an extended conjugated network which is blue and colours the resin beads. Successful peptide bond formation removes the free alpha amino group by coupling to the incoming Fmoc-protected AA. This results in a negative Kaiser test i.e. non-blue resin beads.

The test is performed by mixing a small sample of resin with two drops of Kaiser Reagent A (5% ninhydrin in ethanol (w/v)) and two drops of Kaiser Reagent B (80% phenol in ethanol (w/v) + KCN in pyridine as 2 mL 0.001 M KCN in 98-mL pyridine) in a

microcentrifuge tube and heating to 95 °C for 2 min. Extended heating will give a false positive result due to Fmoc removal by reaction with pyridine [83, 84].

2.3 Cystabn peptide characterization

Crude cystabn peptide was characterized in terms of its purity, molecular weight and concentration using HPLC, MALDI Tof MS and UV spectroscopy techniques respectively. The following section will discuss the theoretical principle and general methods used regarding these techniques.

2.3.1 HPLC

HPLC is the standard technique for the characterization of peptides and proteins. Advantages of this method include high reproducibility and ease of protocol optimisation. It relies on the loading of an analyte (peptide) onto a stationary phase (e.g. octadecyl silica, C18) column through which a pressurized liquid (mobile phase) is pumped. This allows the separation of compounds through interaction with the stationary phase. This interaction is slightly different for each component in the sample. As a result, the elution rate of the components will vary which leads to separation on the column stationary phase. The nature of the interaction can be hydrophobic, dipole–dipole and ionic, or a combination. There are three types of HPLC methods typically used in peptides separation. These include size-exclusion HPLC, ion-exchange HPLC and reversed phase (RP)-HPLC, which rely on differences in size, net charge and hydrophobicity respectively. Silica-based stationary phases are used most frequently because it offers good particle rigidity and stability, allowing the use of high mobile phase flow rates and efficient separation.

RP-HPLC is the standard method for peptide separations. It is preferred over other HPLC types because of its high resolution, speed, operation under wide range of conditions, reproducibility, durability of the stationary phase for long period of time and efficiency. However, it has the disadvantage of irreversible denaturation of some large peptide / protein samples, which leads to loss of biological activity. RP-HPLC involves the separation of molecules on according to their hydrophobicity. The separation is due to the hydrophobic binding of the solute molecule from the mobile phase to the modified packed stationary phase particles. The elution from the column occur by a gradient or isocratic conditions of aqueous and organic mobile phases. Therefore, solute elution can be manipulated by changing hydrophobic interactions. This can be achieved through changing the column temperature, the use of TFA or any ion-pairing modifier, or the composition of the aqueous and organic mobile phase. RP-HPLC can be used for analytical purposes (i.e. checking peptide purity) or for recovery and purification of peptides from synthesis reaction mixtures. This choice of analytical or preparative method will generally require the same mobile and stationary phase conditions but an increase in the size of the stationary phase column and an increase of flow rate to achieve efficient separation and recovery of peptide [85].

2.3.2 MALDI ToF MS

After the introduction of soft ionization methods, mass spectrometry has become feasible tool for biomolecules analysis. The two major techniques are electrospray ionization and matrix assisted laser desorption ionization (MALDI). When these techniques combined with time-of-flight (TOF) mass spectrometry, it produce affordable efficient methods for analysis of biological and organic molecules in laboratories. MALDI was introduced in 1988 by Karas and Hillenkamp as a revolutionary method for analysing the fragile biomolecules [86]. MALDI MS preferred over ESI MS because it usually generates monocharged ions which

make it easy to interpret, while the later tend to produce multiply charged ions especially with large molecules which requires data deconvolution downstream from sample acquisition. However, MALDI MS can be problematic for small molecules analysis as it produces considerable background in the m/z range less than 800, which is attributed to ionization of the matrix.

In principle, MALDI MS proceeds by firstly dissolving the non-volatile analyte with a large excess of small organic molecules called matrix in a volatile solvent. This helps to prevent aggregation of the analyte, which can prevent efficient desorption. Co-crystallization of a few microliters of the mixed sample performed on a metal plate by allowing the solvent to evaporate. The plate placed in the MALDI MS instrument under high vacuum. The sample then irradiated with a pulsed laser beam (usually 337 nm). This allow the matrix molecule to absorb most of the laser energy in the UV region in the form of heat. The analyte molecule is preserved intact due to the large excess of matrix. This absorption of energy causes analyte sublimation and expansion into a dense gas cloud. The gaseous molecules of the matrix along with the adsorbed analyte molecules travels rapidly toward the detector under high vacuum. The MALDI MS can be equipped with a Time of Flight (ToF) analyser, which feature more rapid analysis with high resolution and sensitivity [87].

2.3.3 UV Spectrophotometric determination of peptide concentration:

The lyophilized peptide usually contain non-peptide molecules such as water, salts, absorbed solvents, and counter ions. An accurate peptide concentration can be determined by quantitative amino acid analysis or UV spectrophotometry. If the peptide primary sequence contains a strong chromophore (e.g. tryptophan, tyrosine) the peptide concentration can be

determined conveniently using the extinction coefficient of these residues using the following equation:

$$[\text{peptide}],\text{mg/mL} = \left(\frac{A_{280nm}.M_w}{(5560.\#Trp)+(1200.\#Tyr)} \right)$$

Equation 2.1: for peptide concentration calculation. *Where A280 = the absorbance of the solution at 280 nm in a 1-cm cell, M_W = molecular weight of the peptide, #Trp = number of tryptophan residues in the sequence and #Tyr = number of tyrosines in the sequence. The extinction coefficients of chromophoric residues at 280 nm at neutral pH using a 1-cm cell are 5560 AU/mmole/ml for tryptophan and 1200 AU/mmole/ml for tyrosine [88, 89].*

2.4 Conjugate Synthesis

The targeting peptide (cystabn) was conjugated to one of the lipids components (DSPE-PEG_{2000}-Maleimide) for targeting the liposomes to SCLC cells. The use of a spacer PEG between lipid and peptide is crucial to allow steric stabilisation of the liposomes and to efficiently present the peptide to cell surface receptors.

A great number of attachment chemistries exist for the conjugation of targeting peptides to pegylated–lipids. These include conjugation by thiol–maleimide, or strain-promoted (copper-free) azide–alkyne ‘click’ chemistry. Alternatively, it is possible to couple the lipid to the peptide N’ terminus at the end of the SPPS procedure using an amine reactive N-hydroxysuccinimide ester [90-92].

Conjugating the peptide and PEG-lipid components during the SPPS phase has some disadvantages. These include potentially low yield, especially with long PEG chain and its poor suitability for cyclic peptides. The other peptide conjugation methods are dependent on

the choice of functional groups for both peptide residues and PEG, which match the chosen conjugation chemistry. One of the most commonly used methods is the thiol-maleimide conjugation (scheme 2.3). In this method, the peptide chain must feature thiol functional group typically by adding a cysteine residue at the N-terminal end, which then reacts with the maleimide moiety on a functionalized PEG-lipid after peptide cleavage and purification. The thiol-maleimide Michael addition reaction is very reactive due to selectivity of the thiol-maleimide reaction in aqueous and organic media when performed at pH 6.5 -7.5 [93, 94].

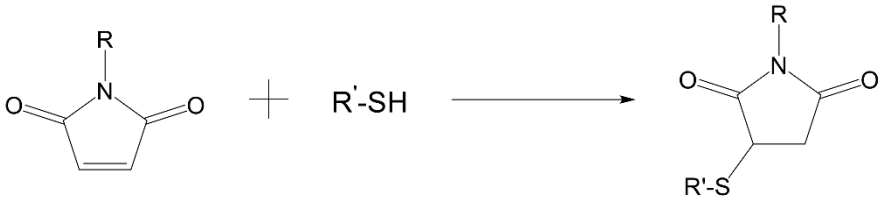

Scheme 2.3: Schematic of the synthesis of thiol-maleimide reaction.

In addition to that, it is rapid reaction with formation of stable product. The high reactivity of the carbon-carbon double bond in maleimide is due to the bond angle distortion and the ring strain [95-97].

2.5 Liposomes preparation

In this study, targeting and control liposomes synthesized by thin film hydration method followed by freeze-thawing and extrusion to produce monodispersed unilamellar vesicles. A major aspect in liposome medical application is the efficient loading of drug needed to achieve therapeutic effect. Liposomes allow encapsulation of both hydrophilic and lipophilic molecules in the hydrophilic core and lipid bilayer respectively. Encapsulation process can be passive (i.e. during liposomes preparation) or active (i.e. after liposomes preparation).

The passive strategy depends on factors including the composition of the formulation, zeta potential, particle size and preparation method. Active loading of compounds into the liposome core *via* ion/pH gradients enables high concentrations of reagents to be stored within vesicles. Many weak acids and bases, such as doxorubicin, can be actively loaded with high efficiency up to concentrations of 130 mM [59, 61].

2.5.1 Thin film hydration

There are several factor affecting the choice of the liposomes preparation method. These include the physicochemical characteristics of the liposomal formulation and the encapsulated material, the dispersion medium; optimum size, polydispersity and shelf-life of the vesicles for the intended application. There are three broad types of liposomes preparation methods including mechanical dispersion, solvent dispersion and detergent removal method [59].

One of the simplest procedure for the liposome formation is the thin film hydration method, although it is often limited by low encapsulation efficiency. The liposomes are prepared, in this method, by mixing and dissolving in a round bottomed flask the individual lipid components of the liposomal formulation in an organic solvent. The non-polar organic solvents used typically include chloroform or a mixture of chloroform and methanol for the more polar lipid derivatives such as pegylated lipids. The organic solvent is then removed by evaporation under vacuum, to produce a thin layer of lipids in the bottom of the flask. Traces of organic solvents which may interfere with liposome assembly are removed under high vacuum. The lipid film is hydrated using aqueous buffer which contains the cargo molecule of choice. Upon agitation, the lipids swell and hydrate to form a heterogeneous suspension of MLVs. A less polydisperse vesicle dispersion can be generated by a freeze-

thawing technique which involves repeated cycles of rapid freezing in a dry ice-acetone bath then rapid thawing at a temperature exceeding the gel-liquid crystalline phase transition. The production of refined monodispersed unilamellar liposomes requires energetic input by extrusion through membrane filters of defined diameters (e.g. 400, 200, 100 nm) or through sonication at high frequency (Figure 2.2) [98-100].

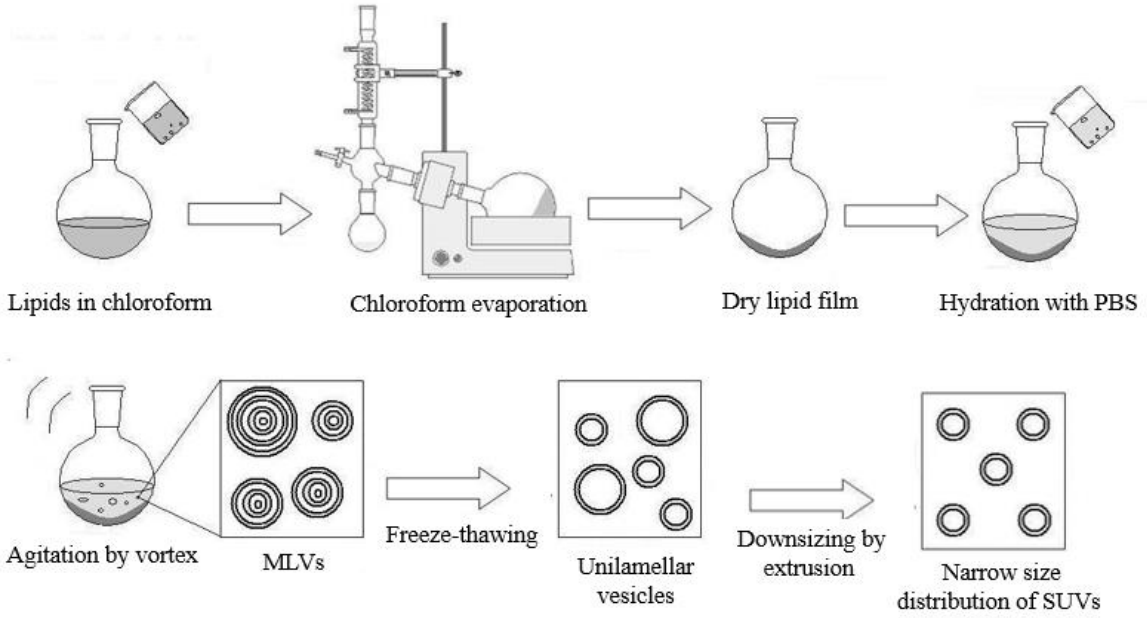

Figure 2.2: Schematic representation of liposome synthesis by thin film hydration method followed by freeze-thawing and extrusion techniques. *Adapted from [101].*

Liposome downsizing can be achieved by sonication or extrusion. Sonication is a commonly used method for the preparation of unilamellar vesicles (ULV). In this method, MLV break up into smaller vesicles by sonic energy. The size of the vesicles depends on the time of sonication as well as other factors such as lipid composition, concentration, temperature, and sonication power. This method is easier to perform in a shorter time compared to extrusion. However, issues with poor batch-to-batch size reproducibility are not uncommon. The other widely used method for ULV preparation is extrusion. It is achieved by forcing the lipid

suspension through a polycarbonate membrane with a well-defined pore size to produce vesicles with a characteristic diameter near the pore size of the membrane used in preparing them. The advantages of this method are good batch-to-batch reproducibility and no requirement to eliminate organic solvents or detergents removal from the final preparations. The exact mechanism of vesicle formation during extrusion is incompletely understood. However, it is clear that MUVs deform into the filter pore due to the applied pressure. This leads to transient rupture and resealing of the vesicles, which contribute to their downsizing during extrusion. A common practice is to apply multiple cycles of freeze thawing onto the suspension prior extrusion. This will lead to an easier and smoother extrusion due to the decrease in lamellarity caused by this method. All downsizing methods must be performed above the lipids' gel-fluid transition temperature to produce the desired size distribution. This is because the lipids fluidity decrease under this temperature [102-105].

2.6 Liposomes Characterization

In order to evaluate the liposome synthesis quality and to ensure reproducibility, various parameters can be measured. The most important parameters are the size and surface charge of liposomes. They give information about the physical stability of the product. In this study, each liposomal formulation was characterized by Zetasizer Nano Zs, for its size using dynamic light scattering (DLS) and its zeta potential using electrophoretic light scattering (ELS).

2.6.1 Size analysis by DLS

There are two important parameters to evaluate physical stability of liposomes intended for therapeutic use. These are the size and surface charge. Several techniques are available for

assessing the average size of liposomes and its disruption which include microscopy techniques, size-exclusion chromatography (SEC), field-flow fractionation and static or dynamic light scattering. One of the most commonly used method is DLS, also called photon correlation spectroscopy (PCS) [106, 107]. DLS measures the dynamic size disruption of particles suspended in liquid indirectly from their diffusion coefficient (D) using Stokes-Einstein equation (Equation 2.2).

$$D = \frac{k_B\, T}{6\pi\eta \mathrm{R}_h}$$

Equation 2.2: The Stokes-Einstein equation, *where (R_h) is the radius of the suspended sphere that have the same diffusion coefficient (D) as the particle, (T) is the absolute temperature of the suspension, (η) is the viscosity of the liquid and (k_B) is Boltzmann's constant ($1.38x10^{-23}$ J/K).*

As shown in the Figure 2.3, DLS works by radiating a beam of laser light onto particles suspended in liquid, which result in the scattering of the light in all directions as it interact with the particles. The scattered light detected by a detector, which is positioned classically at angle of 90° or at the backscatter angel of 173°. The detected scattered light produce a speckle pattern at the detector surface due to interference of light waves. The particles are in continuous motion due to their interaction with the molecule of liquid dispersant. This motion, which is called the Brownian motion, produce a fluctuation in the intensity of the detected light and the speckle pattern moves accordingly. The rates of that fluctuation in the light intensities caused by the apparently moving pattern are detected by the detector and converted into dynamic size distribution by using computer algorithms.

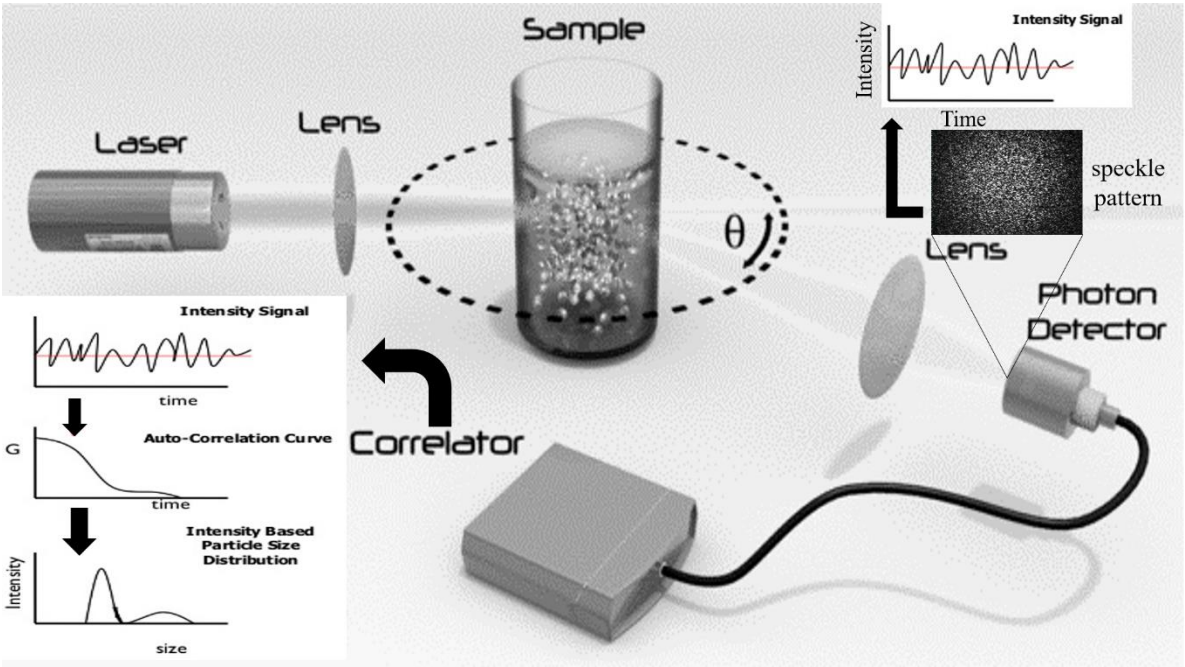

Figure 2.3: Schematic representation of DLS instrument. *A laser (e.g. He-Ne laser 633nm) radiated into the suspended particles in the sample and the light scattered and detected at an angle (e.g. 173°). The correlator uses algorithms to produce the autocorrelation curve from the intensity signals and based on that the particle size distribution produced using Stokes-Einstein equation. Image adapted from [108].*

In a DLS instrument, a digital correlator, calculates the autocorrelation function for the detected photons and plot intensities against time. This fluctuation of intensities with time is random due to the random Brownian motion of the suspended particles. For a relatively large particles or high viscosity medium, the motion (diffusion) of the particle will be slow and lead to slow fluctuation in intensities as function of time and vice versa. Subsequently the diffusion coefficient can be calculated from the correlation function using Equation 2.3.

$$\Gamma = qD$$

Equation 2.3: diffusion coefficient equation. *Γ is the exponential decay rate and q is the modulus of the scattering vector (defined by the scattering angle and wavelength of light). Finally, the hydrodynamic radius can be calculated using the Stokes-Einstein equation.*

DLS method have several advantages including the ability to make measurements in the native sample environment, simplicity of operation, sample easily prepared with low volumes. In addition, it covers the size range from few nanometres to few micrometres range. However, the technique does not yield particle shape information because it gives the diameter of sphere that diffuses the same way as the particle regardless of the particle shape. It also can yield a bias towards reporting larger diameters when small quantities of aggregates or impurities are present in the sample. This is because, the presence of the larger particles will dominate the light scattering signal and mask the presence of the smaller particles because scattering intensity is proportional to the sixth power of the particle diameter [109, 110].

2.6.2 Zeta potential:

One of the most important factors for any colloidal system is the surface charge. Most colloidal dispersions in aqueous media carry an electric charge. The charge between similarly charged particles lead to repulsion between these particles. This repulsion gives stability for the suspended particles in an aqueous media. The surface charge is produced by several factors. Firstly, ionization of surface moieties could lead to negative, positive or zwitterionic charges. Furthermore, the charge could be generated from the adsorption of charged species on the particle surface leading to negatively or positively charged surface

depending on the surfactant nature. The overall charge around the particle surface in a particular medium can be calculated indirectly by zeta potential. This physical property is the potential difference between the medium and the charged layer surrounding the particles (Figure 2.4).

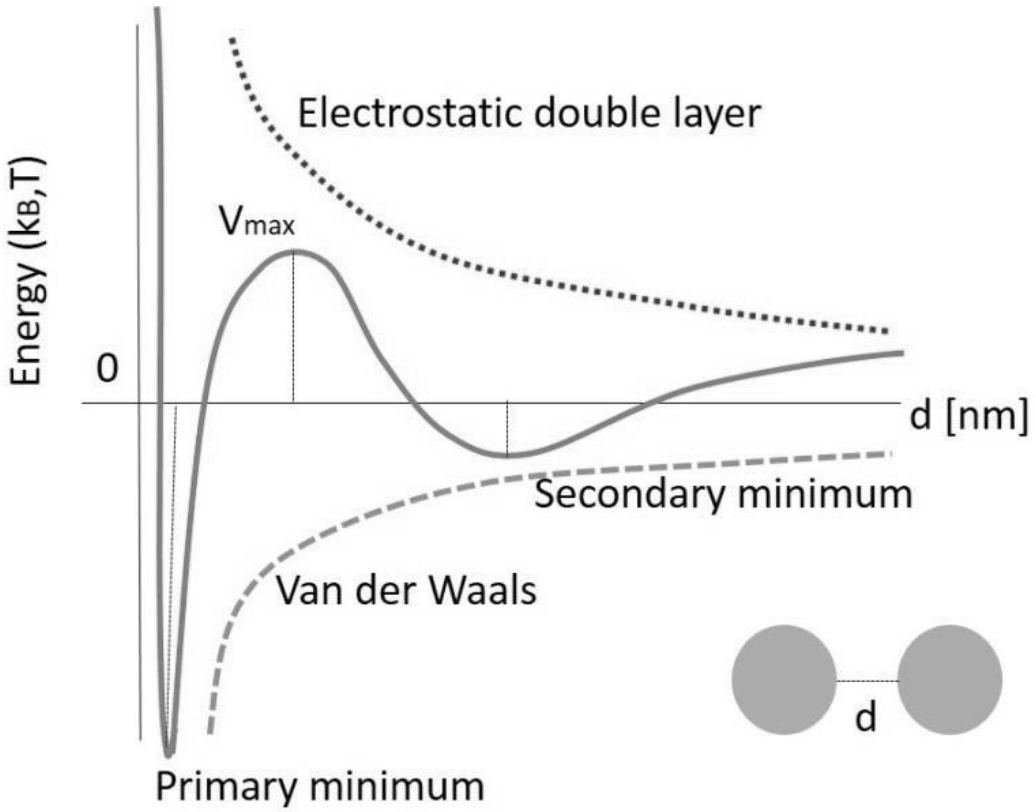

Figure 2.4: DLVO energy graph. *Van der Waals (dashed line) and electrostatic double layer (dotted line) contribute to total DLVO forces represented versus the separation distance between two spheres (d).*

This charged layer is from the attracted molecules from the dispersion medium. Zeta potential are commonly used to predict the stability of colloidal systems. If all the particles in suspension have a large negative or positive zeta potential, then they will tend to repel each other and there will be reduced tendency to aggregation. However, if the particles have

low zeta potential values then there will be not enough force to prevent the particles from aggregating.

The zeta potential of a colloidal system is measured by applying an electric field in a process called electrophoresis. The particle charge dictates the direction and velocity of its motion caused by the electric field. It is also affected by the surrounding medium and the strength of the electric field. In Zetasizer instruments (Figure 2.5), a laser beam is irradiated through optical set up, which split the beam into two beams: the scattering beam which passes through the suspension and a reference beam which passes around the sample cell. The two beams cross each other and create fluctuations in intensity due to particles' motion and create a speckle pattern. This is termed laser Doppler electrophoresis.

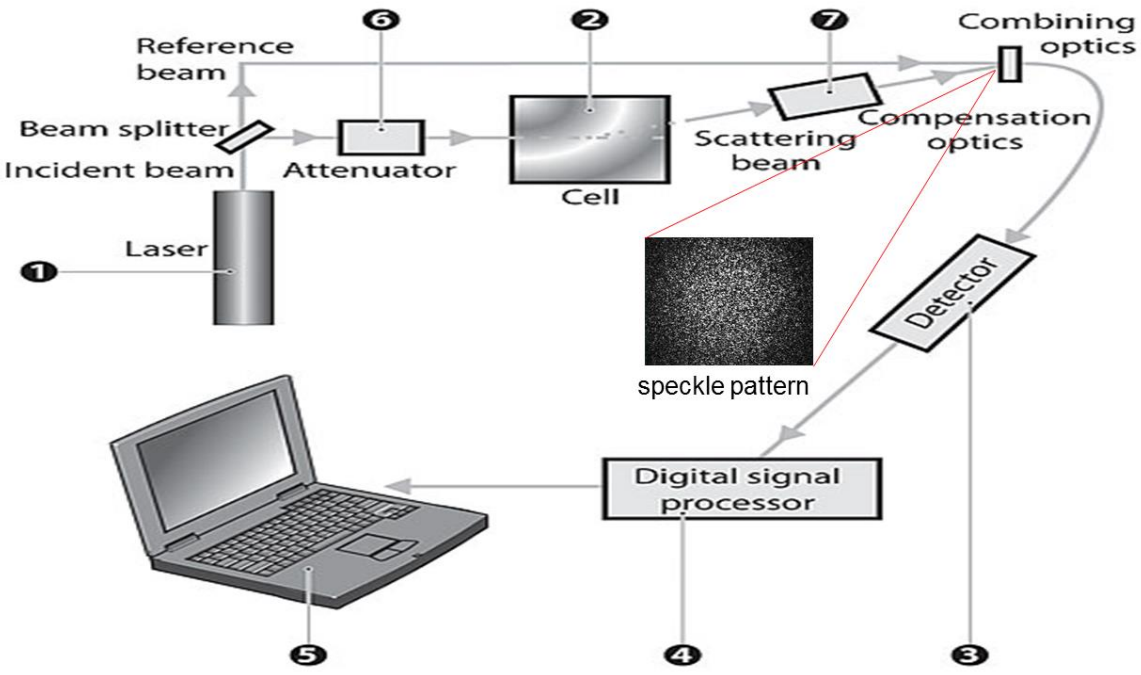

Figure 2.5: Optical configuration of the Zetasizer Nano series for zeta potential measurements.

This frequency of the modulated beam can be used to measure the particle mobility by comparing it with frequency of the reference beam. In conclusion, the laser Doppler electrophoresis method is used to measure the frequency shift. This shift is due to the movement of particles produced by application of electric field. Equation 4 is used to calculate the shift:

$$\Delta f = 2v \sin(\frac{\theta}{2})/\lambda$$

Equation 2.4: frequency shift equation. Δf *is the frequency shift, v is the particle velocity,* λ *the laser wavelength and* θ *the scattering angle.*

In Zetasizer Nano ZS, a new variation of this technique is used. This technique is called phase analysis light scattering (PALS). Instead of measuring the change in frequency of the modulated beam in comparison to reference beam, the phase difference is measured. Basically, it is a measure of the change in phase of the modulated beam relative to a reference beam. The phase is a measure of frequency x time. So, the rate of phase shift between the two signals is measured. From which, the mean phase shift is calculated and then the mean zeta potential is calculated [109, 111-116].

2.7 Cell lines

2.7.1 H345 cell line

The NCI-H345 cell line is a human epithelial lung cells line derived from bone marrow metastasis of small cell lung cancer. The cells were derived from 64 years old Caucasian male in 1981 by D. Carney, A.F. Gazdar. This cell line grow in vitro as multicell aggregates in a gland-like clusters in suspension. The viability of the cells in clusters is better than the viability of the single cells in the cultures. These cells found to be producing gastrin releasing peptide (GRP) as well as expressing its receptor [117].

2.7.2 A549 cell line

A549 cells are adenocarcinoma human alveolar basal epithelial cells. These cells established in 1972 from a 58-year-old caucasian male [118] from which, a malignant lung tumour was removed and cultured. These cells grow *in vitro* as adherent monolayer cells. A549 cells have the ability to synthesize lecithin with high level of unsaturated fatty acids [119]. The cell line are widely used as an in vitro model for a type II pulmonary epithelial cell model for drug metabolism and as a transfection host [120]. The A549 cell line has previsously been classified as a NSCLC model [121].

2.8 MTS cell assay

The MTS assay is a cell proliferation colorimetric assay. It reports cellular viability by measuring the absorbance of a coloured formazan product produced in the mitochondria.

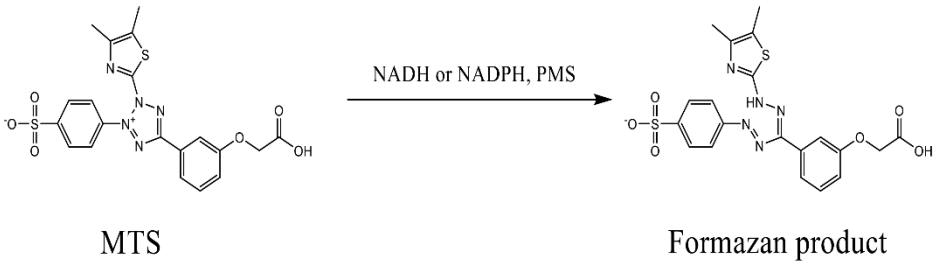

Figure 2.6: MTS reduction scheme by reductases in the mitochondria of live cells.

The MTS reagent is reduced by NADH or NADPH to a water soluble product in the presence of phenazine methosulfate (PMS) as electron coupling agent (Figure 2.6). The NADH/NADPH cofactors are produced by dehydrogenase enzymes in the metabolic pathways of viable cells. This characteristic can be used for sensitive quantification of viable cells. The coloured product produced by viable cells can be quantified by measuring the absorbance at 490-500 nm. The assay can be used for the measurement of cell proliferation in response to growth factors, cytokines, mitogens, and nutrients, etc. It can also be used for the analysis of cytotoxic compounds like anticancer drugs and many other toxic agents and pharmaceutical compounds. MTS assay is performed by adding the MTS/PES reagent mixture directly into the cell culture media of 96-well microtiter plate. Incubation at 37 ºC and absorbance reading without the washing or solubilisation steps involved in the MTT assay [122-124].

2.9 Flow cytometry

Flow cytometer is a technique designed to allow counting and detection of specific cells and their elements in a mixture of cells suspension such as blood. This is achieved by the carefully coordinated components of the flow cytometer including fluidics, optical, and electronic systems (**Figure 2.7**). The fluidics system of the instrument is the key component. Because at this stage the cells are injected into the sheath fluid stream and hydrodynamically focused into a single file at the centre of the stream. Each cell in the stream exited by a light source, typically a laser beam, at a certain point called interrogation point. This lead to light scattering as well as fluorescence. The scattered light in the forward direction is detected by the forward scatter channel. This scattering intensity depends on the refractive index and membrane permeability of the cell membrane as well as the cell size. The light scattered at 90° detected by the side scattering channel. The intensity of this light is proportional to the extent of the cytosolic structures in the cell. The study of both forward and side scattering allow the differentiation between different cell types by size and internal complexity. If cells were also labelled with fluorochrome-linked antibodies the cell associated fluorescence travels through the optic system to be filtered and detected with the detector with appropriate fluorescence emission settings. The florescent intensity is proportional to the number of fluorochrome molecules in each cell. Flow cytometers are equipped with more than one florescence detector in addition to the forward and side scattering detectors, which allow cells to be labelled with more than one fluorochrome[125-127].

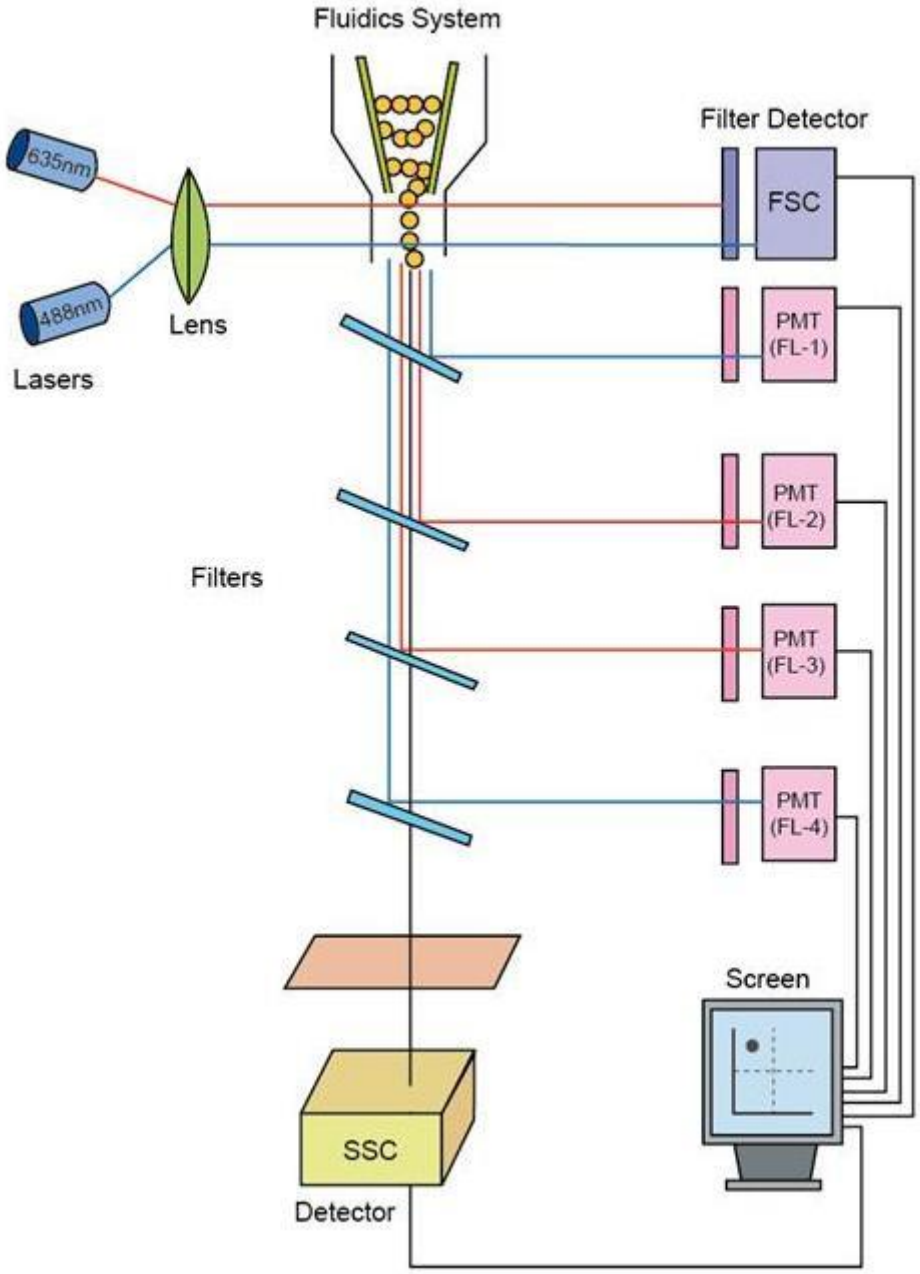

Figure 2.7: schematic representation of a flow cytometer instrumentation setup. *There are two detectors for the scattered light: forward scatter detector and side scatter detector. There are also a number of photomultiplier tubes (PMT) to detect florescence (e.g. FL-1 to FL-4). Image adapted from [128].*

SYNTHESIS OF GRP-R TARGETED LIPOSOMES

Chapter 3

3.1 Introduction

To date there are no clinically approved liposomal formulations that include an active targeting motif for tumour cells [61]. In recent years, however, two antibody-drug conjugates (ADCs) - Kadcyla® (Trastuzumab (Herceptin) targeting HER2+ breast cancer) and Adcetris® (Brentuximab targeting CD30+ Hodgkin's lymphoma)- have been approved which specifically target tumour cells to deliver the potent tubulin inhibitors, vedotin and emtansine, respectively [129, 130]. As is the case for ADCs, active targeting of liposomes has the potential of directing the therapeutic system toward specific diseased target cells. The passive targeting method, even though it offers enhanced therapeutic profile via decreasing toxicity and enhance drug biodistribution by EPR effect and pegylation, it is limited by the variability in the degree of tumour vascularization and porosity of tumour vessels [131, 132]. The active targeting method offers the potential for superior therapeutic index by increasing the targeting and accumulation of the delivery system in the target tumour tissue [133, 134]. The attached targeting motif on the surface of the nanoparticle should bind to its cognate binding partner (e.g. protein, receptor) on the target cell and preferably be internalised into the cell, from where the drug may be liberated into the cytoplasm. Ideally, the target "receptor" should be specific to the target and overexpressed on its surface and trigger endocytosis upon ligand binding [135]. [136-140]. [139, 141].

In this chapter, the GRP receptor was targeted on SCLC cells using a peptide antagonist. The targeting peptide would be presented on the liposomal surface and would afford intracellular delivery of cargo molecules into the target cells.

The aims of this chapter were to:

1) **Confirmation of GRP-R expression in NCI-H345 SCLC and A549 adenocarcinoma cells**
2) **Synthesis and characterisation of the targeting cystabn peptide and preparation of a cystabn-DSPE-PEG2000 conjugate**
3) **Preparation of control (untargeted) and cystabn-targeted liposomal formulations**
4) **Assessment of liposomal stability in different aqueous media**

3.2 Materials & methods

3.2.1 Materials

All materials were of analytical grade and sourced from either Sigma or Fisher unless stated otherwise.

Table 3.1: Antibodies for GRP-R expression

Product	Supplier	Catalogue No.
Rabbit polyclonal antibody to human GRPR (GRPR antibody [N2C3])	GeneTex	GTX113209
Donkey anti-Rabbit IgG (H+L) Secondary Antibody, Alexa Fluor® 488 conjugate	ThermoFisher Scientific	A-21206

Table 3.2: Materials for Cystabn synthesis

Product	**Supplier**	**Catalogue No.**
Rink Amide resin (100-200 mesh)	Merck Millipore	855001
(Fmoc-L-Val-OH)	AGTC Bioproducts Ltd	AGM20
(Fmoc-L-Trp(Boc)-OH)	AGTC Bioproducts Ltd	AGM18
(Fmoc-L-Leu-OH)	AGTC Bioproducts Ltd	AGM11
(Fmoc-L-His(Trt)-OH)	AGTC Bioproducts Ltd	AGM09
(Fmoc-L-Gln(Trt)-OH)	AGTC Bioproducts Ltd	AGM06
(Fmoc-L-Cys(Trt)-OH)	AGTC Bioproducts Ltd	AGM05
(Fmoc-L-Ala-OH*H2O)	AGTC Bioproducts Ltd	AGM01
(Fmoc-Gly-OH)	AGTC Bioproducts Ltd	AGM08
(Fmoc-D-Phe-OH)	AGTC Bioproducts Ltd	AG-140-139-1170
Fmoc-(3S,4S)Sta-OH	Iris Biotech	FAA1630
HCTU	AGTC Bioproducts Ltd	AG330645
HOBt. H2O	AGTC Bioproducts Ltd	AG123333
DIPEA For Peptide Synthesis	AGTC Bioproducts Ltd	AG-BC7012
Dichloromethane (DCM)	Sigma-Aldrich®	24233
Triisopropylsilane (TIPS)	Sigma-Aldrich®	233781
Trifluoroacetic acid (TFA)	Fisher Scientific	10294110
1,2-Ethanedithiol (EDT)	Sigma-Aldrich®	02390
DMF Peptide Synthesis Grade	AGTC Bioproducts Ltd	AGDMF

Table 3.3: Materials for DSPE-PEG2000-Cystabn conjugate synthesis

Product	Supplier	Catalogue No.
1,2-distearoyl-sn-glycero-3-phosphoethanolamine-N-[maleimide(polyethylene glycol)-2000] (ammonium salt) (DSPE-PEG2000-Maleimide)	Avanti® Polar Lipids, INC.	880126
L-cysteinyl-D-phenylalanyl-L-glutaminyl-L-tryptophyl-L-alanyl-L-valyl-L-glycyl-L-histidyl-(3S,4S)-4-amino-3-hydroxy-6-methylheptanoyl-L-Leucinamide (Cystabn)	In-house synthesis and custom synthesis by Cellmano Biotech Ltd	-

Table 3.4: Materials for liposome formulation

Product	Supplier	Catalogue No.
1,2-dioleoyl-sn-glycero-3-phosphocholine (DOPC) (18:1 (Δ9-Cis) PC)	Avanti® Polar Lipids, INC.	850375
1,2-dioleoyl-sn-glycero-3-phosphoethanolamine-N-[methoxy(polyethylene glycol)-2000]	Avanti® Polar Lipids, INC.	880130

(ammonium salt) (DOPE-PEG2000) (18:1 PEG2000 PE)		
Cholesterol (Ovine wool, >98%)	Avanti® Polar Lipids, INC.	700000
DSPE-PEG2000-Cystabn	In-house conjugation	-
(N-(Fluorescein-5-Thiocarbamoyl)-1,2-Dihexadecanoyl-sn-Glycero-3-Phosphoethanolamine, Triethylammonium Salt) (Fluorescein DHPE)	ThermoFisher Scientific	F-362

3.2.2 Cell Culture

All cell cultures were maintained at 37 °C, 5 % CO2, and 95 % air in a humidified incubator and routinely passaged at 80% confluency (A549) or weekly (H345).

3.2.2.1 H345 cell line

The human epithelial metastatic SCLC cell line (NCI-H345) used in this study overexpresses the GRP-R [17, 142, 143] and grows in suspension as multicellular aggregates. H345 cells were grown in RPMI 1640 media supplemented with 10 % FBS, 5 mM L-glutamine, 100 units/ml penicillin, and 100 µg/ml streptomycin (hereafter called full medium). H345 cells were passaged by centrifugation at 200 *g* for 5 min. The supernatant was removed and the

pellet re-suspended in fresh media and counted manually using haemocytometer before passaging it onto the required culture surface (2×10^5 cells/mL).

3.2.2.2 A549 cell line

This adherent cells were grown in DMEM medium supplemented with 10 % FBS, 100 units/ml penicillin, and 100 µg/ml streptomycin. A549 cells passaged by washing with PBS (3 x 5mL) followed by trypsinization (0.25% trypsin + 1mM EDTA for 5 minutes at 37°C). The cells were centrifuged at 200 *g* for 5 min. The supernatant was removed and the pellet re-suspended in fresh media and counted manually using haemocytometer before passaging it onto the required culture surface at density of 3×10^4 cells / cm^2.

3.2.3 GRP-R expression by flow cytometer using fluorescent probe

Both cell lines (A549 and H345) were harvested and diluted to 5×10^5 cells per mL and centrifuged at 1000 rpm at 25 °C for 5 min. The cell pellets were washed (x3) with PBS and resuspended gently in fixation buffer (4% PFA in PBS) for 30 min at RT on a tube roller. The suspension of each cell line was divided into two samples – permeabilized and non-permeabilized. Permeabilized cells were resuspended in ice cold permeabilization buffer (0.5% Triton X-100 in PBS) and incubated for 5 min at RT under gentle rolling agitation before washing with PBS (x3). The nonpermeabilized cells were treated the same with the omission of the permeabilisation buffer (PBS used in lieu). Both samples were pelleted by centrifugation (1000 rpm, 5 min, 25 ^{0}C) and resuspended in blocking buffer (10% FBS in PBS) for 10 min at RT. Wells were washed (PBS x3) and resuspended in rabbit anti-GRP-R antibody (GTX113209 GeneTex, UK, 1µg/ml in blocking buffer) then incubated on ice for 30 minutes. Cells were washed (PBS x3) before incubation with the secondary antibody (donkey, anti-rabbit AlexaFluor 488, 0.5µg/ml in blocking buffer) on ice for 30 min. All

samples were washed (PBS x3) and resuspended in PBS before analysis. Analyses were performed using a Beckman Coulter, Cytomics FC500 flow cytometer equipped with a 15 mW argon-ion laser. Cells were analysed on the basis of forward light scatter (FS), side light scatter (SS) and FL-1 intensity. Typically, fluorescence information for 10000 events was collected for each sample using Kaluza Analysis Software. Data were analysed by gating cells, as judged by FS versus SS dot plots, and plotting the fluorescence of these cells in a histogram. Fluorescence profiles or histograms shown were representative of those obtained from the number of experiments indicated. The increase in fluorescence intensity above background was determined by measuring the shift in fluorescence intensity from peak to peak, relative to the indicated control.

3.2.4 Cystabn synthesis by manual SPPS

Cystabn (Cys-D-Phe-Gln-Trp-Ala-Val-Gly-His-Sta-Leu-NH_2) and scrambled cystabn (Cys-Ala-Gly-Val-Leu-Trp-D-Phe-Sta-Gln-His-NH_2) were synthesized on the Rink Amide MBHA resin. Each coupling step involved addition to 1 eq. of resin Fmoc-AA, HCTU, HOBt and DIPEA (4:4:4:8 eq.) in 1.5 mL DMF. The mixture was reacted for 30 min at RT with occasional gentle agitation then washed with DMF (x3). This process was repeated to achieve a "double coupling" that increases overall coupling efficiency and eventual yield. After confirmation of successful coupling (negative Kaiser test result) the Fmoc deprotection step was performed (2 x 5 min 5% piperazine in DMF). After washing with DMF (3 x 5 mL, 1 min) Fmoc deprotection was confirmed by positive Kaiser test. This coupling and deprotection procedure was repeated until completion of the peptide sequence. The N-terminal amino acid was Fmoc- deprotected, washed with DMF (3 x 5 mL, 1 min), then washed with DCM (3 x 5 mL, 5 min). The resin was then dried under a stream of nitrogen until the resin was free-flowing and dried *in vacuo* for 3-5 h.

The peptide was cleaved from the resin using a cleavage cocktail (5 ml/100 mg resin) comprising TFA (94 %v/v) and scavengers TIPS, EDT and water (2 % v/v each). The cleavage reaction was performed for 7 h to overnight at RT with gentle agitation. The peptide was precipitated in 50 mL diethyl ether that had been pre-chilled on a dry ice-acetone bath. Peptide precipitation was noticeable by the cloudy appearance of ether after slow dropwise addition of the cleavage mixture. In the event of slow peptide precipitation, the ether-peptide mix was sealed in a round bottomed flask and stored overnight at – 20 °C. Precipitated peptide was harvested by centrifugation (3000 rpm, 10 min, 4 °C). Peptide precipitate was washed (x3 cold diethyl ether) then dissolved in 10% aqueous acetic acid before lyophilisation until a dry powder was observed.

3.2.5 Conjugate synthesis

The DSPE-PEG2000-Cystabn conjugate was synthesised using thiol–maleimide conjugation reaction. One equivalent of DSPE-PEG2000 (6.8 μmol in 4 mL chloroform) was added to two equivalents of cystabn (13.3 μmol in 2 mL methanol) in a round-bottomed flask. The mixture was stirred for 24 h at RT under nitrogen gas. After confirmation of successful conjugation by MALDI Tof MS analysis the solvent was evaporated and the reaction mixture redissolved in milliQ water. Unreacted peptide was removed by dialysis against miliQ water at RT for three days (the water changed every 2 h then left overnight) using 2000 MWCO benzoylated dialysis tubing. The purified conjugate was lyophilised to a dry white powder.

3.2.6 Cystabn and conjugate characterization

3.2.6.1 HPLC

Samples were analysed using a gradient elution method using Mobile phase A (H_2O + 0.1% TFA) and B solution (acetonitrile + 0.1% TFA) on a Perkin Elmer HPLC system comprising of binary solvent pump, autosampler, UV/Vis Detector and Peltier Column Oven. Mobile phases were membrane degassed using Millipore Vacuum filtration using 0.2 µm nitrocellulose filter. The gradient profile was 0-5 min. 5% B, 5-25 min 5-95% B and 5 min 5% B. Peptide samples (~1 mg/mL in miliQ water) were prepared in HPLC vials after centrifugation at 13000 rpm for 10 min. Peptide was eluted on a Phenomenex Luna® C18 (2) LC Column (particle size 5 µm, pore size 100 Å, 150 length x 4.6 mm diameter). Samples injected as 10 µl and analysed using UV/Vis detector at 280 nm wavelength. For the conjugate, the same method used with Thermo Scientific Hypersil™ BDS C8 LC Column (particle size 3 µm, pore size 130Å, 150 length x 4.6 mm diameter). Samples were injected in 10 µl volumes and elution monitored at 280 nm.

3.2.6.2 Development of a MALDI ToF MS method for conjugate analysis

Peptide samples (2 mg/mL) was prepared in 1:1 acetonitrile: miliQ water + 0.1% TFA. A saturated matrix solution (5 mg/mL) of α-cyano hydroxycinnamic acid was prepared in 1:1 acetonitrile: water + 0.1% TFA. Equal volumes (5 µL) of the matrix and sample solutions were mixed together and 1 µL spotted twice onto the same well of a clean MALDI sample plate. Samples were left to dry for 5 min in between each drop. Samples were analysed using linear ion detection mode on a SHIMADZU Axima-CFR MALDI-TOF.

The method used for MALDI analysis of peptides was unsuitable for conjugate analysis. A new sample layering method was developed for conjugate sample. Briefly, the conjugate was dissolved in chloroform at 2 mg/mL. A saturated matrix solution (10 mg/mL) of universal MALDI matrix (1:1 mixture of DHB and α-cyano-4-hydroxy-cinnamic acid, Sigma Aldrich, Poole, UK) was prepared in methanol. The sample was applied directly as a 1 µl spot onto a MALDI plate well followed by rapid evaporation by stream of hot air. The matrix solution was then applied as 1 µl on the same well followed by rapid evaporation by stream of hot air. The dried sample taken to be analysed by SHIMADZU Axima-CFR MALDI-TOF and Launchpad software.

3.2.6.3 UV Spectrophotometry for peptide concentration determination

Samples (~1 mg/mL & ~0.5 mg/mL) were prepared in milliQ water (for the peptide samples) and chloroform (for the conjugate samples) in clean quartz UV cuvettes. The samples were scanned at wavelengths range of 400 nm to 200 nm. The absorbance at 280 nm was used to determine the concentration using the molar extinction coefficient for the peptide tryptophan residue (5560 AU/mmole/ml).

3.2.7 Preparation of control and cystabn-targeted liposomal formulations

Lipids for each liposomal formulation (Table 3.5) were dissolved in chloroform and mixed in a round-bottomed flask. A thin lipid film was produced by evaporation of the solvent in vacuo. The film maintained under high vacuum for one hour to remove traces of organic solvent. The film was hydrated with PBS to a final lipids concentration of 10 mg/mL then heated to 55 ºC and vortexed extensively to produce MLVs [98]. Five cycles of freeze-thawing (dry ice-acetone followed by heating to 55 ºC) were performed to reduce the lamellarity of the vesicles [99]. Finally lipid suspensions were extruded (21 x) through

polycarbonate membranes of 200 nm, 100 nm and 50 nm pore sizes to produce a narrow size distribution of ULVs [100].

Table 3.5: Liposomal Formulations Composition

Control Formulation	DOPC: Chol: DOPE-PEG2000 (57: 38: 5 mol. %)
Targeted Formulation	DOPC: Chol: DOPE-PEG2000: DSPE-PEG2000-Cystabn (57: 38: 4: 1 mol. %)
FL-Control Formulation	DOPC: Chol: DOPE-PEG2000: DHPE-Fluorescein (56: 38: 5: 1 mol. %)
FL-Targeted Formulation	DOPC: Chol: DOPE-PEG2000: DSPE-PEG2000-Cystabn: DHPE-Fluorescein (56: 38: 4: 1: 1 mol. %)

3.2.8 Characterization of liposomal formulations

Liposomes were characterized for size and zeta potential using Zetasizer Nano ZS. For size measurements the liposomal suspension was diluted 1:10 with PBS and sealed with parafilm.

For zeta potential measurements, the liposomal suspension was diluted 1:10 with PBS and transferred to a clean folded capillary cell (Malvern, DTS1070).

3.2.9 Liposomal stability in PBS and 10% serum

An aliquot of the liposomal suspension was diluted 1:10 with either PBS or 10% FBS in PBS After 0, 24 and 72 hours the samples were transferred to cuvettes and measured for size and zeta potential as described above.

3.3 Results

3.3.1 GRP-R expression in SCLC cells (H345)

To examine for differences in the GRP-R expression levels in the two cells lines an indirect immunolabelling was performed followed by semi-quantitative detection by flow cytometry. Figure 3.1 shows the flow cytometric characterisation the two cell lines, A549 and H345. Specifically, Figures 3.1A-B show the forward and side scatter profiles of the A549 and H345 lines, respectively. Subtle differences in cell size and granularity were evident from the different locations of the two cell line profiles on the dot plot. This was consistent with microscopic inspection of cell morphology (data not shown). The cells were gated based on FS/SS of the control cells (i.e. without treatment), and the fluorescence of these cells subtracted from treatment groups to yield the median fluorescence intensity (MFI) for each group.

The GRP-R expression in non-permeabilised H345 (primary and secondary antibody) was 51 ± 27 and about 5-fold greater than the MFI of the secondary-only control (10 ± 1.7) indicating specific labelling of surface expressed receptor. In contrast, the surface expression of GRP-R in A549 was lower. Specifically, the MFI was only 2-fold higher than the secondary only control (24 ± 6 versus 10 ± 3).

Flow cytometry analysis of permeabilised cells revealed a greater extent non-specific binding of the secondary antibody in both cell lines, compared to non-permeabilised cells (compare Figure 3.1C and D). However, this increased "background" staining was accompanied by an increase in specific GRP-R staining in both cell lines. In H345 cells the total cellular expression increased to 130. A549 cells displayed the greatest expression with

an MFI of 318. The sum of the surface and total expression MFI for A549 cells is significantly greater ($P < 0.05$) than H345 cell line.

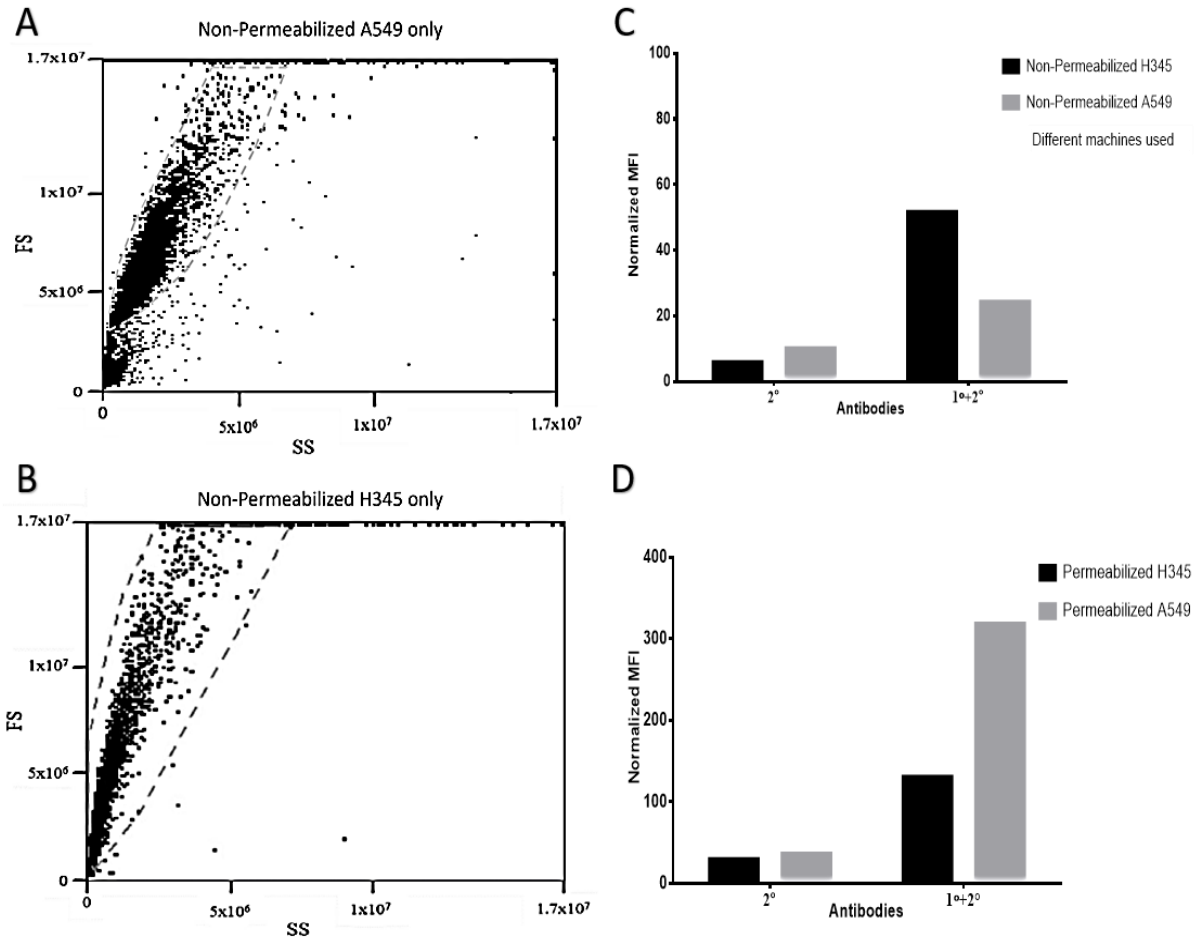

Figure 3.1: GRP-R expression data in H345 and A549 cells. *A & B: Forward scatter (FS) and side scatter (SS) flow cytometry profiles of control non-permeabilized A549 and NCI-H345 cells, respectively. Gates are shown in the dotted lines. C & D: Median FL-1 fluorescence intensity (MFI) of non-permeabilised (C) and permeabilised (D) H345 and A549 cells. Data shown in C are from two separate experiments. Data in D are from a single experiment due to limited antibody availability.*

3.3.2 Peptide synthesis

Early studies involved synthesis of an N-terminal cysteine mutant of the agonist bombesin peptide including residues 6-14 (Cys-Gln-Trp-Ala-Val-Gly-His-Lue-Met-NH_2) after which the project moved towards the use of an unnatural antagonist peptide, Cystabn (Cys-D-Phe-Gln-Trp-Ala-Val-Gly-His-Sta-Leu-NH_2).

3.3.2.1 Cys-bombesin (6-14)

Cys-bombesin (6-14) synthesis was performed using manual Fmoc SPPS using standard double coupling approach with a good crude yield of 78 %. HPLC analysis of crude peptide revealed a retention time (RT) of the peptide was 14.0 minutes and a purity of 85% (Figure 3.2A). MALDI ToF MS analysis confirmed the presence of the intact peptide. The mass spectrum shown in Figure 3.2B included $[M+H]^+$ = 1043.1 Da, $[M+Na]^+$ = 1065.1 Da, $[M+K]^+$ = 1081.1 Da. UV-Vis spectroscopic analysis of the peptide included absorbance bands at 280 nm (Figure 3.2C) corresponding to the tryptophan indole side chain (Figure 3.2D).

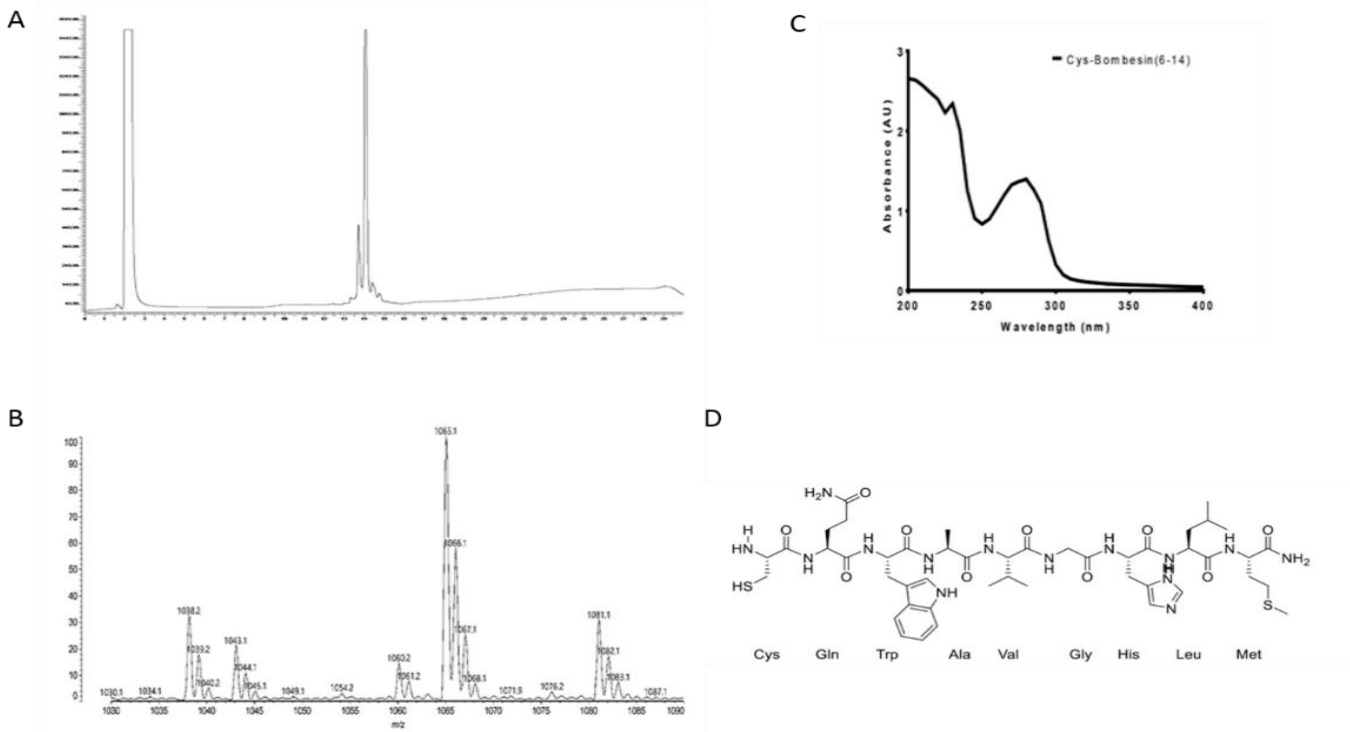

Figure 3.2: Characterisation of Cys-bombesin(6-14). *(A) RP-HPLC chromatogram, (B) MALDI ToF MS spectrum and (C) UV absorbance spectrum of crude Cys-bombesin (6-14). Panel B show the correct masses of peptide. Mass data* $[M+Na]^+$ *(calculated) = 1065.48 Da,* $[M+Na]^+$ *(observed) = 1065.1 Da,* $[M+H]^+$ *= 1043.1 Da,* $[M+K]^+$ *= 1081.1 Da). D: structural formula of Cys-bombesin(6-14) along with the corresponding three letter amino acid annotation.*

3.3.2.2 Cystabn

The antagonist peptide, Cystabn was synthesized by manual Fmoc SPPS with a good yield of 92 % post-cleavage. RP-HPLC analysis using a 30 minute gradient program (Figure 3.3a) revealed number of unresolved peaks. Peak integration of the largest peak (R_T = 14.5 min.) estimated the yield to be ~55%. Figure 3.3a shows the MALDI ToF mass spectrum of crude Cystabn (Exact mass = 1215.62 Da). The mass spectrum includes: $[M+Na]^+$ = 1238.3 Da as the predominant ion (calculated $[M+Na]^+$ = 1238.62 Da), $[M+H]^+$ = 1216.3 Da. The UV absorbance (Figure 3.3C) corresponds mainly to tryptophan shown in the peptide sequence (Figure 3.3D).

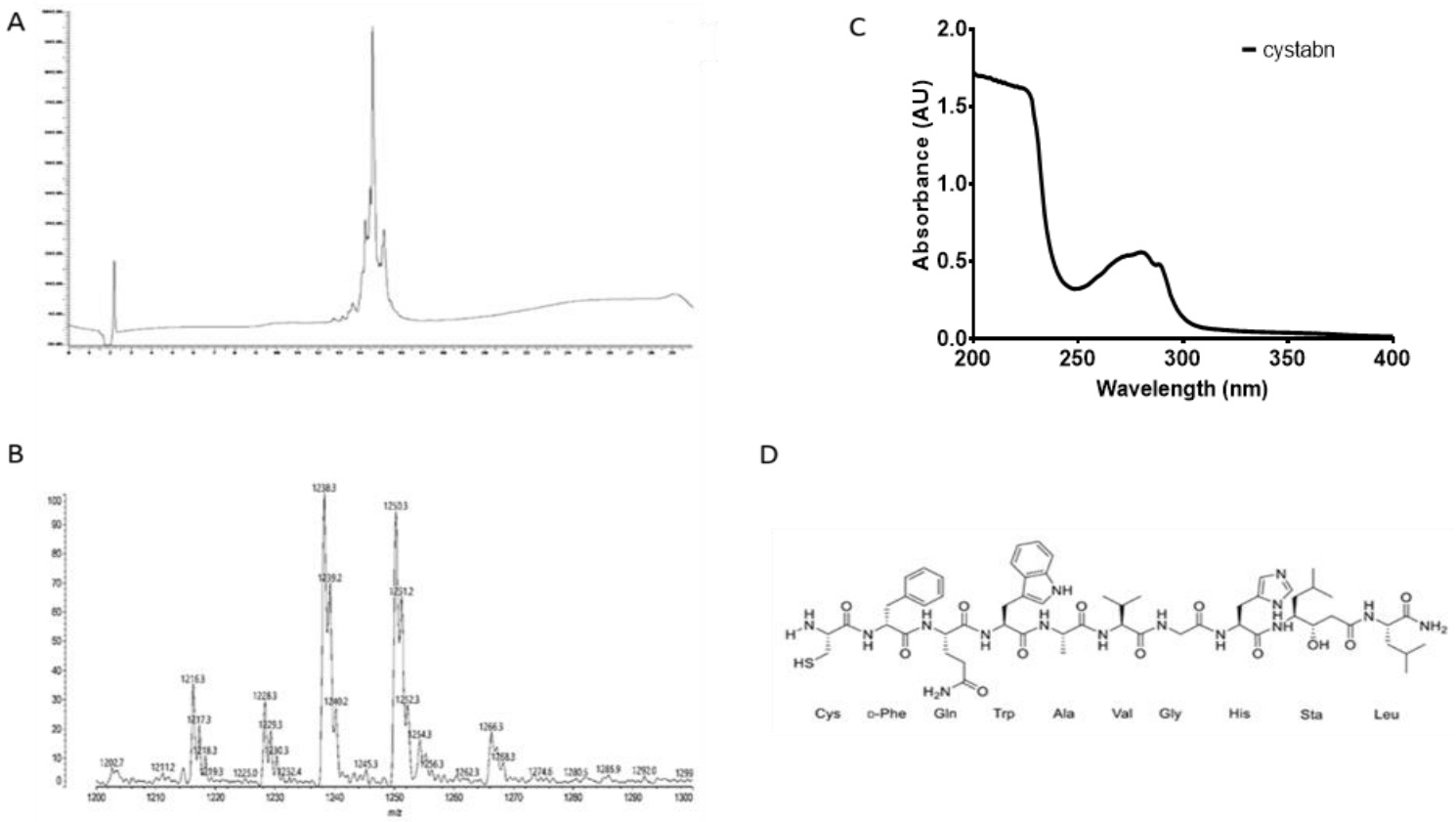

Figure 3.3: Characterisation of Cystabn peptide. *RP-HPLC chromatogram (A), MALDI ToF MS spectrum (B) and UV absorbance spectrum (C) of crude Cystabn. Panel B show the correct masses of peptide. Mass data $[M+Na]^+$ (calculated) = 1238.62 Da, $[M+Na]^+$ (observed) = 1038.3 Da, $[M+H]^+$ = 1216.3 Da) D: structural formula of Cystabn along with the corresponding three letter amino acid annotation. Sta = gamma amino acid, statine.*

3.3.2.3 Scrambled Cystabn peptide

Scrambled cystabn was synthesized by manual Fmoc SPPS with a good yield of 94 %. HPLC analysis showed crude peptide purity to be 70% with a R_T of 14.8 minutes (Figure 3.4A). Scrambled cystabn was analysed with MALDI ToF MS (Figure 3.4B) to confirm the mass of the peptide (Exact mass = 1215.62 Da). The spectrum showed $[M+Na]^+$ (observed) = 1238.3 Da high, (calculated $[M+Na]^+$ = 1238.62 Da), [M] = 1215.4 Da. The UV absorbance spectrum (Figure 3.4C) includes the expected absorbance bands at 280nm corresponding to the tryptophan indole ring expected from the peptide primary sequence (Figure 3.4D).

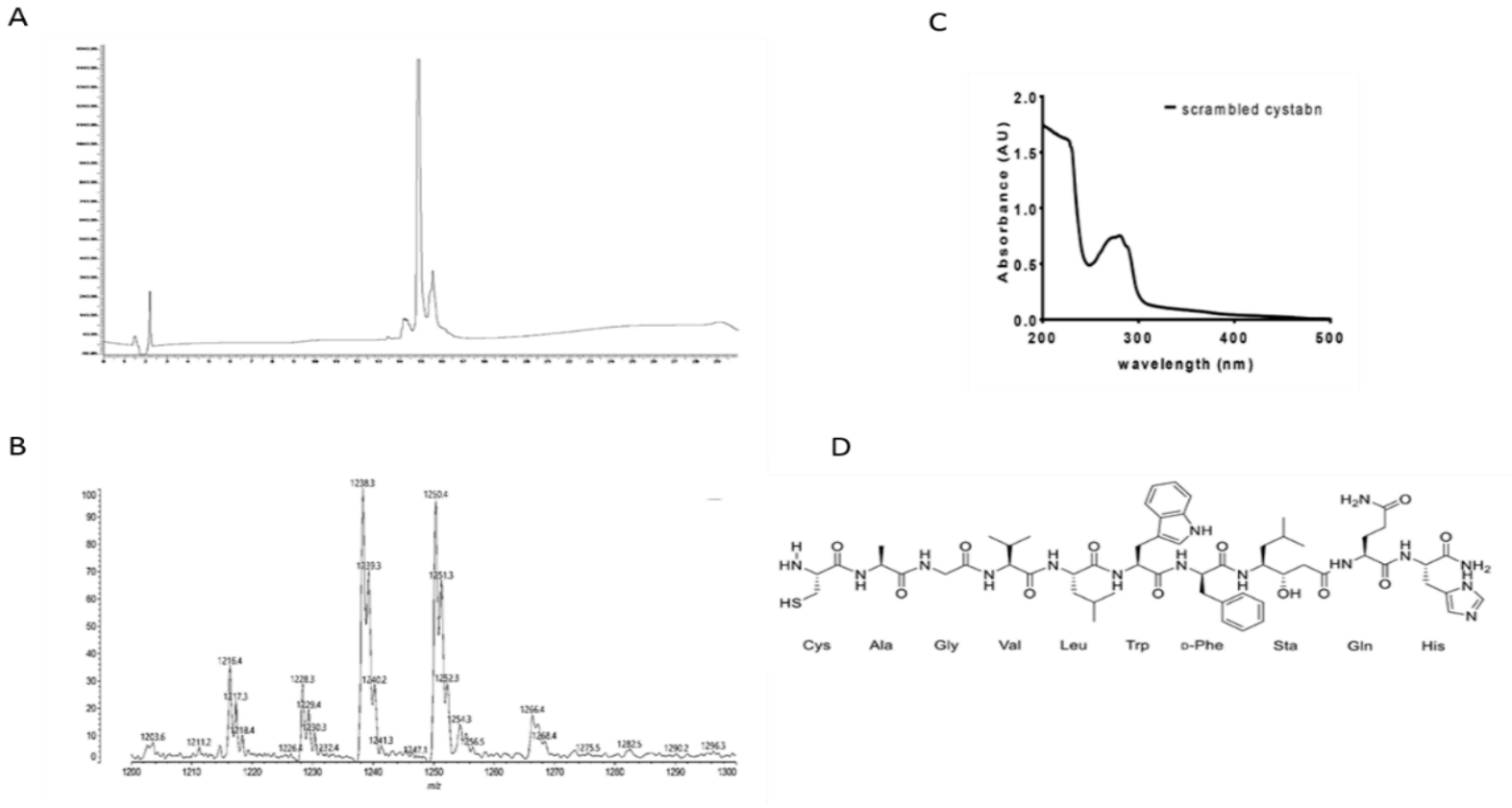

Figure 3.4: Characterisation of scrambled Cystabn peptide. *RP-HPLC chromatogram (A), MALDI ToF MS spectrum (B) and UV absorbance spectrum (C) of crude scrambled Cystabn. Panel B show the correct masses of peptide. Mass data $[M+Na]^+$ (calculated) = 1238.62 Da, $[M+Na]^+$ (observed) = 1038.3 Da, $[M]^+$ = 1215.4 Da). D: structural formula of Cystabn along with the corresponding three letter amino acid annotation. Sta = gamma amino acid, statine.*

3.3.3 Conjugate synthesis (DSPE-PEG2000-cystabn)

The DSPE-PEG2000-Cystabn conjugate was synthesised using thiol–maleimide conjugation reaction with a good yield of 98 % (scheme 3.1). After purification by dialysis, the conjugate was characterized by HPLC on a C8 column to afford analysis of the less polar conjugate (Figure 3.5A). Purity of the peptide was determined to be 86% upon peak integration. The retention time (R_T) of the peptide was 18.94 min. The conjugate was analysed with MALDI ToF MS to confirm the mass of the conjugate (Figure 3.5B). The exact mass of the DSPE-PEG2000 maleimide was calculated as 4137.41 Da but is unreliable due to the polydisperse nature of the PEG linker. The mass spectrum include the most abundant ion at 4188 Da. The expected mass difference between ion peaks is 44 Da, which represents ethylene glycol monomers (C_2H_4O = 44.05). Figure 3.5b includes, for example, a mass difference from 4277.57 Da to 4321.49 Da, which is equal to one monomer. Two monomer mass differences of ~ 88 Da (4100.68 Da to 4188.41 Da) equivalent to two ethylene glycol monomers were also recorded.

The conjugate also, characterized by UV spectrometer. The conjugate dissolved in chloroform and analysed over the UV range of 200 nm to 400 nm. At 280 nm, the observed absorbance (Figure 3.5C) corresponds mainly to tryptophan shown in the conjugate structure (Figure 3.5D). The noisy background lower than ~ 250 nm is attributable to the interference presented by solvent contaminants.

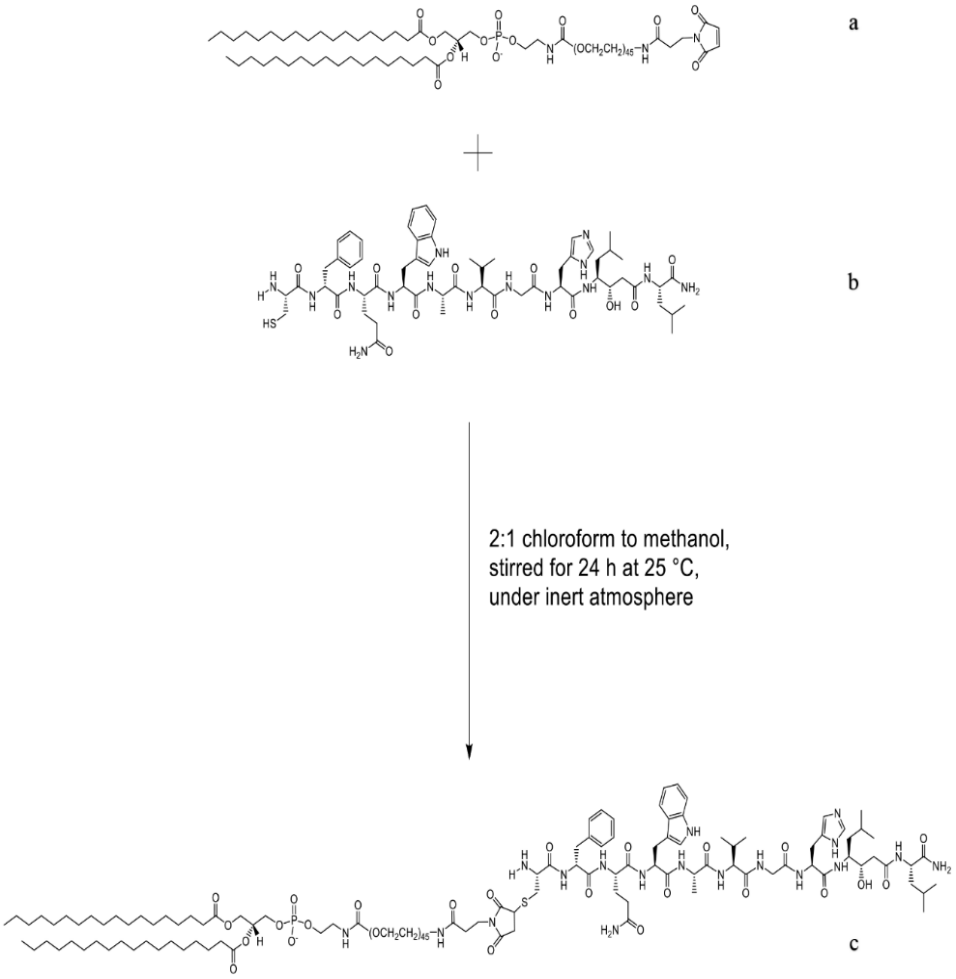

Scheme 3.1: Synthesis of the DSPE-PEG2000-cystabn. *Thiol–maleimide conjugation reaction between one equivalent of DSPE-PEG2000-maleimide (a) and two equivalents of cystabn (b) to give DSPE-PEG2000-cystabn (c).*

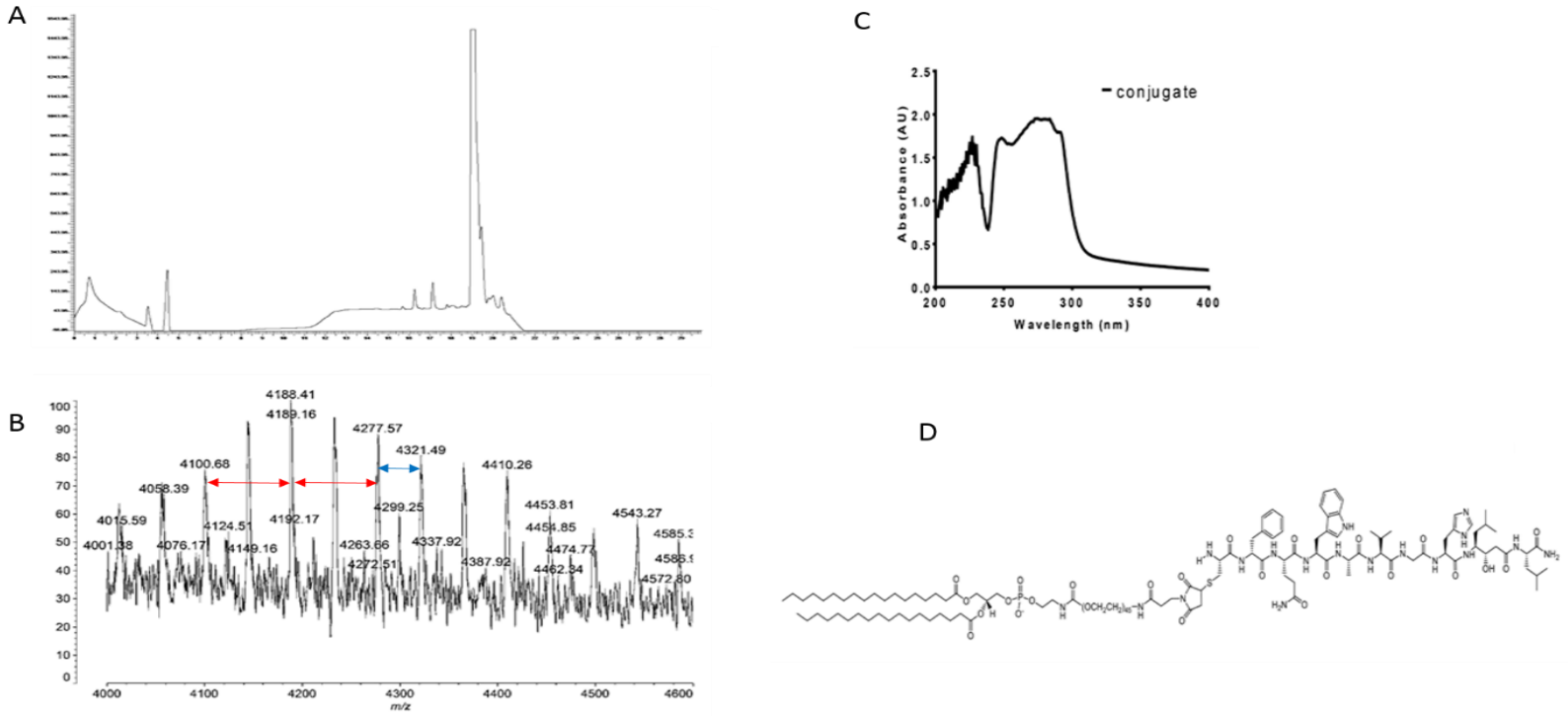

Figure 3.5: Characterisation of DSPE-PEG2000-cystabn conjugate. *RP-HPLC chromatogram (A), MALDI ToF MS spectrum (B) and UV absorbance spectrum (C) of the crude conjugate. Panel B show the masses spectra of the conjugate spread around (4137.41 Da calculated, which is the mass of the conjugate) with 44.05 Da peak separation. This 44.05 difference in masses between peaks equal to one ethylene glycol monomer. Blue and red arrows indicate peak separation by one or two glycol monomers, respectively. D: structural formula representation of DSPE-PEG2000-cystabn conjugate. N.B. the exact structure of the PEG chain is unknown.*

3.3.4 Formulation of the targeted and control liposomes

The thin film hydration protocol used to prepare liposomes produced reproducible monodispersed SUVs. The mean diameters for both liposomal were 101± 2.1 nm and 101± 2.3 nm for control and targeted liposomes, respectively. The polydispersity index is < 0.1 for both formulations indicating monodispersed population (0.058 ± 0.007 and 0.068 ± 0.019 for control and targeted liposomes, respectively). The zeta potential of both formulations were slightly negative i.e. -1.64 ± 2.13 mV and -1.86 ± 1.64 mV for control and targeted liposomes, respectively. Representative size and zeta potential measurements are summarized in Table 3.2.

Figure 3.6a and 3.6c shows the DLS autocorrelation function data for both formulations (control and targeted formulations respectively). Both correlation curves produced show smooth single exponential decay function, which indicates mono-disperse particle suspensions. Cumulants analysis used to extract the Z-average and polydispersity index from the curve. Figure 3.6b and 3.6d shows the intensity weighted size distribution with good reproducibility for both formulations (control and targeted formulations respectively).

Freshly prepared control and targeted liposomes showed consistent ($p>0.05$) size, zeta potential and polydispersity measurements. A Z-average diameter of 101 nm and a zeta potential of -1.6 mV with a narrow polydispersity index of 0.06 indicating a refined unilamellar formulation for the control formulation. Similarly, the targeted formulation showed size, zeta potential and polydispersity measurement of 100 nm, -1.9 mV and 0.07, respectively.

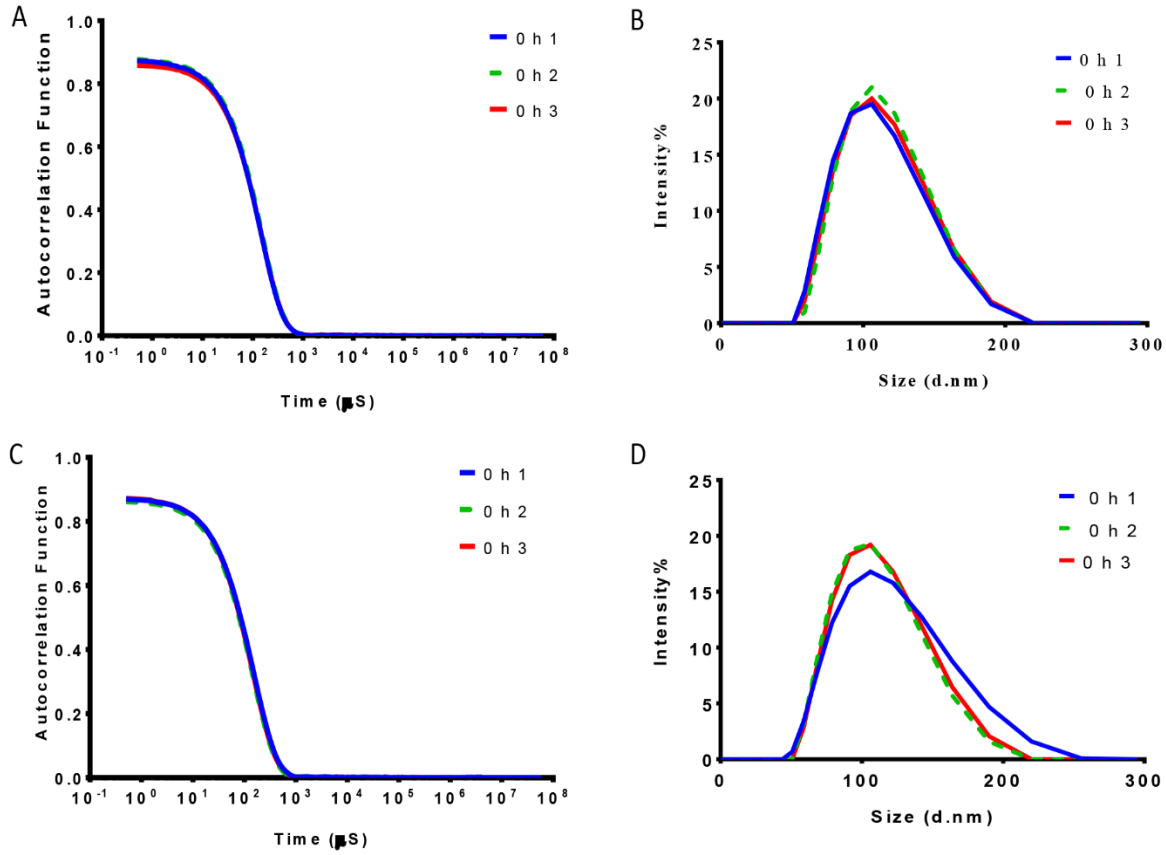

Figure 3.6: DLS characterisation of control and cystabn-targeted liposomes. *Autocorrelation functions (A & C) and intensity weighted size distribution date for (B & D) of control liposomes (top row) and targeted liposomes (lower row). Each panel shows results from three independent experiments in red, green and blue.*

Table 3.6 : Summary of liposomes physical characteristics

	Control liposomes	**Cystabn-targeted liposomes**
Z-Ave (d.nm) [1]	101 ± 2.1	100 ± 2.3
PDI [2]	0.058 ± 0.007	0.068 ± 0.019
ZP (mV) [3]	-1.64 ± 2.13	-1.86 ± 1.64

Data shown are mean ± SD, n=3 independent experiments.

[1] Z-averaged hydrodynamic diameters (Z-Ave) obtained by cumulant analysis of the auto-correlation functions.

[2] Polydispersity indexes (PDI) obtained by cumulant analysis of the auto-correlation functions.

[3] Zeta potential (ZP) was measured in PBS with 137 mM NaCl.

3.3.5 Liposome physical stability study

The colloidal stability of liposomes is an important factor for *in vitro* and *in vivo* application of liposomes. The physical stability of targeted and control liposomes was studied in PBS and 10% serum over three days. The physical stability of the liposomes in PBS monitored using the size and the zeta potential over the period of the study whereas only the size parameter used to monitor the physical stability of the liposomes in 10% serum.

Both liposomal formulations showed a good stability in PBS along the storage period reflected by their size (Figure 3.7A-B) and zeta potential (*Table 3.7***)**. Compared to the respective freshly prepared formulations, there no significant change ($p>0.05$) in the size, polydispersity and zeta potential of either liposomal formulations upon storage in PBS for the whole storage period at the three different temperatures i.e. 4 °C, 25 °C and 37 °C. The largest change recorded for the control formulation from 0.058 ± 0.007 to 0.098 ± 0.07 PDI

after incubation at 25 °C for 72 h. In general, the PDI for the targeted formulation increased greater than that of control liposomes. For example, the PDI rose from 3-fold from 0.068 ± 0.019 to 0.176 ± 0.08 after 72 h incubation at 25 °C. There were no significant changes in zeta potential ($p>0.05$) for both formulations. For the control formulation, the zeta potential decreased from -1.64 ± 1.42 to -2.57 ± 1.15 mV after incubation at 25 °C for 24 h. For the targeted formulation, the zeta potential decreased from -1.76 ± 0.56 to -3.55 ± 1.96 mV after incubation at 37 °C for 72 h.

As expected, storage of liposomes in 10% FBS caused more physical instability than storage in PBS (Figure 3.8 *cf.* Figure 3.7). There was non-significant change in the parameters of the control and targeted formulations ($p>0.05$) immediately after addition of 10% FBS. For the freshly prepared control formulation, the size slightly decreased from 93.93 ± 1.78 to 89.79 ± 1.52 nm with slight increase in PDI from 0.083 ± 0.002 to 0.160 ± 0.012 immediately after addition of 10% FBS. For the freshly prepared targeted formulation, the size slightly increased from 105.5 ± 3.42 to 113.37 ± 20.51 nm with slight decrease in PDI from 0.055 ± 0.019 to 0.241 ± 0.148 immediately after addition of 10% FBS. However, the targeted formulation (figure 3.8b) showed trending instabilities reflected by its polydispersity values proportional to the storage temperature and duration. For example, storage of targeted liposomes at 37 °C after 72 hours showed the highest PDI (0.7, $p<0.05$) compared to the freshly prepared sample (PDI=0.068 ± 0.019). After storage for 72 hours, the PDI of the targeted formulation increased greatly from 0.19 at 4 °C to 0.56 at 25 °C to 0.70 at 37 °C ($p<0.05$). This indicates that the colloidal stability decreases with storage duration and temperature. Storage at 37 °C in 10% FBS caused the most instability regardless of duration. It is also noted that, no increases in size or PDI ($p>0.05$) were seen when targeted liposomes were stored in 10% FBS at 4 °C.

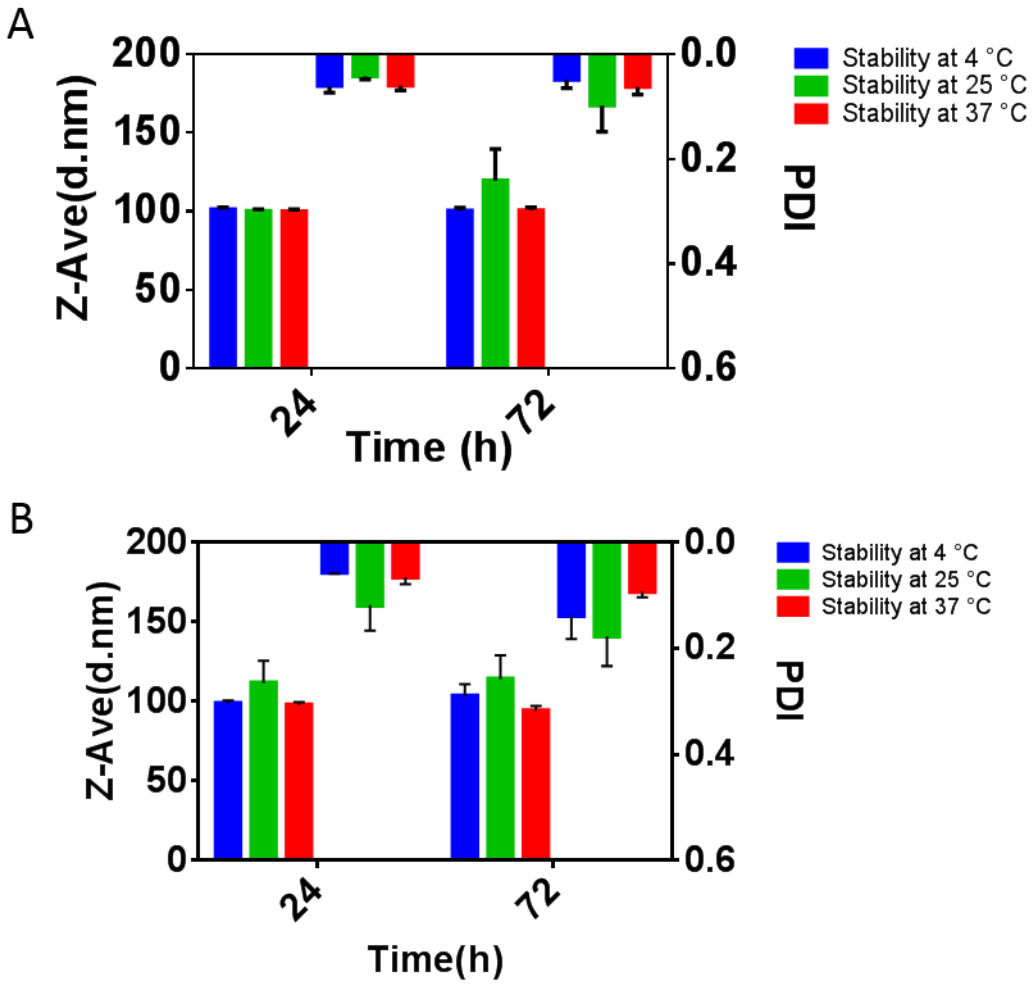

Figure 3.7: Physical stability in PBS: *(A) and (B) are the Z- average and PDI data for the control and targeted liposomes respectively. Mean ± SD, n=3.*

Table 3.7: Zeta Potential for the control and targeted liposomes

Control liposomes							
Time (h)	0	24			72		
Temperature (°C)	RT	4	25	37	4	25	37
ZP (mV)[1]	-1.64 ±1.42	-2.59 ±0.95	-2.57 ±1.15	-1.50 ±0.80	-1.28 ±0.87	-1.57 ±0.91	-1.66 ±0.72
Targeted liposomes							
Time (h)	0	24			72		
Temperature (°C)	RT	4	25	37	4	25	37
ZP (mV)[1]	-1.76 ±0.56	-1.40 ±0.56	-2.12 ±0.69	-3.76 ±1.11	-2.73 ±1.15	-1.65 ±0.54	-3.55 ±1.96

Data shown are mean ± SD

[1] Zeta potential (ZP) was measured in PBS with 137 mM NaCl.

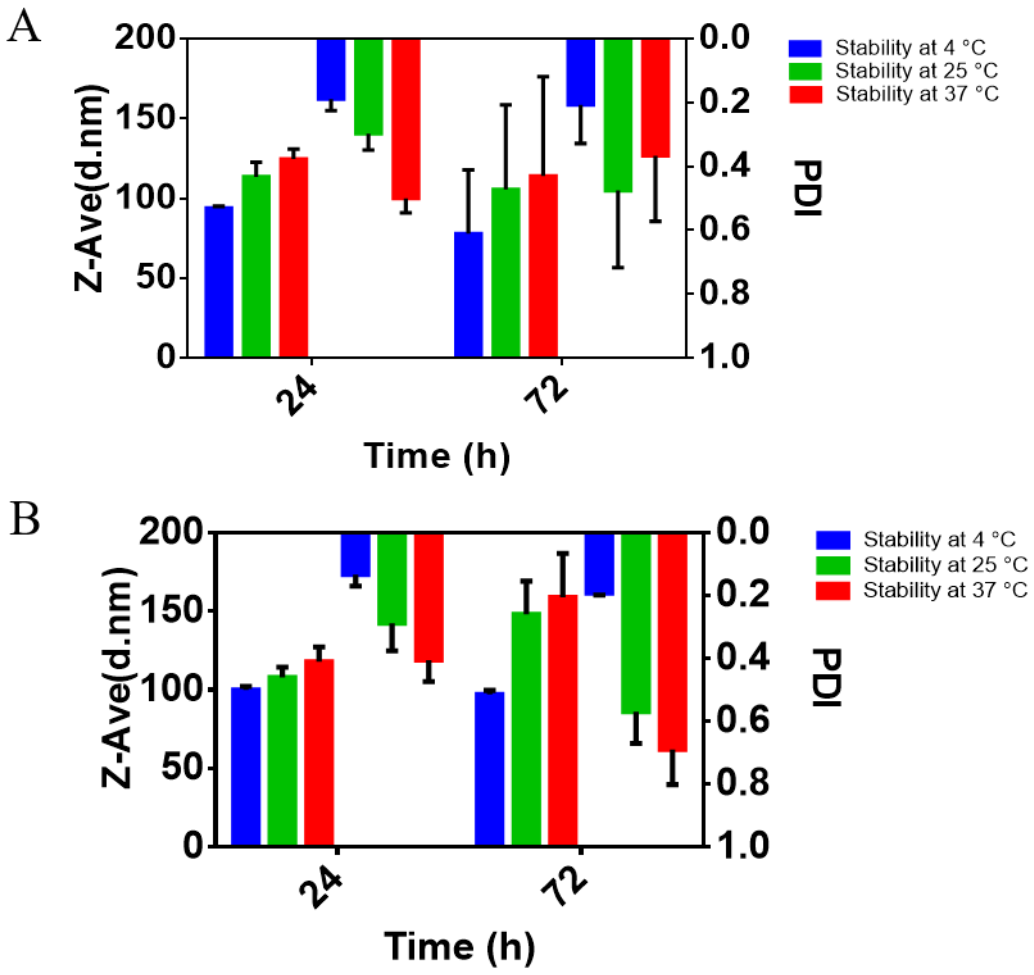

Figure 3.8: Physical stability of liposomes in 10% serum: *(A) and (B) are the Z- average and PDI data (n=3) for the control and targeted liposomes respectively.*

3.4 Discussion

In order to work towards a targeted liposomal formulation or SCLC it is necessary to identify an appropriate targeting strategy such that liposomes can be appropriately enriched at the target site. Here, the GRP-R was targeted in light of the growing evidence for the role of bombesin-related peptides and their cognate receptors (e.g. GRP-R) in cancer biology and targeting.

To examine for differences in the GRP-R expression levels in the two lung cancer cells lines (one SCLC and one NSCLC) an indirect antibody labelling was performed followed by semi-quantitative detection by flow cytometry. The relative amount of GRP-R expressed on the cell surface of non-permeabilised cells was >2-fold greater in H345 cells than A549 cells indicating a wider availability of the target on this cell type. Intriguingly, analysis of permeabilised cells revealed that A549 cells express a greater total amount of GRP-R compared to H345. This result was however accompanied by a greater amount of background non-specific binding of the secondary antibody in both cell lines, compared to non-permeabilized cells. This observation of increased cell surface expression does support the rationale for targeting GRP-R on this cell type in spite of evidence to suggest a sub-optimal antibody labelling protocol for potentially both primary and secondary antibodies.

The antibody clone used in this study was raised against the second extracellular loop of the GRP-R and therefore affords the detection of both surface expressed and intracellular protein. It is not possible to state conclusively whether the antibody recognises optimally its antigen in the intracellular environment where there is potential for receptor folding or conformational distortion that might lead to weak binding and /or non-specific binding to other bombesin receptor family members. Due to the limited availability of the GRP-R

antibody it was impossible to properly optimise the antibody labelling technique. An optimised protocol would afford the titration of both primary and secondary antibody solution for the studyof GRP-R expression in a wider range of SCLC, NSCLC and normal lung epithelial cell lines.

As summarised in the introduction there are various and sometimes contradictory data in the published literature regarding the expression of GRP-R mRNA and protein in lung cancer models and patient tissues Moreover, the growth of NSCLC tumours in mice was suppressed by more than 30% using GRP-R antagonist [32]. Although the A549 cell line was not intended to serve a GRP-R negative cell line in this study it would be appropriate in future studies to incorporate normal human lung epithelial lines as a control to appropriately measure the targeting indices if GRP-R targeted liposomes.

The development of a targeted liposomal drug platform relies on the use of an appropriately specific targeting moiety. In this work an antagonist peptide was used as a high affinity targeting ligand for GRP-R in place of the widely used bombesin (6-14) peptide which has been shown to impart an autocrine growth effect on SCLC lines. Fmoc-SPSS was used to prepare C' terminal amidated peptides on a small scale of ~50-100mg. Initial work on the synthesis of Cys-bombesin (6-14) delivered a product in good yield, however HPLC analysis indicated the presence of a closely related structural impurity account for >40% of the product. It would be expected that the contaminant would be a truncated or otherwise modified peptide from the synthetic procedure. Surprisingly, MALDI-TOF analysis revealed no such truncated or related peptides and the UV absorbance spectrum indicated the presence of a native tryptophan without the presence of an oxidise tryptophan that would present an altered UV absorbance spectrum in addition to distinct HPLC peaks and MALDI-TOF peaks. Similar levels of impurities were observed in HPLC analyses of the Cystabn and

scrambled cystabn peptides. Nonetheless, confirmatory UV and MALDI-TOF data supported the use of these crude peptides without further purification. Indeed, conjugation of the Cystabn peptide to DSPE-PEG-maleimide proceeded successfully to yield a peptide-PEG-lipid conjugate with a mass around 4.5kDa. Significant method development was required to establish the reaction solvent conditions that encouraged reactant and product solubility while maintaining reaction efficiency in addition to the choice of purification method. The choice of dialysis as a purification method is favourable to HPLC which has the drawback of sample losses on repeated injection as well as time consuming testing of column fractions and solvent evaporation to recover the product.

MALDI-TOF MS was chosen as the definitive analytical technique of choice for proving successful peptide-PEG-lipid conjugation. However, initial attempts were unsuccessful due to inefficient sample ionisation and a predominance of matrix-associated ions at low *m/z*. The technique was optimised through iterative trialling of MALDI matrices (e.g. α-cyanohydroxycinnamic acid, DHB, dithranol) as well as a number of sample mixing or layering techniques such as mixing, layering, sandwiching. Mass spectra with good resolution were achieved following optimal mixing of a high sample concentration with a mixture of matrices in a layer on layer approach. Successful conjugation was concluded when regions of the mass spectrum, centred around the expected product mass range, included the signature pattern of 44 Da peak spacing consistent with a PEG polymer. Moreover, reaction completion was indicated by the absence of peaks in the mass range occupied by the DSPE-PEG-maleimide.

Time constraints prohibited the synthesis of the scrambled Cystabn-PEG-lipid conjugate although the product was tested in cell growth assays (Chapter 4). In place of a control liposome presenting the scrambled Cystabn peptide a control liposome formulation was

prepared in which 5% total DOPE-PEG was included rather than 4% DOPE-PEG + 1% cystabn-PEG-DSPE. The use of this as a control was sub-optimal as judged by the lower colloidal stability of the peptide-loaded formulation compared to the bare control liposome. The observed increases in PDI and particle size over the 72 h time period could result from interference by the displayed peptide on the liposomal surface charge. Alternatively, the presence of protease substrates on the vesicle surface might also have attracted enzymes that indirectly destabilise the liposome through surface charge modification. It should be noted however the times scale for peptidase/protease instability are likely to be considerably shorter than the first 24 hour timepoint. This increase in size probably caused by opsonisation process. Opsonization of liposomes by plasma proteins plays a critical role in the clearance of injected liposomes in vivo. Upon exposure to serum or plasma, liposomes rapidly adsorb a vast collection of protein molecules, as demonstrated by isolation of liposomes from in vitro incubations with serum/plasma [144, 145]. Szebeni et al. demonstrated that using DSPE-PEG2000 in the liposomal formulation (HSPC/Chol), with same size and lipid composition as Doxil®, promoted complement activation and opsonisation in human serum in vitro, compared to HSPC/Chol as control [146]. Key information on particle stability in physiological fluids could be extracted from zeta potential measurements although it is extremely difficult to monitor the zeta potential in 10% serum as it presents a diverse collection of proteins which may bind in dynamic equilibrium with the liposome and affect greatly the accuracy of the zeta potential measurement.

Initial work involved a successful synthesis of Cys-bombesin (6-14) however it was abandoned at an early stage of the project in order to focus on an antagonistic peptide sequence. Chandra et al [147] used bombesin (6-14), without the N terminal cysteine residue) a targeting ligand for the delivery of starch-stabilised gold nanoparticles to PC-3

prostate cancer cells in vitro. *In vivo* studies indicate that their functionalised nanoparticles are able to target the GRP receptor-enriched pancreatic tissue such that ~45% of the injected dose of ^{198}Au-labelled particles were recovered from the pancreas. Nonetheless, it was decided that a more rational alternative would involve the deployment of an antagonistic peptide (Cystabn) that does not carry the risk of a mitogenic effect on target cells. However, antagonistic peptide as will be shown in the next chapter, will not stimulate cell growth. There is a study which also suggest that using antagonistic peptide for Bombesin may be preferable in cancer targeting over agonist due to higher tumour uptake and longer tumour washout [148]. Others have developed GRP-like peptides with antagonist activity at their receptor. One such peptide, [D-Phe6, Sta13, Leu14] Bombesin(6-14), shows high affinity binding to GRP-R (IC_{50} = 2.2 nM by competitive binding method) and stimulates receptor internalisation. A structurally related peptide, KJGJKG displayed a higher binding affinity (IC_{50} 0.5 nM by competitive binding method) but includes a complex Psi amino acid that is synthetically challenging to prepare [49, 149]. In this project, the [D-Phe6, Sta13, Leu14] Bombesin(6-14) sequence was chosen as a compromise between high affinity antagonist activity with ease of peptide synthesis.

This pepide-PEG-lipid conjugate was subsequently used to prepare unilamellar liposomes in which the extent of loading of targeting conjugate was 1% of the total 5 % mol of pegyated lipid. The characterization of the liposomes showed a monodisperse liposome suspension with a slightly negative zeta potential (-1.64 for control and -1.76 for targeted liposomes in PBS). The value of zeta potential is closer to zero because the formulations contain the zwitterionic phospholipid (DOPC). The colloidal and biological stability of the system is provided through the steric hindrance effect caused by pegylation. Pegylation achieved by inclusion of 5 mole % DOPC-PEG_{2000}. The pegylation of the surface of liposomes in the

range of 5-10 mole % using PEG_{2000}-lipid found to provide the longest circulation time *in vivo* [150, 151]. At this range, a dense polymer brush formed at the surface and yielding the repulsive steric interaction For anticancer application, the optimal size of < 200 nm provide highest tumour retention by utilizing Enhanced Permeability and Retention (EPR) of the tumour. Most current approved anticancer nanomedicines have sizes range from 100-200 nm. However, size range of < 20 nm will cause removal of nanoparticles by renal clearance and fenestrated capillaries. In addition to that, as the size increase >150 nm, the accumulation in the spleen, liver and bone marrow enhanced [152]. The mean size of the liposomes were about 100 nm even though they were extruded finally though a 50 nm filter. To further enhance the tumour accumulation, targeting moiety were incorporated as 1 mole % DSPE-PEG_{2000}-maleimid. By using this approach, cystabn will be available unhindered to identify and bind to its receptor on the cancer cell [75, 153].

Liposomes are limited by their physical instability caused by aggregation or fusion of vesicles to form larger particles [154]. This can affect both in vitro and in vivo liposomal behaviour. The stability of a colloidal system is determined by the balance of attractive and repulsive forces between suspended particles in the medium. An increased repulsive contribution increases the colloidal stability. Increased steric repulsion by particle pegylation is one type of the approaches that is commonly used to provide liposomal stability. This type of stabilization provides increased colloidal stability for slightly charged nanoparticles. In addition to that, it provides *in vivo* stability by preventing rapid clearance by the immune system [155]. Although the exact mechanism for pegylation induced stability is not understood, the hypothesized mechanism by which steric stabilization work is preventing electrostatic, hydrophobic and van der waals interactions [156].

3.5 Conclusion

In this chapter we confirmed GRP-R to be overexpressed on the surface of the SCLC cells (H345), which justifies targeting SCLC cells by targeting the receptor for delivery of drugs. The receptor shown to be expressed in both cell lines (H345 and A549) with >2 fold increased surface expression in SCLC cells. Cys-bombesin(6-14), cystabn and scrambled cystabn were successfully synthesised using the Fmoc SPPS method. This confirmed using MALDI-ToF MS and the UV data. In addition to that, conjugation with DSPE-PEG_{2000}-Mal was evidently successful. Targeted and control liposomes were synthesised and tested for their stability in aqueous media. The data revealed monodispersed formulation with size of about 100 nm for both formulation. Good stability demonstrated in PBS for both formulation whereas time-dependant instability in 10% FBS.

CELLULAR UPTAKE OF LIPOSOMES BY LUNG CELL MODELS

Chapter 4

4.1 Introduction

Liposomes have several advantages as drug carriers including biocompatibility, biodegradability and a capacity to entrap hydrophilic and lipophilic molecules within their aqueous core and bilayer respectively. Conventional liposomes have been shown to be rapidly eliminated from the bloodstream by mononuclear phagocyte system. Further development of these vesicles led to the use of polymers (mainly PEG) to be grafted onto liposomal surface. This improves the passive targeting of liposomes to malignant tissue through the enhanced permeability and retention (EPR) effect. To achieve active targeting to cancer cells the liposome surface can also be modified with specific targeting moieties such as antibodies, sugars, peptides to further refine biodistribution to target tissue and to improve drug pharmacokinetics. One of the most important aspect of liposomal drug formulation is its cellular uptake in the target tissue of interest such that the extent of drug accumulation in the tumour can be predicted when delivered in vivo.

In this chapter, the cellular uptake of fluorescently labelled Cystabn-targeted liposomes was determined in the A549 and NCI-H345 cell lines by flow cytometry. Liposomes prepared without the Cystan-targeting peptide were used as control to determine the specificity of peptide-targeting to the GRP receptor.

The aims of this chapter were to:

1) **Evaluate the targeting moiety mitogenicity to SCLC cells (H345)**
2) **Study the targeted liposomal uptake in SCLC cells**

4.2 Materials & methods

4.2.1 Materials

All materials were of analytical grade and sourced from either Sigma or Fisher unless mentioned otherwise.

4.2.2 Cell Culture

All cell cultures were maintained at 37 °C, 5 % CO2, and 95 % air in a humidified incubator and routinely passaged at confluency. Further details are found in Chapter 3.

4.2.3 MTS proliferation assay with bombesin-derived peptides

The A549 and H345 cell lines were seeded in 96 well plates at 5000 cells/well. Cystabn and its scrambled form were serially diluted 4-fold from 742.4 nM to 11 pM. Both cell lines were incubated with the peptides in complete medium containing 2% FBS for various time points. For A549 cells, the doubling time is 22 h, so the cells treated with reagent at 24 h, 48 h and 72 h. In contrast, H345 cell doubling time is 122 h, so the treatment performed at 5 days, 7 days and 10 days. At each time point 10 µL MTS/PES reagent was added per 100 µL (stock concentration of 2 mg/mL MTS and 0.92 mg/mL PES) to the A549 and H345 cells and were incubated at 37 °C for 4 hours and 6 hours respectively. The absorbance at 492 nm was measured using BMG LABTECH FLUOstar OPTIMA Microplate Reader. The positive control was 1% Triton X-100 and the negative control was 2% FBS medium without peptides.

4.2.4 Liposomes uptake experiment by flow cytometer using fluorescent probe

The Cystabn-targeted fluorescent liposomes and control florescent liposomes (both including 1 mole % DHPE-fluorescein) were prepared by thin film hydration method as described in the Chapter 2/3. The two formulation characterized in terms of their size and surface charge using Zetasizer Nano ZS.

To perform uptake experiments the H345 cell line was subcultured into 12 well plates as described in chapter 3 and incubated overnight. The cell media was removed by centrifugation (200 *g*, 5 min) and replenished with serum-free DMEM and incubated at 37 °C and 4 °C (as control). The stock fluorescent liposome solution (10 mg/mL lipid) was diluted 1:13 in serum-free medium such that the final lipid concentration was 0.769 mg/mL and a final targeting peptide concentration was 38 μg/mL (31.24 nM). These conditions were chosen according to the published literature [157, 158] as those suitable for generating a measurable fluorescence response for flow cytometry. Cells were incubated at 37 °C or 4 °C for 15-120 min before transfer to ice to stop liposome internalisation. Cells were transferred into microfuge tubes and washed with PBS (x3), then cells were resuspended in PBS. Flow cytometry analysis was performed using a Beckman Coulter Cytomics FC500 flow cytometer equipped with a 15 mW argon-ion laser. Cells were analysed on the basis of forward light scatter (FS), side light scatter (SS) and DHPE- fluorescein fluorescence (excitation/emission maxima ~496/519 nm) by FL-1 detector. Typically, fluorescence information for 10000 events was collected for each sample using Kaluza Analysis Software. Data were analysed by gating live cells, as judged by FS versus SS dot plots, and plotting the fluorescence of these cells in a histogram. Fluorescence profiles or histograms shown were representative of those obtained from the number of experiments indicated. The

increase in fluorescence intensity above background was determined by measuring the shift in fluorescence intensity from peak to peak, relative to the indicated control.

4.3 Results

4.3.1 Mitogenicity of cystabn

The effect of cystabn peptide on the proliferation of both cell lines was determined by MTS assay. Both cell lines were treated with a dose-range of cystabn and scrambled cystabn control across the concentration range ~750 nM to 11.5 pM. For the slow dividing H345 cell line the effect of peptides was determined over 5, 7 and 10 days (Figure 4.1). There was no observed increase or decrease in absorbance across the tested concentration range of either peptide at any of the time points. The low absorbance values measured in Figure 4.1 a-c were recorded after an extended incubation time with the MTS reagent and indicate a low metabolic capacity of this cell line. Absorbance values measured for the 1% Triton control, was 0.33 AU for A549 cells and 0.2 AU for H345 cells.

In A549 cells (Figures 4.1 d-f) the Cystabn and scrambled peptide antagonists had no measurable effect on proliferation and there was no significant difference ($P > 0.05$) in the absorbance values across time points. The consistenecy of absorbance values at the lowest peptide concentrations reflects the fast growing nature of A549 cells and the rapid achievement of 85-100% confluency by 24 hours and beyond.

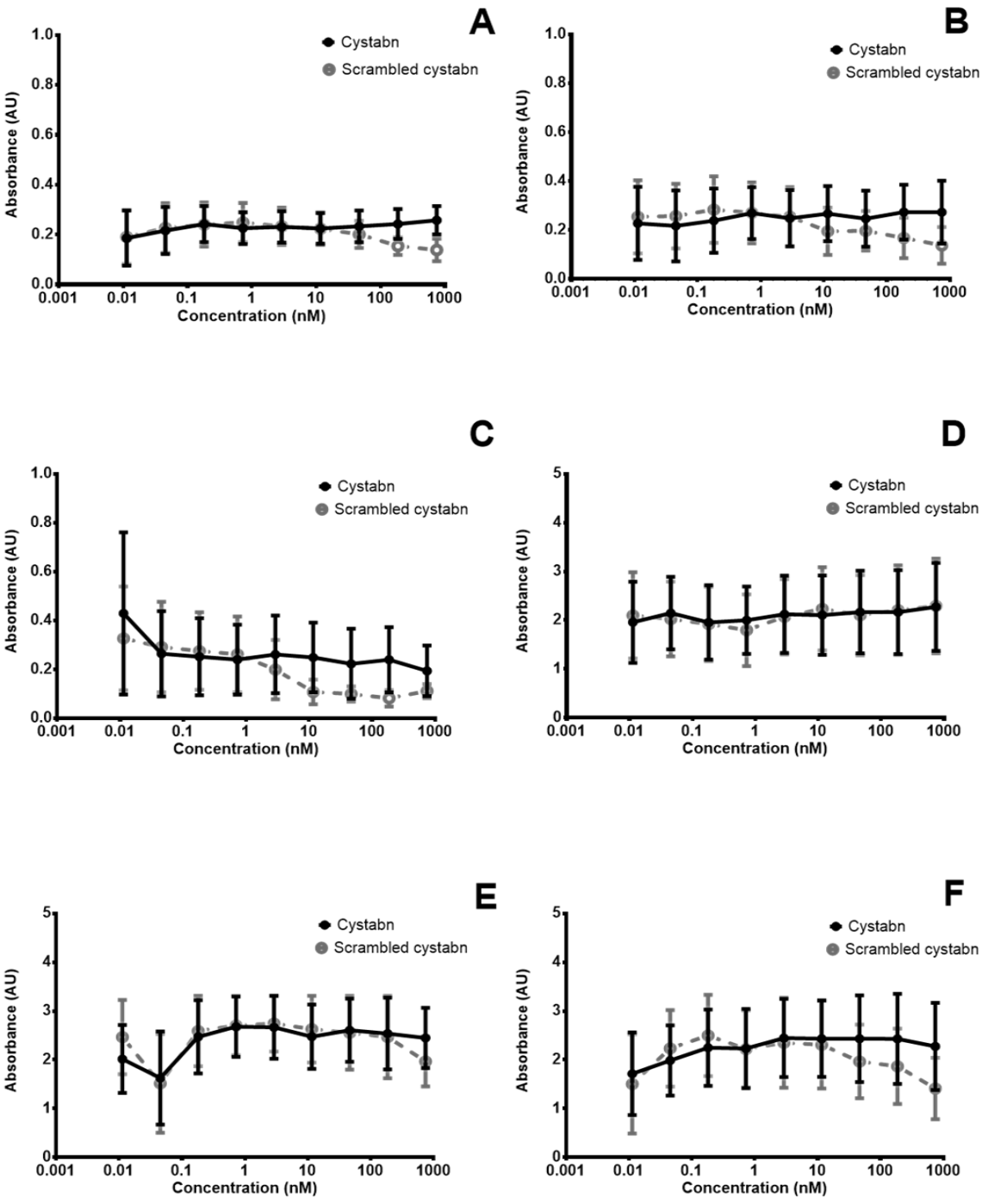

Figure 4.1: MTS cell proliferation assays. *Viability of cells was measured at 492 nm for H345 cells at 5 days (A), 7 days (B) and 10 days (C); and for A549 cells at 24 h (D), 48 h (E) and 72 h (F). prior to measurement, H345 and A549 cells were incubated with MTS/PES reagent for 6 hours and 4 hours respectively. Error bars show standard error of the mean (n=3 independent experiments).*

4.3.2 Uptake of targeted liposomes

Flow cytometry was used to evaluate the uptake, into A549 and H345 cells, of targeted and control liposomes (without the targeting moiety) labelled with 1 mole % DHPE-fluorescein. Due to time constraints these studies were performed only in H345 cells. H345 has higher surface GRP-R expression as discussed in Chapter 3 and it is the cell line of interest in this study.

The liposomes were incubated with H345 cells for 15 - 120 minutes at 37 °C and for 120 minutes at 4 °C (as no-uptake control). The cell suspensions presented a homogenous dispersion and cells were gated based on FS/SS of the control cells (i.e. without treatment) as shown in example scatter plot Figure 4.3A and fluorescence histogram of the gated population (Figure 4.2B). It is apparent from Figure 4.2 B that the control population showed negligible background fluorescence. Figures 4.2C and 4.2D show the fluorescence histogram of the gated populations of H345 cells for control and targeted liposomes respectively. The shift in the florescence intensity of samples from three independent experiments are shown in Figure 4.2E.

From Figure 4.2C it is apparent that cells incubated at 4°C with fluorescently labelled control liposomes marginally higher MFI than untreated control cells (1.6 and 2.5 for control and targeted liposomes respectively). For the control formulation experiment shown in Figure 4.2c there was a marginal rightward shift in the FL-1 intensity upon increased incubation time indicating an increased uptake of fluorescent liposomes. Calculation of the median fluorescence intensity (MFI) of each histogram from there independent experiments indicated that there was no increase in the FL1 intensity over the 120 min.. For example, the MFI decreased from 4.24 ± 0.8 at 15 min to 3.76 ± 0.02 at 120 min.

Over the time course of the experiment there was a small increase in the MFI for H345 cells incubated with the targeted formulation (Figure 4.2D). There was an observable shift in the florescent signal of all time points at 37 °C compared to the florescent signal of 120 minutes at 4 °C. This indicate that liposomes are internalised by H345 cells but to a limited extent. However, there are no significant difference between time points of the same formulation at 37 °C as well as between formulations ($p > 0.05$). however, there is a slight increase in the uptake of the targeted formulation at 60 °C compared to the control formulation (4.58 ± 0.77 and 3.32 ± 0.24 respectively).

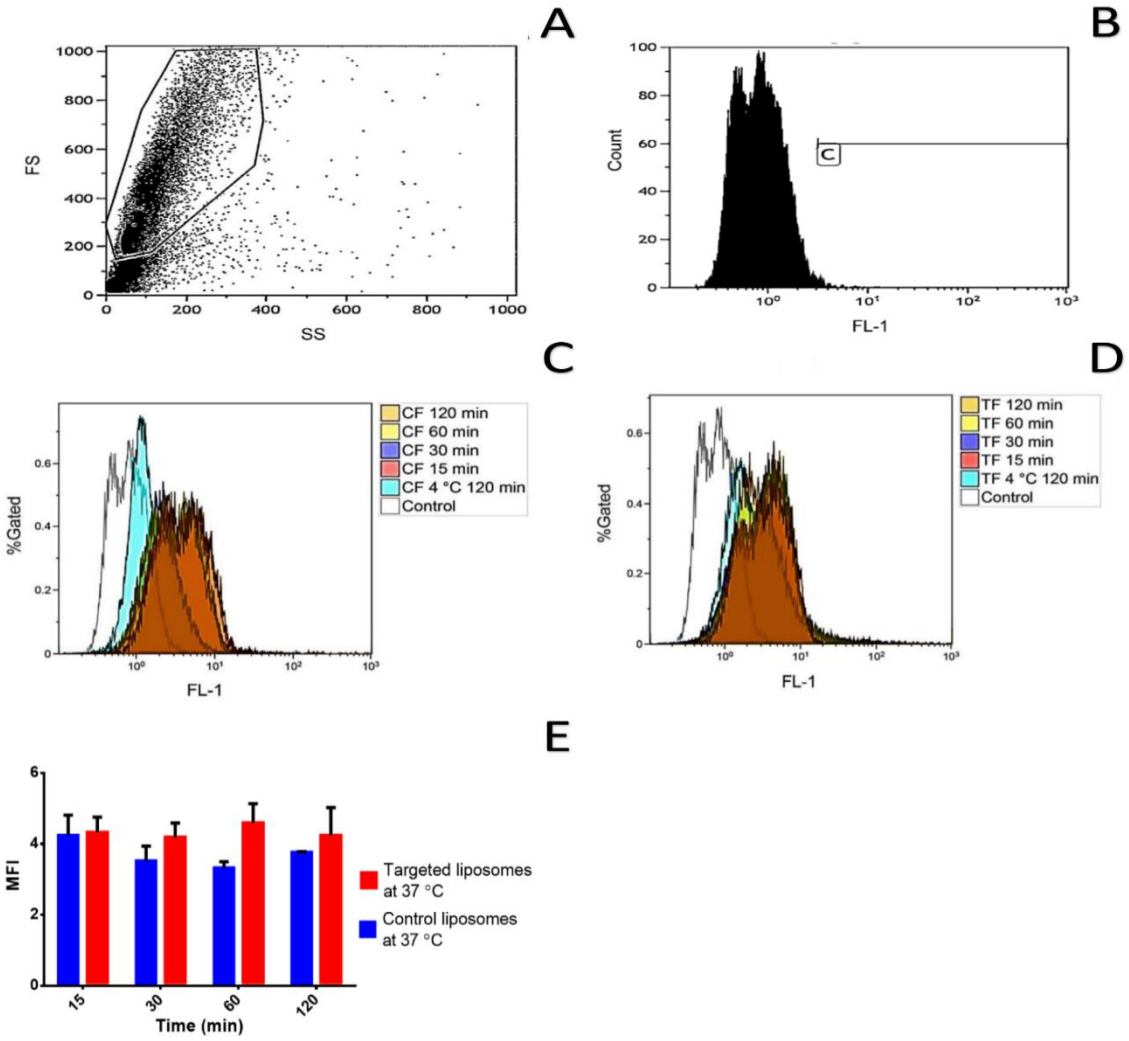

Figure 4.2: Flow cytometry analysis of liposomes uptake by H345 cells. *(A) example of* cell gating strategy dot plot for H345 control cells (without treatment). FS: Forward scattering, SS: side scattering. (B) FL-1 fluorescence histogram shift of the control sample. The bar labelled C indicates the exterior of the gate in which increased FL-1 fluorescence was detected. *(*C*) and (*D*) show the FL-1 histograms of control formulations (CF) and targeted formulations (TF) after incubation with H345 cell line for 120, 60, 30 and 15 minutes at 37 °C and for 120 minutes only at 4 °C (as control). Cell suspensions were analysed with a Cytomics FC500 flow cytometer. The median florescence intensities (MFI)* represented for both formulations at *37 °C. Error bars show standard error of the mean (n=3 independent experiments).*

4.4 Discussion

Active targeting of nanomedicines to cancer cells is a challenging concept to achieve. In the case of SCLC targeting we sought in this work to exploit bombesin-derived peptides in order to target the cognate GRP receptor that is reported to be upregulated in SCLC cells. We hypothesised that the use of a N-terminal cysteine derived GRP receptor antagonist peptide (Cystabn) avoids the mitogenic effect of bombesin peptides that might compromise this targeting approach by causing agonist-induced GRP receptor activation and stimulation of cancer growth [4, 27].

The effect of Cystabn peptide on the proliferation of two GRP-R positive cell lines (A549 and H345) was evaluated by MTS assay after incubation with a dose-range of cystabn and scrambled cystabn control peptide. There was no change in the absorbance of either cell cultures caused by either peptide indicating the absence of a pro-mitogenic response. These experiments were designed such that any increase in cell proliferation would be registered as an increase in MTS absorbance. In the case of A549 cells (doubling time 22 h) the MTS absorbance was high at each of the timepoints of indicating high confluency even at 24 hours. Visual inspection of the A549 cell monolayers confirmed the confluency to be <100% so further studies would be required in order to optimise the seeding density and peptide treatment times. In contrast, the slow-growing H345 cells (doubling time, 122 h) displayed very low MTS absorbance levels that were comparable to the 1% Triton X-100 control at 5, 7 and 10 days post-treatment. The 10 day exposure for H345 cells was designed to include two population doubling times and this sub-optimal result warrants further investigation. The reduction of serum concentration from 10% to 2% would have a direct negative effect on the cellular proliferation rate but also reduces the exposure to serum-derived mitogenic factors that drive cell proliferation in faster growing cells such as A549. In summary, the

absence of a pro-proliferative activity of Cystabn justifies its use as a targeting ligand as opposed to the agonist peptides which have been shown to promote cell proliferation of SCLC cells in vitro (using NCI-N592 cells). In the work of Cuttitta et al [42] an anti-GRP antibody (2A11) supressed SCLC xenograft growth in mice by 50% in mass compared to the control group. Distinct from GRP and bombesin-related peptides other small proteins/peptideshave been shown to act as growth factors in malignancies such as bladder [159] and prostate [160] cancer. For example, vascular endothelial growth factor (VEGF), acts as angiogenetic factor in several tumours and the use of an anti-VEGF receptor 3 antibody (mF4-31C1), the growth of several tumours such as prostate cancer in mice have been suppressed [160].

With evidence of cell surface expression of GRP receptor and the absence of mitogenic effects associated with Cystabn treatment targeted liposomes were prepared. Specific binding of targeted liposomes to their target site is an important factor in optimising the targeted delivery to cancer cells. In this study, we have performed semi-quantitative analysis of the internalization of cystabn targeted fluorescent liposomes to H345 cells in comparison to control. In general, the extent of liposome internalisation was low, as evidenced by a marginal increase in the FL-1 detector signal over the 120 min time course. More significantly, for both control and targeted formulation there were no significant differences in cellular MFI between time points. There was a noticeable increase in the MFI between control cells incubated at 4 °C and those incubated at 37 °C. These largely inconclusive data demand further investigation into the reasons for low cellular uptake. The studies presented here were performed on freshly cultured cells and which would be expected to have a typical endocytic internalisation rate that would be measured as a time-dependent increase in MFI over a 2 hour time period as reported for other probes [161, 162].

To achieve effective drug delivery, internalization into the cell is required because most anti-cancer drugs act on intracellular targets. There are generally three possible mechanisms of liposome cargo delivery into target cells. Firstly, upon binding to their cell surface bound target liposomes can release their contents in the extracellular region of the target cells. This increases the local drug concentration which drives passive uptake into the cell. The major challenge to the exploitation of this mechanism is to ensure selective extracellular drug release. Secondly, liposomes can fuse with the cell membrane and release their contents intracellularly. An example of this is using diplasmenylcholine to formulate plasma-stable liposome which release its content intracellularly at endosomal pHs [163]. Thirdly, cell-bound liposomes can be internalised by the target cells via receptor-mediated endocytosis and release their contents intracellularly. Internalization of liposomes is dependent on many factors, such as liposome size, type of cell and type of target receptor [164-174].

GPR-R is an example of an internalising receptor [175]. It has been shown that [D-Phe6, Sta13, Leu14]Bombesin(6-14), which is an antagonist can bind to GRP-R with high affinity (IC_{50} = 2.2 nM by competitive binding method) and internalize into the cell [50]. The radiolabelled (via ^{111}In-DOTA-(β-Ala)$_2$) peptide antagonist for GRP-R, [Cys5, D-Phe6, Sta13, Leu14]Bombesin(5-14) showed promising features. It showed high affinity (binding IC_{50} 1.3 nM) to GRP-R *in vitro* using prostate cancer cell line (PC-3). In another study, the internalization of a number of radio-analogues of the peptide was studied using a temperature shift experiment from 4 °C to 37 °C [176]. The internalized fraction after 4 h at 37C was less than 20% for the peptide radioanaloges, which is characteristic for antagonists. Biodistribution of the peptide in mice showed very high uptake of radioactivity in the GRP-R expressing prostate cancer line (PC-3) with high rate of clearance by kidney from non-malignant tissues [50, 177].

The targeted liposomes would be expected to include on average 50% of the loaded targeting Cystabn-PEG-lipid conjugate on the liposome surface i.e. 19 µg/ml (15.6 µM) which is some 80-fold higher than the IC50 of this peptide for the GRP-receptor in Swiss 3T3 cells [48]. In addition to that, the targeted liposome formulation showed good stability in PBS and time-dependant stability in 10% FBS. When studied i*n vivo* the metabolic stability of [Cys5, D-Phe6, Sta13, Leu14]Bombesin(5-14) it was reported that 60% of intact radiopeptides were still detectable after 5 min of injection using HPLC [50]. after 5 minutes, two major hydrophilic radiometabolites revealed. In summary, both control liposomes and cystabn-targeted formulation failed to show significant internalisation into H345 SCLC cell. This is most likely attributable to an intrinsically low endocytic capacity in these cells. Future studies will seek to confirm the endocytic capacity of this cell line using robust fluorescent endocytic probes such as fluorescently labelled transferrin, dextrans and cholera toxin.

4.5 Conclusion

In this chapter, we have demonstrated that cystabn does not induce accelerated growth in A549 and NCI-H345 cells, both of which have been shown to express GRP-R to varying extents. Hence it is favourable to be used rather than GRP-R agonists, such as bombesin, for targeting functionality. GRP-R confirmed to be overexpressed on the surface of the SCLC cells (H345), which justifies targeting SCLC cells by targeting the receptor for delivery of drugs. Flow cytometry analysis of H345 cells showed that the extent of fluorescent liposome uptake was negligible over the time points tested, was equivalent for control and targeted formulations. This indicates that the current formulation approach is inappropriate for the preparation of targeted liposomes. Further work will focus on the confirmation of Cystabn uptake into both cell lines prior to formulation work to optimise the presentation of the targeting ligand on the liposome surface. With evidence of rapid peptide internalisation into the H345 and other SCLC cell lines further formulation work will be conducted to optimise ligand presentation to the GRP-R on the SCLC cell surface.

GENERAL DISSCUSION AND CONCLUSION

Chapter 5

5.1 General discussion

In this study, the GRP-R expression measured. The idea of targeting this receptor came from its important role as autocrine growth factor in SCLC. Two lung cancer cells lines (SCLC and NSCLC) used in the study. The expression detected by indirect antibody measurement by flow cytometer. H345 cells showed higher surface expression of GRP-R (>2 fold, compared to A549), which suggest higher availability of the receptor. A549 cells showed greater total amount of GRP-R. This could be explained as higher non-specific binding. This data support SCLC targeting using this receptor.

Another important factor in targeting is the use of highly specific targeting moiety. In this study, an antagonist peptide (cystabn) was used for targeting as an alternative to bombesin (6-14) peptide. It has high affinity for GRP-R. the reason is that bombesin shown to cause cancer growth by autocrine manner. In addition, antagonistic peptide can cause tumour growth inhibition. Antagonistic peptide shown to not stimulate cell growth by using MTS proliferation assay. Cystabn synthesised by SPPS and successfully characterized by HPLC, MALDI-ToF MS and UV spectrometer. In addition to that, conjugation of the Cystabn peptide to DSPE-PEG-maleimide proceeded successfully to yield a peptide-PEG-lipid conjugate.

Liposomes prepared by thin-film hydration as control liposome formulation (5% total DOPE-PEG) and targeted formulation (4% DOPE-PEG + 1% cystabn-PEG-DSPE). There was an increase in PDI and particle size over the 72 h time period for targeted liposome. This increase in size probably caused by opsonisation process. The characterization of the liposomes showed a monodisperse liposome suspension with a slightly negative zeta potential (-1.64 for control and -1.76 for targeted liposomes in PBS). The targeted liposome

formulation showed good stability in PBS and time-dependant stability in 10% FBS. The colloidal and biological stability of the system is provided through the steric hindrance effect caused by pegylation. Pegylation achieved by inclusion of 5 mole % DOPC-PEG_{2000}. In this study, a 5 mole % pegylation is used to provide long circulation time *in vivo* by greatly decrease opsonisation.

In this study, the internalization of cystabn targeted fluorescent liposomes to H345 cells in comparison to control was evaluated using flow cytometry. In general, the extent of liposome internalisation was low over the 120 min time course. In addition, there were no significant differences in cellular internalization between formulations over 120 min. However, there was observable increase in the MFI of both formulation and the control at 4 °C. Further investigation needed for the low cellular uptake.

5.2 General conclusion

In this study, we have demonstrated that GRP-R expressed on the surface of the SCLC cells higher than NSCLC cells. We have also demonstrated that cystabn does not induce growth in A549 and NCI-H345 cells. In addition to that, cystabn has high affinity and selectivity to the GRP-R. Therefore, the use of this antagonist is favourable over GRP-R agonists as a targeting moiety.

Successful synthesis of cystabn, by SPPS and DSPE-PEG_{2000}-cystabn conjugation is demonstrated. The characterization by three methods – HPLC, MALDI ToF and UV spectrometry – performed. The control and the targeted liposomes were synthesised and characterised by DLS. Both formulations showed monodispersed population. Further investigation into the stability of both formulation performed in PBS and 10% FBS. Both formulations showed good stability in PBS. The targeted formulation showed time-dependant instability in 10% serum.

Flow cytometry analysis of H345 cells showed internalization of both formulations compared to control cells at 4 °C. However, there was no significant diffrance between formulations. This indicates the need for invistgating other liposomes synthesis methods to improve the uptake.

Bibliography

1. UK, C.R. *Lung cancer statistics: Lung cancer incedance*. 2013 [cited September 20165; Available from: http://www.cancerresearchuk.org/health-professional/cancer-statistics/statistics-by-cancer-type/lung-cancer#heading-Zero.
2. UK, C.R. *Cancer mortality for all cancers combined: Cancer mortality by sex and UK resion*

2014 [cited September 2016; Available from: http://www.cancerresearchuk.org/health-professional/cancer-statistics/mortality/all-cancers-combined#heading-Zero.

3. Travis, W.D., *Update on small cell carcinoma and its differentiation from squamous cell carcinoma and other non-small cell carcinomas.* Modern Pathology, 2012. **25**: p. S18-S30.
4. Jackman, D.M. and B.E. Johnson, *Small-cell lung cancer.* The Lancet, 2005. **366**(9494): p. 1385-1396.
5. Kahnert, K., D. Kauffmann-Guerrero, and R.M. Huber, *SCLC–state of the art and what does the future have in store?* Clinical Lung Cancer, 2016.
6. Ren, Y., et al., *Multiple paraneoplastic syndromes associated with small cell lung cancer: a unique case of concomitant Lambert-Eaton myasthenic syndrome, paraneoplastic cerebellar degeneration and syndrome of inappropriate secretion of antidiuretic hormone.* INTERNATIONAL JOURNAL OF CLINICAL AND EXPERIMENTAL MEDICINE, 2016. **9**(2): p. 4939-4942.
7. Hobbs, C. and A. Miller, *Review of endocrine syndromes associated with tumours of non-endocrine origin.* Journal of clinical pathology, 1966. **19**(2): p. 119-127.
8. Wang, X., R. Jiang, and K. Li, *Prognostic significance of pretreatment laboratory parameters in combined small-cell lung cancer.* Cell biochemistry and biophysics, 2014. **69**(3): p. 633-640.
9. Guidance, N. *Lung cancer: diagnosis and management*. 2011 September 2016]; Available from: https://www.nice.org.uk/guidance/cg121/chapter/Patient-centred-care.
10. Moody, T.W., et al., *BN/GRP-like peptides and receptors in small cell lung cancer.* Int J Neurosci, 1988. **40**(1-2): p. 141-8.
11. Carney, D.N., et al., *Selective stimulation of small cell lung cancer clonal growth by bombesin and gastrin-releasing peptide.* Cancer Res, 1987. **47**(3): p. 821-5.
12. Jaques, G., et al., *Production of insulin-like growth factor binding proteins by small-cell lung cancer cell lines.* Exp Cell Res, 1989. **184**(2): p. 396-406.
13. Anastasi, A., V. Erspamer, and M. Bucci, *Isolation and amino acid sequences of alytesin and bombesin, two analogous active tetradecapeptides from the skin of European discoglossid frogs.* Arch Biochem Biophys, 1972. **148**(2): p. 443-6.
14. McDonald, T., et al., *Characterization of a gastrin releasing peptide from porcine non-antral gastric tissue.* Biochemical and biophysical research communications, 1979. **90**(1): p. 227-233.
15. Minamino, N., K. Kangawa, and H. Matsuo, *Neuromedin B: a novel bombesin-like peptide identified in porcine spinal cord.* Biochemical and biophysical research communications, 1983. **114**(2): p. 541-548.
16. Patel, O., A. Shulkes, and G.S. Baldwin, *Gastrin-releasing peptide and cancer.* Biochimica et Biophysica Acta (BBA)-Reviews on Cancer, 2006. **1766**(1): p. 23-41.
17. Cornelio, D., R. Roesler, and G. Schwartsmann, *Gastrin-releasing peptide receptor as a molecular target in experimental anticancer therapy.* Annals of Oncology, 2007.

18. Jensen, R., et al., *International Union of Pharmacology. LXVIII. Mammalian bombesin receptors: nomenclature, distribution, pharmacology, signaling, and functions in normal and disease states.* Pharmacological reviews, 2008. **60**(1): p. 1-42.
19. Wasilenko, W.J., et al., *Calcium signaling in prostate cancer cells: evidence for multiple receptors and enhanced sensitivity to bombesin/GRP*. Prostate, 1997. **30**(3): p. 167-73.
20. Zachary, I. and E. Rozengurt, *Modulation of the epidermal growth factor receptor by mitogenic ligands: effects of bombesin and role of protein kinase C.* Cancer surveys, 1984. **4**(4): p. 729-765.
21. Slice, L.W., H.F. Yee, Jr., and J.H. Walsh, *Visualization of internalization and recycling of the gastrin releasing peptide receptor-green fluorescent protein chimera expressed in epithelial cells.* Receptors Channels, 1998. **6**(3): p. 201-12.
22. Cuttitta, F., et al., *Bombesin-like peptides can function as autocrine growth factors in human small-cell lung cancer.* 1985.
23. Burns, D., et al., *Breast cancer cell-associated endopeptidase EC 24.11 modulates proliferative response to bombesin.* British journal of cancer, 1999. **79**(2): p. 214.
24. Narayan, S., et al., *Specific binding and growth effects of bombesin-related peptides on mouse colon cancer cells in vitro.* Cancer research, 1990. **50**(21): p. 6772-6778.
25. Bologna, M., et al., *Bombesin stimulates growth of human prostatic cancer cells in vitro.* Cancer, 1989. **63**(9): p. 1714-1720.
26. Moody, T.W., et al., *Neuromedin B binds with high affinity, elevates cytosolic calcium and stimulates the growth of small-cell lung cancer cell lines.* Journal of Pharmacology and Experimental Therapeutics, 1992. **263**(1): p. 311-317.
27. Toi-Scott, M., C.L. Jones, and M.A. Kane, *Clinical correlates of bombesin-like peptide receptor subtype expression in human lung cancer cells.* Lung Cancer, 1996. **15**(3): p. 341-354.
28. Xiao, D., et al., *The human gastrin-releasing peptide receptor gene structure, its tissue expression and promoter.* Gene, 2001. **264**(1): p. 95-103.
29. Kane, M.A., et al., *Isolation of the bombesin/gastrin-releasing peptide receptor from human small cell lung carcinoma NCI-H345 cells.* J Biol Chem, 1991. **266**(15): p. 9486-93.
30. Corjay, M.H., et al., *Two distinct bombesin receptor subtypes are expressed and functional in human lung carcinoma cells.* Journal of Biological Chemistry, 1991. **266**(28): p. 18771-18779.
31. Uchida, K., et al., *Expression of progastrin-releasing peptide and gastrin-releasing peptide receptor mRNA transcripts in tumor cells of patients with small cell lung cancer.* Journal of cancer research and clinical oncology, 2002. **128**(12): p. 633-640.
32. Hohla, F., et al., *Growth inhibition of non-small-cell lung carcinoma by BN/GRP antagonist is linked with suppression of K-Ras, COX-2, and pAkt.* Proceedings of the National Academy of Sciences, 2007. **104**(47): p. 18671-18676.
33. Detterbeck, F.C., D.J. Boffa, and L.T. Tanoue, *The new lung cancer staging system.* CHEST Journal, 2009. **136**(1): p. 260-271.
34. Sørensen, J., et al., *Performance status assessment in cancer patients. An inter-observer variability study.* British journal of cancer, 1993. **67**(4): p. 773.
35. Kurup, A. and N.H. Hanna, *Treatment of small cell lung cancer.* Critical reviews in oncology/hematology, 2004. **52**(2): p. 117-126.
36. Morabito, A., et al., *Treatment of small cell lung cancer.* Critical reviews in oncology/hematology, 2014. **91**(3): p. 257-270.

37. Veronesi, G., et al., *When is surgery indicated for small-cell lung cancer?* Lung Cancer, 2015. **90**(3): p. 582-9.
38. Bosch, F. and L. Rosich, *The Contributions of Paul Ehrlich to Pharmacology: A Tribute on the Occasion of the Centenary of His Nobel Prize.* Pharmacology, 2008. **82**(3): p. 171-179.
39. Maeda, H., et al., *Tumor vascular permeability and the EPR effect in macromolecular therapeutics: a review.* J Control Release, 2000. **65**(1-2): p. 271-84.
40. Allen, T.M., *Ligand-targeted therapeutics in anticancer therapy.* Nature Reviews Cancer, 2002. **2**(10): p. 750-763.
41. Lembo, D. and R. Cavalli, *Nanoparticulate delivery systems for antiviral drugs.* Antiviral Chemistry and Chemotherapy, 2010. **21**(2): p. 53-70.
42. Cuttitta, F., et al., *Bombesin-like peptides can function as autocrine growth factors in human small-cell lung cancer.* Nature, 1985. **316**(6031): p. 823-6.
43. *Antitumor activity of an anti-gastrin releasing peptide (GRP) murine monoclonal antibody (2A11). Phase II trial and in vitro correlation with peptide and receptor expression.* Lung Cancer, 1994. **11**: p. 4.
44. Koppan, M., et al., *Bombesin/gastrin-releasing peptide antagonists RC-3095 and RC-3940-II inhibit tumor growth and decrease the levels and mRNA expression of epidermal growth factor receptors in H-69 small cell lung carcinoma.* Cancer, 1998. **83**(7): p. 1335-43.
45. Kiaris, H., et al., *Targeted cytotoxic analogue of bombesin/gastrin-releasing peptide inhibits the growth of H-69 human small-cell lung carcinoma in nude mice.* British journal of cancer, 1999. **81**(6): p. 966.
46. Thomas, F., et al., *Antitumoral activity of bombesin analogues on small cell lung cancer xenografts: relationship with bombesin receptor expression.* Cancer research, 1992. **52**(18): p. 4872-4877.
47. Mahmoud, S., et al., *[Psi13, 14] bombesin analogues inhibit growth of small cell lung cancer in vitro and in vivo.* Cancer research, 1991. **51**(7): p. 1798-1802.
48. Llinares, M., et al., *Syntheses and biological activities of potent bombesin receptor antagonists.* J Pept Res, 1999. **53**(3): p. 275-83.
49. Tokita, K., et al., *Molecular basis for selectivity of high affinity peptide antagonists for the gastrin-releasing peptide receptor.* Journal of Biological Chemistry, 2001. **276**(39): p. 36652-36663.
50. Marsouvanidis, P.J., et al., *Gastrin releasing peptide receptor-directed radioligands based on a bombesin antagonist: synthesis, 111In-labeling, and preclinical profile.* Journal of medicinal chemistry, 2013. **56**(6): p. 2374-2384.
51. Bangham, A.D. and R. Horne, *Negative staining of phospholipids and their structural modification by surface-active agents as observed in the electron microscope.* Journal of molecular biology, 1964. **8**(5): p. 660IN2-668IN10.
52. Sessa, G. and G. Weissmann, *Phospholipid spherules (liposomes) as a model for biological membranes.* Journal of lipid research, 1968. **9**(3): p. 310-318.
53. Daoud, S.S., L.R. Hume, and R.L. Juliano, *Liposomes in cancer therapy.* Advanced Drug Delivery Reviews, 1989. **3**(3): p. 405-418.
54. Meybeck, A., *Past, present and future of liposome cosmetics*, in *Liposome Dermatics*. 1992, Springer. p. 341-345.
55. Kim, H.-H.Y. and I.C. Baianu, *Novel liposome microencapsulation techniques for food applications.* Trends in Food Science & Technology, 1991. **2**: p. 55-61.
56. Gregoriadis, G., P. Leathwood, and B.E. Ryman, *Enzyme entrapment in liposomes.* FEBS letters, 1971. **14**(2): p. 95-99.

57. Michel, S. *Predicting the fate of liposomes*. 2014 January 2014 [cited 2016 september 2016]; Available from: http://www.materials-talks.com/blog/2014/01/20/predicting-the-fate-of-liposomes/.
58. Koshkaryev, A., et al., *Immunoconjugates and long circulating systems: origins, current state of the art and future directions.* Advanced drug delivery reviews, 2013. **65**(1): p. 24-35.
59. Akbarzadeh, A., et al., *Liposome: classification, preparation, and applications.* Nanoscale Research Letters, 2013. **8**(1): p. 1-9.
60. Allen, T.M. and P.R. Cullis, *Liposomal drug delivery systems: From concept to clinical applications.* Advanced Drug Delivery Reviews, 2013. **65**(1): p. 36-48.
61. Torchilin, V.P., *Recent advances with liposomes as pharmaceutical carriers.* Nat Rev Drug Discov, 2005. **4**(2): p. 145-160.
62. Vaage, J., et al., *Tissue distribution and therapeutic effect of intravenous free or encapsulated liposomal doxorubicin on human prostate carcinoma xenografts.* Cancer, 1994. **73**(5): p. 1478-1484.
63. Gabizon, A., et al. *Prolonged circulation time and enhanced accumulation in malignant exudates of doxorubicin encapsulated in polyethylene-glycol coated liposomes*. Cancer Res 1994 Jnne 2015 [cited 54 4]; 1994/02/15:[987-92]. Available from: https://www.doxil.com/hcp/mechanism-of-action.
64. Krishna, R., et al., *Liposomal and nonliposomal drug pharmacokinetics after administration of liposome-encapsulated vincristine and their contribution to drug tissue distribution properties.* J Pharmacol Exp Ther, 2001. **298**(3): p. 1206-12.
65. Gabizon, A., H. Shmeeda, and Y. Barenholz, *Pharmacokinetics of Pegylated Liposomal Doxorubicin.* Clinical Pharmacokinetics, 2003. **42**(5): p. 419-436.
66. Li, J., et al., *A review on phospholipids and their main applications in drug delivery systems.* Asian Journal of Pharmaceutical Sciences, 2015. **10**(2): p. 81-98.
67. Sułkowski, W., et al., *The influence of temperature, cholesterol content and pH on liposome stability*. Journal of molecular structure, 2005. **744**: p. 737-747.
68. Akbarzadeh, A., et al., *Liposome: classification, preparation, and applications.* Nanoscale Res Lett, 2013. **8**(1): p. 102.
69. Philippot, J., S. Mutaftschiev, and J. Liautard, *A very mild method allowing the encapsulation of very high amounts of macromolecules into very large (1000 nm) unilamellar liposomes.* Biochimica et Biophysica Acta (BBA)-Biomembranes, 1983. **734**(2): p. 137-143.
70. Sercombe, L., et al., *Advances and challenges of liposome assisted drug delivery.* Frontiers in pharmacology, 2015. **6**.
71. Klibanov, A.L., et al., *Amphipathic polyethyleneglycols effectively prolong the circulation time of liposomes.* FEBS Lett, 1990. **268**(1): p. 235-7.
72. Gabizon, A.A., *Pegylated liposomal doxorubicin: metamorphosis of an old drug into a new form of chemotherapy*. Cancer investigation, 2001. **19**(4): p. 424-436.
73. van den Hoven, J.M., et al., *Complement activation by PEGylated liposomes containing prednisolone*. European journal of pharmaceutical sciences, 2013. **49**(2): p. 265-271.
74. Gabizon, A., et al., *Prolonged circulation time and enhanced accumulation in malignant exudates of doxorubicin encapsulated in polyethylene-glycol coated liposomes.* Cancer research, 1994. **54**(4): p. 987-992.
75. Noble, G.T., et al., *Ligand-targeted liposome design: challenges and fundamental considerations.* Trends in biotechnology, 2014. **32**(1): p. 32-45.

76. Honda, M., et al., *Liposomes and nanotechnology in drug development: focus on ocular targets.* International journal of nanomedicine, 2013. **8**: p. 495.
77. Merrifield, R.B., *Solid phase peptide synthesis. I. The synthesis of a tetrapeptide.* Journal of the American Chemical Society, 1963. **85**(14): p. 2149-2154.
78. Sheppard, R., *The fluorenylmethoxycarbonyl group in solid phase synthesis.* Journal of Peptide Science, 2003. **9**(9): p. 545-552.
79. Ramakers, B.E.I., J.C.M. van Hest, and D.W.P.M. Lowik, *Molecular tools for the construction of peptide-based materials.* Chemical Society Reviews, 2014. **43**(8): p. 2743-2756.
80. Shelton, P.T. and K.J. Jensen, *Linkers, Resins, and General Procedures for Solid-Phase Peptide Synthesis*, in *Peptide Synthesis and Applications*, J.K. Jensen, P. Tofteng Shelton, and L.S. Pedersen, Editors. 2013, Humana Press: Totowa, NJ. p. 23-41.
81. Behrendt, R., P. White, and J. Offer, *Advances in Fmoc solid‐phase peptide synthesis.* Journal of Peptide Science, 2016. **22**(1): p. 4-27.
82. El-Faham, A. and F. Albericio, *Peptide coupling reagents, more than a letter soup.* Chemical reviews, 2011. **111**(11): p. 6557-6602.
83. Kaiser, E., et al., *Color test for detection of free terminal amino groups in the solid-phase synthesis of peptides.* Analytical Biochemistry, 1970. **34**(2): p. 595-598.
84. Sarin, V.K., et al., *Quantitative monitoring of solid-phase peptide synthesis by the ninhydrin reaction.* Analytical biochemistry, 1981. **117**(1): p. 147-157.
85. Aguilar, M.-I., *HPLC of Peptides and Proteins.* HPLC of peptides and proteins methods and protocols, 2004: p. 3-8.
86. Karas, M. and F. Hillenkamp, *Laser desorption ionization of proteins with molecular masses exceeding 10,000 daltons.* Analytical chemistry, 1988. **60**(20): p. 2299-2301.
87. Hoffmann, E.d. and V. Stroobant, *Mass spectrometry : principles and applications*. 2007: Chichester : John Wiley & Sons, Ltd., c2007.

3rd ed. / Edmond de Hoffmann, Vincent Stroobant.

88. Aitken, A. and M.P. Learmonth, *Protein Determination by UV Absorption*, in *The Protein Protocols Handbook*, J.M. Walker, Editor. 2002, Humana Press: Totowa, NJ. p. 3-6.
89. Sapan, C.V. and R.L. Lundblad, *Review of methods for determination of total protein and peptide concentration in biological samples.* PROTEOMICS – Clinical Applications, 2015. **9**(3-4): p. 268-276.
90. Hackenberger, C.P.R. and D. Schwarzer, *Chemoselective Ligation and Modification Strategies for Peptides and Proteins.* Angewandte Chemie International Edition, 2008. **47**(52): p. 10030-10074.
91. Pounder, R.J., et al., *Metal free thiol-maleimide 'Click' reaction as a mild functionalisation strategy for degradable polymers.* Chemical Communications, 2008(41): p. 5158-5160.
92. Jewett, J.C. and C.R. Bertozzi, *Cu-free click cycloaddition reactions in chemical biology.* Chemical Society Reviews, 2010. **39**(4): p. 1272-1279.
93. Northrop, B.H., S.H. Frayne, and U. Choudhary, *Thiol–maleimide "click" chemistry: evaluating the influence of solvent, initiator, and thiol on the reaction mechanism, kinetics, and selectivity.* Polymer Chemistry, 2015. **6**(18): p. 3415-3430.
94. Gorin, G., P.A. Martic, and G. Doughty, *Kinetics of the reaction of N-ethylmaleimide with cysteine and some congeners.* Archives of Biochemistry and Biophysics, 1966. **115**(3): p. 593-597.

95. Schelté, P., et al., *Differential reactivity of maleimide and bromoacetyl functions with thiols: application to the preparation of liposomal diepitope constructs.* Bioconjugate chemistry, 2000. **11**(1): p. 118-123.
96. Lee, C.C. and E.R. Samuels, *THE KINETICS OF REACTION BETWEEN L-CYSTEINE HYDROCHLORIDE AND SOME MALEIMIDES.* Canadian Journal of Chemistry, 1964. **42**(1): p. 168-170.
97. Saito, F., H. Noda, and J.W. Bode, *Critical Evaluation and Rate Constants of Chemoselective Ligation Reactions for Stoichiometric Conjugations in Water*. ACS Chemical Biology, 2015. **10**(4): p. 1026-1033.
98. Bangham, A., M.M. Standish, and J. Watkins, *Diffusion of univalent ions across the lamellae of swollen phospholipids.* Journal of molecular biology, 1965. **13**(1): p. 238-IN27.
99. Mayer, L., et al., *Solute distributions and trapping efficiencies observed in freeze-thawed multilamellar vesicles.* Biochimica et Biophysica Acta (BBA)-Biomembranes, 1985. **817**(1): p. 193-196.
100. Berger, N., et al., *Filter extrusion of liposomes using different devices: comparison of liposome size, encapsulation efficiency, and process characteristics.* International Journal of Pharmaceutics, 2001. **223**(1–2): p. 55-68.
101. de Araújo Lopes, S.C., et al., *Liposomes as Carriers of Anticancer Drugs.* Cancer Treatment—Conventional and Innovative Approaches; Rangel, L., Ed, 2013.
102. Cho, N.-J., et al., *Comparison of extruded and sonicated vesicles for planar bilayer self-assembly*. Materials, 2013. **6**(8): p. 3294-3308.
103. Hunter, D. and B. Frisken, *Effect of extrusion pressure and lipid properties on the size and polydispersity of lipid vesicles.* Biophysical journal, 1998. **74**(6): p. 2996-3002.
104. Lapinski, M.M., et al., *Comparison of liposomes formed by sonication and extrusion: rotational and translational diffusion of an embedded chromophore.* Langmuir, 2007. **23**(23): p. 11677-11683.
105. Gregoriadis, G., *Liposome Technology: Liposome Preparation and Related Techniques*. 2016: CRC Press.
106. Hoo, C.M., et al., *A comparison of atomic force microscopy (AFM) and dynamic light scattering (DLS) methods to characterize nanoparticle size distributions.* Journal of Nanoparticle Research, 2008. **10**(1): p. 89-96.
107. Fissan, H., et al., *Comparison of different characterization methods for nanoparticle dispersions before and after aerosolization.* Analytical Methods, 2014. **6**(18): p. 7324-7334.
108. Instruments, L. *Dynamic Light Scattering: Measuring the Particle Size Distribution*. Available from: http://www.lsinstruments.ch/technology/dynamic_light_scattering_dls/.
109. McNeil, S.E., *Characterization of nanoparticles intended for drug delivery*. Vol. 697. 2011: Springer.
110. Hassan, P.A., S. Rana, and G. Verma, *Making sense of brownian motion: colloid characterization by dynamic light scattering.* Langmuir, 2014. **31**(1): p. 3-12.
111. Cosgrove, T., *Colloid science: principles, methods and applications*. 2010: John Wiley & Sons.
112. Moghimi, S.M. and J. Szebeni, *Stealth liposomes and long circulating nanoparticles: critical issues in pharmacokinetics, opsonization and protein-binding properties.* Progress in Lipid Research, 2003. **42**(6): p. 463-478.

113. Xu, R., *Progress in nanoparticles characterization: Sizing and zeta potential measurement.* Particuology, 2008. **6**(2): p. 112-115.
114. McNeil-Watson, F., W. Tscharnuter, and J. Miller, *A new instrument for the measurement of very small electrophoretic mobilities using phase analysis light scattering (PALS).* Colloids and Surfaces A: Physicochemical and Engineering Aspects, 1998. **140**(1–3): p. 53-57.
115. Corbett, J.C.W., et al., *Measuring surface zeta potential using phase analysis light scattering in a simple dip cell arrangement.* Colloids and Surfaces A: Physicochemical and Engineering Aspects, 2012. **396**: p. 169-176.
116. Thomas, J.C., et al., *Observation of Field-Dependent Electrophoretic Mobility with Phase Analysis Light Scattering (PALS).* Langmuir, 2002. **18**(11): p. 4243-4247.
117. Trepel, J.B., et al., *A novel bombesin receptor antagonist inhibits autocrine signals in a small cell lung carcinoma cell line.* Biochem Biophys Res Commun, 1988. **156**(3): p. 1383-9.
118. Giard, D.J., et al., *In vitro cultivation of human tumors: establishment of cell lines derived from a series of solid tumors.* J Natl Cancer Inst, 1973. **51**(5): p. 1417-23.
119. Lieber, M., et al., *A continuous tumor-cell line from a human lung carcinoma with properties of type II alveolar epithelial cells.* Int J Cancer, 1976. **17**(1): p. 62-70.
120. Stearns, R.C., J.D. Paulauskis, and J.J. Godleski, *Endocytosis of Ultrafine Particles by A549 Cells.* American Journal of Respiratory Cell and Molecular Biology, 2001. **24**(2): p. 108-115.
121. Siegfried, J.M., et al., *Evidence for Autocrine Actions of Neuromedin B and Gastrin-releasing Peptide in Non-small Cell Lung Cancer.* Pulmonary Pharmacology & Therapeutics, 1999. **12**(5): p. 291-302.
122. Mori, H., et al., *Cell proliferation in cancer prevention; effects of preventive agents on estrogen-related endometrial carcinogenesis model and on an in vitro model in human colorectal cells.* Mutation Research/Fundamental and Molecular Mechanisms of Mutagenesis, 2001. **480–481**: p. 201-207.
123. Malich, G., B. Markovic, and C. Winder, *The sensitivity and specificity of the MTS tetrazolium assay for detecting the in vitro cytotoxicity of 20 chemicals using human cell lines.* Toxicology, 1997. **124**(3): p. 179-192.
124. Goodwin, C.J., et al., *Microculture tetrazolium assays: a comparison between two new tetrazolium salts, XTT and MTS.* Journal of Immunological Methods, 1995. **179**(1): p. 95-103.
125. Henel, G. and J.L. Schmitz, *Basic theory and clinical applications of flow cytometry.* Laboratory Medicine, 2007. **38**(7): p. 428-436.
126. Shapiro, H.M., *Practical flow cytometry*. 2005: John Wiley & Sons.
127. Rahman, M., *to Flow Cytometry.* AbD seroTEC a divizion of morphoSys, 2006.
128. NPTEL. *Lecture 19 : Flow Cytometry and Cell Sorting*. 2012 September 2016]; Available from: http://nptel.ac.in/courses/102103016/19#.
129. Barenholz, Y.C., *Doxil®–the First FDA-approved Nano-drug: from Basics via CMC, Cell Culture and Animal Studies to Clinical Use*, in *Nanomedicines*. 2016. p. 315-345.
130. Duan, X., et al., *Nanoparticle formulations of cisplatin for cancer therapy.* Wiley Interdisciplinary Reviews: Nanomedicine and Nanobiotechnology, 2016.
131. Pandey, H., R. Rani, and V. Agarwal, *Liposome and Their Applications in Cancer Therapy.* Brazilian Archives of Biology and Technology, 2016. **59**.

132. Suzuki, R., et al., *Cancer therapy with nanotechnology-based drug delivery systems: applications and challenges of liposome technologies for advanced cancer therapy.* Nanomaterials in Pharmacology, 2016: p. 457-482.
133. Verma, S., et al., *Trastuzumab emtansine for HER2-positive advanced breast cancer.* New England Journal of Medicine, 2012. **367**(19): p. 1783-1791.
134. Mehta, A., V.V. Reddy, and U. Borate, *Anti CD-30 Antibody-Drug Conjugate Brentuximab Vedotin (ADCETRIS®) May Be a Promising Treatment Option for Systemic Mastocytosis (SM).* Blood, 2012. **120**(21): p. 2857-2857.
135. Yu, M.K., J. Park, and S. Jon, *Targeting strategies for multifunctional nanoparticles in cancer imaging and therapy.* Theranostics, 2012. **2**(1): p. 3.
136. Danhier, F., O. Feron, and V. Préat, *To exploit the tumor microenvironment: passive and active tumor targeting of nanocarriers for anti-cancer drug delivery.* Journal of Controlled Release, 2010. **148**(2): p. 135-146.
137. Torchilin, V.P., *Passive and active drug targeting: drug delivery to tumors as an example*, in *Drug delivery*. 2010, Springer. p. 3-53.
138. Bertrand, N., et al., *Cancer nanotechnology: the impact of passive and active targeting in the era of modern cancer biology.* Advanced drug delivery reviews, 2014. **66**: p. 2-25.
139. Sapra, P., P. Tyagi, and T.M. Allen, *Ligand-targeted liposomes for cancer treatment.* Current drug delivery, 2005. **2**(4): p. 369-381.
140. Wang, X. and W. Lu, *Active Targeting Liposomes: Promising Approach for Tumor-Targeted Therapy.* J Bioequiv Availab, 2016. **8**: p. 013-014.
141. Yao, V.J., et al., *Ligand-targeted theranostic nanomedicines against cancer.* Journal of Controlled Release, 2016.
142. Siegfried, J., et al., *Evidence for autocrine actions of neuromedin B and gastrin-releasing peptide in non-small cell lung cancer.* Pulmonary pharmacology & therapeutics, 1999. **12**(5): p. 291-302.
143. Siegfried, J.M., et al., *Production of gastrin-releasing peptide by a non-small cell lung carcinoma cell line adapted to serum-free and growth factor-free conditions.* Journal of Biological Chemistry, 1994. **269**(11): p. 8596-8603.
144. Chonn, A., S. Semple, and P. Cullis, *Association of blood proteins with large unilamellar liposomes in vivo. Relation to circulation lifetimes.* Journal of Biological Chemistry, 1992. **267**(26): p. 18759-18765.
145. Moghimi, S.M. and H.M. Patel, *Tissue specific opsonins for phagocytic cells and their different affinity for cholesterol- rich liposomes.* FEBS letters, 1988. **233**(1): p. 143-147.
146. Szebeni, J., et al., *Role of complement activation in hypersensitivity reactions to doxil and hynic PEG liposomes: experimental and clinical studies.* Journal of liposome research, 2002. **12**(1-2): p. 165-172.
147. Chanda, N., et al., *Bombesin functionalized gold nanoparticles show in vitro and in vivo cancer receptor specificity.* Proc Natl Acad Sci U S A, 2010. **107**(19): p. 8760-5.
148. Cescato, R., et al., *Bombesin receptor antagonists may be preferable to agonists for tumor targeting.* Journal of Nuclear Medicine, 2008. **49**(2): p. 318-326.
149. Llinares, M., et al., *Syntheses and biological activities of potent bombesin receptor antagonists.* The Journal of peptide research, 1999. **53**(3): p. 275-283.
150. Allen, C., et al., *Controlling the physical behavior and biological performance of liposome formulations through use of surface grafted poly(ethylene glycol).* Biosci Rep, 2002. **22**(2): p. 225-50.

151. Kenworthy, A.K., et al., *Range and magnitude of the steric pressure between bilayers containing phospholipids with covalently attached poly(ethylene glycol).* Biophysical Journal, 1995. **68**(5): p. 1921-1936.
152. Tang, L., et al., *Investigating the optimal size of anticancer nanomedicine.* Proceedings of the National Academy of Sciences, 2014. **111**(43): p. 15344-15349.
153. Deshpande, P.P., S. Biswas, and V.P. Torchilin, *Current trends in the use of liposomes for tumor targeting.* Nanomedicine, 2013. **8**(9): p. 1509-1528.
154. Sharma, A. and U.S. Sharma, *Liposomes in drug delivery: progress and limitations.* International journal of pharmaceutics, 1997. **154**(2): p. 123-140.
155. Allen, T.M., et al., *Liposomes containing synthetic lipid derivatives of poly(ethylene glycol) show prolonged circulation half-lives in vivo.* Biochim Biophys Acta, 1991. **1066**(1): p. 29-36.
156. Lasic, D.D., *Doxorubicin in sterically stabilized liposomes.* Nature, 1996. **380**(6574): p. 561-562.
157. Van Broekhoven, C.L. and J.G. Altin, *A novel system for convenient detection of low-affinity receptor-ligand interactions: chelator-lipid liposomes engrafted with recombinant CD4 bind to cells expressing MHC class II.* Immunol Cell Biol, 2001. **79**(3): p. 274-84.
158. Danila, D., et al., *Antibody-Labeled Liposomes for CT Imaging of Atherosclerotic Plaques.* Texas Heart Institute Journal, 2009. **36**(5).
159. Laskin, J.J. and A.B. Sandler, *Epidermal growth factor receptor: a promising target in solid tumours.* Cancer Treat Rev, 2004. **30**(1): p. 1-17.
160. Laakkonen, P., et al., *Vascular endothelial growth factor receptor 3 is involved in tumor angiogenesis and growth.* Cancer research, 2007. **67**(2): p. 593-599.
161. Vorauer-Uhl, K., et al., *Determination of liposome size distribution by flow cytometry.* Cytometry, 2000. **39**(2): p. 166-71.
162. Childers, N.K., et al., *Characterization of liposome suspensions by flow cytometry.* J Immunol Methods, 1989. **119**(1): p. 135-43.
163. Rui, Y., et al., *Diplasmenylcholine-folate liposomes: an efficient vehicle for intracellular drug delivery.* Journal of the American Chemical Society, 1998. **120**(44): p. 11213-11218.
164. Daleke, D.L., K. Hong, and D. Papahadjopoulos, *Endocytosis of liposomes by macrophages: binding, acidification and leakage of liposomes monitored by a new fluorescence assay.* Biochimica et Biophysica Acta (BBA)-Biomembranes, 1990. **1024**(2): p. 352-366.
165. Ishii, Y., et al., *Preparation of EGF labeled liposomes and their uptake by hepatocytes.* Biochemical and biophysical research communications, 1989. **160**(2): p. 732-736.
166. Lundberg, B., K. Hong, and D. Papahadjopoulos, *Conjugation of apolipoprotein B with liposomes and targeting to cells in culture.* Biochimica et Biophysica Acta (BBA)-Biomembranes, 1993. **1149**(2): p. 305-312.
167. Machy, P. and L.D. Leserman, *Small liposomes are better than large liposomes for specific drug delivery in vitro.* Biochimica et Biophysica Acta (BBA)-Biomembranes, 1983. **730**(2): p. 313-320.
168. Matthay, K.K., et al., *Role of ligand in antibody-directed endocytosis of liposomes by human T-leukemia cells.* Cancer research, 1989. **49**(17): p. 4879-4886.
169. Nassander, U.K., et al., *Design of immunoliposomes directed against human ovarian carcinoma.* Biochimica et Biophysica Acta (BBA)-Biomembranes, 1995. **1235**(1): p. 126-139.

170. Storm, G. and D.J. Crommelin, *Liposomes: quo vadis?* Pharmaceutical Science & Technology Today, 1998. **1**(1): p. 19-31.
171. Straubinger, R.M., et al., *Endocytosis of liposomes and intracellular fate of encapsulated molecules: strategies for enhanced cytoplasmic delivery*, in *Receptor-Mediated Targeting of Drugs*. 1984, Springer. p. 297-315.
172. Straubinger, R.M., et al., *Endocytosis of liposomes and intracellular fate of encapsulated molecules: encounter with a low pH compartment after internalization in coated vesicles.* Cell, 1983. **32**(4): p. 1069-1079.
173. Suzuki, S., et al., *Modulation of doxorubicin resistance in a doxorubicin-resistant human leukaemia cell by an immunoliposome targeting transferring receptor.* British journal of cancer, 1997. **76**(1): p. 83.
174. Vingerhoeds, M., et al., *Immunoliposome-mediated targeting of doxorubicin to human ovarian carcinoma in vitro and in vivo.* British journal of cancer, 1996. **74**(7): p. 1023.
175. Abd-Elgaliel, W.R., et al., *Design, Synthesis, and Biological Evaluation of an Antagonist− Bombesin Analogue as Targeting Vector.* Bioconjugate chemistry, 2008. **19**(10): p. 2040-2048.
176. Abiraj, K., et al., *Bombesin antagonist-based radioligands for translational nuclear imaging of gastrin-releasing peptide receptor-positive tumors.* J Nucl Med, 2011. **52**(12): p. 1970-8.
177. de Jong, M., et al., *Radiopeptide antagonists for imaging and therapy of GRPR+ tumors.* Journal of Nuclear Medicine, 2011. **52**(supplement 1): p. 189-189.